USING NOVEL SURFACE-ENHANCED RAMAN SPECTRSCOPY (SERS)-SILVER NANOROD BIOSENSING ASSAYS AND CHEMOMETRIC METHODS TO DETECT LOW-LEVELS OF MEASLES VIRUS

by

TASADAY LYNCH

(Under the Direction of Richard Dluhy)

ABSTRACT

Measles is a very contagious disease that is the leading cause of death of children. Traditionally, the measles virus (MV) can be detected using qRT-PCR, ELISA, and IFA assays. However, these techniques often provide inconclusive information and do not allow for low-level detection. Since, viral shedding of an infected person can be from 1 to 10,000 pfu, it is important to attain an assay capable of low level MV detection. Surface-enhanced Raman spectroscopy (SERS) demonstrates a quick, label-free spectroscopic method for detection of low levels of molecular samples. In this study, SERS- Ag nanorods assays were used with the Partial Least Squares-Discriminant Analysis (PLS-DA) chemometric method to classify D4, A, and H1 measles genotypes with 100% sensitivity and specificity. Additionally, the SERS assay was combined with Partial Least Squares (PLS) to accurately (RMSECV=0.024) estimate low molecular concentrations (10^3 -10 pfu/ml) of MV samples with high linearity (R^2=0.99).

INDEX WORDS: infectious disease, spectroscopy, chemometrics

USING NOVEL SURFACE-ENHANCED RAMAN SPECTRSCOPY (SERS)-SILVER NANOROD BIOSENSING ASSAYS AND CHEMOMETRIC METHODS TO DETECT LOW-LEVELS OF MEASLES VIRUS

by

TASADAY LYNCH

BS, UNIVERSITY OF GEORGIA, 2007

A Thesis Submitted to the Graduate Faculty of The University of Georgia in Partial Fulfillment of the Requirements for the Degree

MASTER OF SCIENCE

ATHENS, GEORGIA

2010

USING NOVEL SURFACE-ENHANCED RAMAN SPECTRSCOPY (SERS)-SILVER NANOROD BIOSENSING ASSAYS AND CHEMOMETRIC METHODS TO DETECT LOW-LEVELS OF MEASLES VIRUS

by

TASADAY LYNCH

Major Professor: Richard Dluhy

Committee: I. Jonathan Amster
John Stickney

Electronic Version Approved:

Maureen Grasso
Dean of the Graduate School
The University of Georgia
August 2010

TABLE OF CONTENTS

Page

LIST OF TABLES

Page

LIST OF FIGURES

Page

Chapter 1

Introduction

1.1 Summary.

The measles can be deadly to both children and adults, particularly when it leads to pneumonia and encephalitis. The infection is one of the leading causes of death among young children even though a safe and cost-effective vaccine is available. In 2008, there approximately 10 million cases and 164,000 measles deaths globally. More than 95% of these deaths occurred in low-income countries with weak health infrastructures and inaccessibility to vaccination. Nonetheless, the disease still affects populations in developed nations with access to vaccination due to virus importation. Therefore, a need for reliable laboratory surveillance of the measles remains an issue especially as disease prevalence declines.

Laboratory surveillance for measles is based on detection of virus-specific antibodies and detection of viral proteins or viral RNA.[1] Detection of virus-specific antibodies such as immunoglobin M (IgM) occurs using serologic methods like immunofluorescent antibody (IFA) and enzyme-linked immunosorbent assays (ELISA or EIA) by documentation of IgG seroconversion or four-fold rise in IgG EIA titer between acute- and convalescent-phase sera, and by isolation of MV or deletion of MV RNA from a clinical specimen. Serologic methods, however, are not measles specific, meaning they

cannot distinguish between wild-type infections and vaccine-associated cases because they merely measure levels of antibodies (IgG or IgM) that can be attributed to a number of infections. Additionally, these tests are not time-efficient, have low sensitivity, poor detection limit, and frequently lead to false negatives.[2-4]

Sensitive viral detection methods like reverse transcription-polymerase chain reaction (RT-PCR) also do not enable the capacity to detect low levels of viral sample even though the use of the technique (*i.e.,* for the detection of MV RNA in a variety of clinical samples) has served as a valuable, alternative procedure for cases in which serologic testing results are inconclusive, inconsistent, or unavailable.[1] RT-PCR is a technique carried out through the detection of viral RNA via nucleic acid extraction and amplification. Low levels of virus typically found in clinical samples limit the sensitivity of this viral antigen detection method. For example, previously vaccinated individuals who experience the reoccurrence of a measles outbreak have decreased amount of viral shedding, thereby low levels of RNA cannot be detected by RT-PCR. In addition to its limitations with sensitivity, RT-PCR viral RNA or viral isolation samples are often inadequate because of improper collection, storage, and processing and transportation.[5] Sample preparation alone is a lengthy and requires much precision to produce consistent and conclusive results. Likewise, it takes hours to obtain results. Finding a method that increases the reliability and speed of viral detection assays is advantageous in the future of measles surveillance and to establish a basis for further studies concerning virus discrimination.

One alternative to existing laboratory surveillance technique is surface-enhanced Raman spectroscopy (SERS), a nano-optical method that provides a fast, label free

method for the determination of the viral samples. SERS is an extension of Raman spectroscopy, which is a vibrational spectroscopic technique used to provide high structural information useful in real-world applications in biochemistry and the life sciences.[6] SERS differs from Raman scattering in that the incoming laser beam interacts with the oscillations of plasmonic electrons in metallic nanostructures to enhance, by 14 orders of magnitude, the vibrational spectra of molecules adsorbed to the surface.[7-9] SERS is an extremely sensitive method that has been used for virus detection by either direct spectroscopic characterization of the intact virus,[10] indirect detection of virus biomarkers,[11] or by the use of reporter molecule assemblies.[12]

Over the past few years, SERS has been used as a biomedical-sensing device to detect viruses and differentiate between various viral strains with the use of silver nanorods as biosensing platforms. Nano-array surface-enhanced Raman spectroscopic substrates, created by an oblique angle deposition (OAD) technique,[13] have been recently used for the detection and differentiation of closely related respiratory syncytial virus.[10] In these studies by Dluhy et al. SERS substrates have demonstrated extreme sensitivity with enhancement factors of greater than 10^8.[14,15] These nano-array surface-enhanced Raman spectroscopic substrates, silver nanorod-based SERS (AgNR-SERS) substrates, demonstrated the possibility of rapidly (<60 sec) detection of various virus types in minute specimen volumes (0.75 ± 0.25 μL) without biochemical manipulation of the virus sample.[16] The high signal enhancement obtained from the AgNR-SERS substrates, as well as the small amount of analyte is need for detection, proves that SERS has the potential of being a reliable method for low level virus detection.

While the SERS-AgNR substrates provide the sensitivity of the SERS method, they do not convey selectivity possibilities of SERS assays.[1] The selectivity of the SERS technique can be provided by multivariate statistical analysis of the spectral data.[17] In past studies, it has been shown that the SERS technique can be a qualitative methodology when combining the sensitivity and reproducibility of the AgNR-SERS substrates with the classification abilities of multivariate analytical tools (i.e. chemometrics). [1,18] In addition to being a qualitative methodology, SERS can be used for quantitative information about viral strains. Specifically, combining SERS with chemometrics one can relate the relative intensity of spectral data to the change in viral concentration. This cannot be accomplished by directly relating the intensity of one band to the concentration in a univariate form. Thus, it is believed that AgNR-SERS substrates can be used to determine the limit of detection of MV strains using partial least squares (PLS), a chemometric method, because PLS is suitable for the analysis of complex mixtures since it is able to allow fast and simultaneous determination of each component in a mixture without time-consuming separations and with minimum sample preparation.

In this two-part study, SERS measles detection was achieved with minimal sample preparation. First, it was demonstrated that the SERS methodology could be used as a highly sensitive qualitative technique. This was expressed by the classification of various MV genotypes (viral strains A1, H, and D4) using Ag-SERS substrates, in conjunction with multivariate analytical methods (i.e. principle components analysis and partial least squares-discriminant analysis; PCA and PLS-DA). In the second study, demonstrated was the possibility of using the SERS methodology as a quantitative tool that can provide a relationship between SERS spectral intensity to changes in measles

viral concentration for the determination of the limit of detection. This was shown in PLS models, regression curves that relate the relative intensity of SERS spectral data to the change in viral concentration.

1.2 Measles virus

Background of the measles

The measles is a very contagious disease known by a prodromal* illness of fever, coryza, cough, and conjunctivitis followed by the appearance of a generalized maculopapular rash. It is an infection of the respiratory system caused by the measles virus (MV), which is spread by aerosol or respiratory droplets and enters by the respiratory route. An infection has an average incubation period of 14 days and infectivity from 2 to 4 days prior, until 2 to 5 days following the onset of the rash.[19] The onset of the rash coincides with the appearance of the immune response and initiation of virus clearance.[20] The disease can often lead to pneumonia and encephalitis if not treated. The Centers for Disease Control and Prevention deem the disease the deadliest to unvaccinated children; the infection is one of the leading causes of death among young children throughout the world. Needless to say, availability of the MV vaccine in industrialized nations make it less fatal, however, endemic transmission of the disease into underdeveloped nations, populations with inadequate medical care, is associated with high mortality. Likewise, in industrialized nations, measles outbreaks reoccur due to the transmission and mutation of the virus, as well as the re-infection of people with failed immunity to the disease.[21-24] Measles is a current global concern and attaining the

* up to four days before the rash

quickest method of detection will aid diagnosis of the disease and contribute to the global measles surveillance.[18]

Large numbers of people are needed to generate adequate susceptible individuals to maintain measles in a population. It is postulated that the measles evolved in the early centers of civilization in the Middle East where populations attained sufficient densities to sustain continued transmission[25]. Scientists assume that the disease evolved from animal morbillivirus mainly because, phylogenetically, MV is most closely related to Rinderpest virus (RPV), a pathogen of cattle (Figure 1.1), therefore it is assumed that MV evolved in an environment where cattle and humans lived in close proximity[25]. Arabian physician Abu Becr is credited with distinguishing small pox from the measles in the 9th century. Becr referred to the measles as *hasbah* (eruption) and noted that it causes an "anxiety of mind, sick qualms and heaviness of heart, oppress more in the measles than in the smallpox".[26] Between 1 and 1200 A.D., numerous epidemics of illnesses characterized by a rash were recorded in European and Far Eastern populations. In the 8th century, it is recorded that the measles spread across the Pyrenees into France with the Saracen invasion.[27] Continual epidemics identified as measles were recorded in the 11th and 12th centuries, and in 1224 it was considered a childhood disease.[25]

Introduction of measles into previously unexposed populations has been associated with high morbidity and mortality.[27,28] Epidemics of rash illnesses were associated with episodes of depopulation in China, India, and the Mediterranean region. Introduction of measles into the Fiji Islands in 1875 resulted in 26% morality[27]. An estimated 56 million people died as a result of European exploration of the New World,

mainly due to the introduction into native Amerindian populations of Old World diseases, like smallpox and measles[25].

Peter Panum, a Danish physician, deduced the contagious nature of the disease in his visit to Faroe Islands in 1846. In the large-scale measles epidemic, Panum observed many attributes of the virus from the 14-day incubation period, the lifelong immunity present in older residents, and postulated a respiratory route of transmission. Within the pervious century, complications of the measles were first described.[20] In 1790, James Lucas, an English surgeon, described the first case of post-measles encephalomyelitis in a woman who developed paraparesis as the rash was fading[29]. In the nineteenth century, measles was associated with the exacerbation of tuberculosis and in 1908 a physician recorded the disappearance of delayed-type hypersensitivity skin test responses to tuberculin[30]. In 1933, Subacute sclerosing pan-encephalitis (SSPE) was first described by Dawson in a young boy with progressive neurologic deterioration. Histologic examination of the brain showed eosinophilic intranuclear and intracytoplasmic inclusions in neurons and glial cells. Reports of paramyxoviruslike particles in the inclusions[31] were followed rapidly by documentation of elevated MV antibody in serum and cerebrospinal fluid and staining of the inclusions with antibody to MV.[32]

In 1954, the measles virus was first grown in tissue culture by Enders and Peebles,[33] who inoculated primary human kidney cells with the blood of David Edmonston, a child with measles. MV isolates were also prepared from peripheral blood leukocytes or respiratory secretions inoculated onto primary monkey kidney cells.[33] Continuous monkey kidney cell lines subsequently replaced primary kidney cell cultures for MV isolation.[34] Isolation of wild-type strains is most often successful, however,

using an Epstein-Barr virus-transformed marmoset B lymphocyte line, B95-8[35] or vero cells engineered to express the MV receptor signaling lymphocyte activation molecule (SLAM)[36]. Generally, the first observable sign of virus growth is cell-cell fusion and syncytial formation.

When MV is isolated in cell culture, it can be grown in a variety of cells in culture. This method of growth, specifically growing MV in foreign hosts (e.g. chick embryo and canine and bovine kidney cells), led to the development of live-attenuated vaccine strains.[37] Currently, virus stocks are grown in vero cells at a low multiplicity of infection to prevent accumulation of defective interfering particles. These tissue culture-adapted strain lines are most useful for titration of adapted virus by plaque formation.[38] The virus replicates slowly and in 3 to 5 days it typically becomes visible on plaques. Longer time periods may be required to reach the endpoint of a titration.

Molecular epidemiology of measles virus

MV is an RNA virus in the *Morbillivirus* genus within the family of *Paramyxovirdae* that causes an infection of the respiratory system.[5] Morbilliviruses form two genetically distinct groups of viruses related to either canine distemper virus (CDV) or RPV (Figure 1.1)[39]. Although other members of the genus infect various animal species, measles only infects humans and nonhuman primates.[5] Morbilliviruses are distinct from other paramyxoviruses in formation of intranuclear inclusion bodies. Virions are pleomorphic and range in size from 100 to 300 nm. The genome consists of 15,894 nucleotides, which code for the six structural proteins (nucleoprotein [N], phosphoprotein [P], and matrix [M], fusion [F], hemaggltinin [H], and large protein [L]).[5]

It is a nonsegmented, single—strained, negative-sense genomic material encapsidated by a N to form a helical nucleocapsid that reaches a length of 1.2 μm with the P and L proteins attached. This ribonucleoproteic complex is the substrate for both transcription and replication. The RNA-dependent RNA polymerase binds to the nucleocapsid template using its co-factor, the P.[40] The envelope carries surface projections that are composed of the viral transmembrane H and F glycoproteins (Figure 1.2). The M protein lines the interior of the virion envelope.[39]

The MV remains an antigenically stable monotypic virus for the mere fact that the antisera[†] from individuals infected decades ago retain the ability to neutralize current wild-type strains of MV and vice versa, however with varying efficiencies.[41] Variability in the N and H genes has been recognized by nucleotide sequence analysis[42,43] and monoclonal antibody reactivity[44-46]. The N proteins of wild-type viruses contain antigenic heterogeneity in that N genes differ by up to 7% in the C-terminal N_{TAIL} region.[44,47] Likewise, the H gene nucleotide sequence varies between residues 167 and 241, where the five potential N-linked glycosylation sites are located.[43] The apparent rate of mutation of H in virus circulating in defined geographic locations is low, approximately 5×10^{-4} per year for a selected nucleotide,[42] whereas the rate of mutation during growth in vitro is higher, estimated at 9×10^{-5} per replication for a nucleotide[48]. Wild-type strains separate into eight different clades (A-H) and at least 22 different genotypes based on sequencing of the C-terminal 450 nucleotides of the N gene or the entire coding region of H.[49] Genotypes are classified as distinctive of one another if the

[†] blood serum containing polyclonal antibodies

nucleotide sequence differs from the closest reference sequence by more than 2.5% in N or 2.0% in H.[50] Some genotypes are found in one geographical region, others are co-circulating, while other are inactive and may be extinct. Many laboratories have conducted sequence analysis of wild type measles and demonstrated that molecular epidemiologic techniques could be used to study the transmission patterns of measles virus.[51-56]

1.3 Conventional methods of detection.

To confirm that a patient has measles, clinical diagnosis alone is not adequate, a reliable laboratory test is needed to examine serum samples obtained from the patient.[57] A confirmed case must have serologic affirmation or be epidemiologically associated to a confirmed measles case.[58] It is recommended that a patient's blood sample be collected at the first contact with a suspected case.[59] Blood samples should be collected within 30 days of rash onset for reliable laboratory results. The sample should be handled aseptically and put on ice. Afterwards, the sample should be centrifuged and the serum separated and delivered to an appropriate laboratory for testing.

In the past, the laboratory diagnosis of MV has been detected with methods like Reverse transcription-polymerase chain reaction (RT-PCR), indirect immunofluorescent assay (IFA), and enzyme-linked immunosorbent assay (ELISA or EIA). RT-PCR is a method used to amplify one or more copies of a segment of DNA several orders of magnitude using specific genome- and antigenome-sense primers, usually separated by 200 to 400 nucleotides on the genome of interest for diagnostic reasons. This technique can be performed in a single tube due to the availability of thermostable DNA

polymerases derived from thermophillic bacteria. The process is done through thermal cycling, a series of heating and cooling the DNA. The cycle begins by heating the DNA to high temperature (94ºC) so as to dissociate the DNA duplex, and then cooling to allow annealing of the primers (37ºC to 50ºC) and finally heating to the optimum temperature (72ºC) for the polymerase to copy new DNA. The cycles are repeated 25 to 35 times (25 cycles is said to increase the initial DNA up to 10^7 times) to produce a DNA product that can be visualized by ethidium bromide staining on an agarose gel. The size of the DNA product is defined by the location of the two primers on the virus genome and non-specific DNA products can sometimes be produced and care is needed when interpreting these results. The genome of all morbilliviruses consists of a single strand of negative sense RNA and therefore cannot be amplified directly by PCR but must first be copied into DNA by reverse transcription in a two-step reaction, reverse-transcription/ polymerase chain reaction (RT-PCR).[60] Therefore, RT-PCR is a time consuming step. Additionally, the process may be constrained by the need for an adequate amount of input nucleic acids for quantitation purposeses.[61]

Serologic assays are commonly used to detect virus samples. The most widely used assays are ones that directly measure binding of molecules of antibodies to viral antigens. Examples of these assays include ELISA (or EIA), radioimmunoassay, and the indirect immunofluorescent antibody assay (IFA) (Fields Ch 17 pg 582). Binding assays like IFA can be used in many different formats and in one common format, a viral antigen—that can consist of virally infected cells, a purified viral preparation, or a recombinant viral protein—is attached to a solid surface such as the inner surface of the well of a microtiter tray, a plastic bead or a microscope slide in the case of IFA. Serum is

then added to allow for the binding of antiviral antibodies that might be present in the serum. After the incubation period, the serum is removed and the well is washed several times. The next step includes the addition of a second antibody (i.e. detector antibody) with specificity for human immunoglobulins. The second antibody is usually a mouse monoclonal or a polyclonal antibody from a nonhuman species. The antibody is linked to an enzyme such as horseradish peroxidase. The second antibody binds to any human antibody present. The well is then washed again and the presence of a second antibody is detected based on a colorimetric or fluorescence signal. An advantage of binding assays is that they can be modified to detect IgM or IgA-specific antiviral antibodies through the use of isotype-specific detector antibodies.[62]

A serologic method very similar to IFA used commonly in immunology to detect the presence of an antibody or antigen in a blood sample is ELISA, also referred to as enzyme immunoassay (EIA). The procedure is carried out by immobilizing a known amount of antigen to a solid support then washing a specific antibody over it, to bind the two. The antibody is linked to an enzyme, and in the final step a substance is added that the enzyme can convert to some detectable signal. In fluorescence ELISA, when light of a certain wavelength is shown on the sample, the antigen/antibody complex will fluoresce so that the amount of antigen in the sample can be inferred through the magnitude of fluorescence. A cut-off point maybe is determined by comparing the results by a known standard. For example, the cut-off concentration for drug screening in the workplace is 50 ng/mL, a concentration higher than 50 ng/mL would be considered positive. The most controversial aspect of this test is the cut-off point in distinguishing a positive result from a negative one.

Commercial test kits that detect IgM class antibodies are commonly used and validated by the Global Measles Laboratory Network to be sensitive and specific.[63-65] Laboratory results can be obtained hours after sample collection, however, IgM titers become negative as time passes thereby producing more false-positive results.[66] In fact, ELISA is a more sensitive method than IFA and has the sensitivity of only 50% for the first few weeks of infection.[67] In previously vaccinated persons who become infected, the timing of the IgM response may be altered or the response is absent or undetectable.[68] When these tests fail several other laboratory tools can be used to validate the results. They include an IgM antibody-capture immunoassay, the measurement of IgM anti-measles antibody levels in blood samples obtained from an individual at the onset of disease and at least 14 days after onset, and molecular techniques. An IgM-positive result can occur for at least 6 weeks following vaccination, and seldomly IgM can be detected 2 months or more after vaccination. A person with a rash 2 weeks after vaccination may really have the measles or might be having a reaction to some other disease or allergen. In this case, the presence of IgM in the serum will not be helpful since one cannot distinguish between IgM response from vaccination and wild measles infection.

Although many methods exist for the serological detection of the MV, this process can be long and costly. Similar to IFA and ELISA, RT-PCR has the limitation of not being a low-limit detection method for viral detection. This is an issue for those who have low levels of MV RNA shedding due to failed immunity or a reoccurrence of the virus. In conclusion, a more dependable, inexpensive, and time efficient method of low-level MV detection is desired.

1.4 Raman Spectroscopy.

Raman spectroscopy is an analytical tool, used in chemistry and biology, which was discovered by C.V. Raman in 1928. Classical Raman spectroscopy is described as a vibrational spectroscopic technique produced by inelastic scattering. It occurs when the monochromatic radiation of energy, via a photon, that strikes a molecule is not conserved. In contrast, elastic scattering occurs when the radiation of energy that strikes a molecule is mostly scattered (>99.9%) at the same energy (i.e. Rayleigh scattering). In the case of inelastic scattering it is much weaker than elastic scattering, therefore Raman scattering is weaker than Rayleigh scattering.

In Rayleigh scattering, a photon strikes the molecule with excitation energy at $\tilde{\nu}_0$ frequency. The molecule re-emits the light with energy at the same $\tilde{\nu}_0$ frequency. In Raman scattering, however, the energy of light is re-emitted at a frequency greater or less than the initial frequency of the molecule ($\tilde{\nu}_0 \pm \tilde{\nu}_v$). When the re-emitted energy is less than the initial energy the scattering is known as Stokes Raman scattering. It specifically occurs when the molecule absorbs energy from the photon and the transition of energy occurs from the ground state to the excited state. Thus, for absorbed energy at $\tilde{\nu}_v$ frequency, light is scattered at a frequency of $\tilde{\nu}_0 - \tilde{\nu}_v$. In contrast, in anti-Stokes Raman scattering, molecules in the excited state are radiated and transition from the excited state to the ground state. Therefore, the energy of the re-emitted light is at a higher frequency than the initial energy, $\tilde{\nu}_0 + \tilde{\nu}_v$. Raman vibrational bands are defined by the wavenumber shifts from the excitation energy . Since more molecules populate the ground state at

ambient temperature, Stokes scattering is more common than anti-Stokes scattering for Raman.

In the Raman spectrum, the high structural information about various samples can be determined from the relative intensity of the Raman band and frequency. Since Raman scattering is weak, the reduction of stray light contributed by Rayleigh scattering is essential. This is because elastic scattering is 10^4 to 10^6 times stronger than Raman scattering, Rayleigh scattering can overwhelm the Raman signal. Rayleigh scattering occurs in each spectroscopic measurement since approximately 99.9% of the incident light scatters to produce elastic scattering. Spectrometer filters are used to eliminate the band attributed to Rayleigh scattering, therefore allowing weak Raman bands to appear with higher signal-to-noise in the spectrum.[69,70] After Rayleigh rejection, the detector measures the filtered Raman signal and structural information about one's sample is obtained.

One of the most commonly used detectors used in Raman spectroscopy is the charge-coupled device (CCD) detector. The CCD is a type of multichannel detector capable of simultaneous detection of dispersed radiation in the focal plane.[71] Conventional CCD detectors are two-dimensional solid-state sensors in integrated-circuit form that contain as many as 10^6 pixels on a single silicon chip. A pixel of the detector consists of a thin conducting electrode and p-type silicon body surrounded by an insulating oxide. Upon detection, charges are collected and then stored in the metal-oxide semiconductor (MOS) electrodes. Following the generation of electron-hole pairs, about 10^5 to 10^6 electrons are stored in each pixel, also known as a "potential" well. The charge is moved from pixel to pixel to generate integrated and amplified signals. The

charge accumulation varies directly with the incident intensity and integration time. [71] One disadvantage of CCD detectors is the "blooming" effect, one that occurs when charges from over-illuminated pixels are spread to adjacent pixels. This effect occurs when the CCD is exposed to strong radiation, which limits the dynamic range at the upper end of the detector. Therefore, CCD detectors are more useful for weak sources of monochromatic light like Raman scattering. In addition, the CCD provides high quantum efficiency for light in the UV to near-IR range. The high sensitivity of the detector is useful in Raman spectroscopy and the use of CCD detectors greatly enhances the signal-to-noise ratio of bands in Raman spectra. Other advantages of CCD include low read noise, low dark current, and readout flexibility.[72]

The spectral image of the signal detected at the CCD detector depends on the type of Raman imaging selected. There are three types of Raman imaging: single point microscopy, line imaging, and global illumination. In single point imaging, the Raman spectrum is acquired for one point at a time. Moving the sample stage allows one to perform point-by-point data collection of a sample. Single point imaging acquires spatially resolved spectra in a sequential manner. In line imaging, the laser is focused so that spectral data is collected along a line focused on the sample. The product is a 2-dimensional representation of the intensity versus the Raman shifts along the imaged line. The simultaneous measurement in line imaging generates a spatially resolved spectra along the focused line. In global illumination, the laser is defocused to generate an eclipse-like illumination on the sample. Thus, the illumination covers a larger area on the sample, and a spatially resolved spectra is obtained for the area. The scattered radiation is detected at the specific Raman shift wavelengths. If the detected shifts are characteristic

of the sample components, then the 2D image reflects the chemical composition. In global illumination, the laser is defocused to illuminate a larger area on the sample. This method expands the full view of the microscope.

Line-focused lasers make line imagining possible. In this imaging mode, a laser beam is scanned onto the image plane by a scanning mirror. The microscope objective then focuses the laser beam onto the sample in the shape of a line with an adjustable length. The light is scattered back into the same microscope objective and is focused along the entrance slit of the spectrograph. The CCD detector at the spectrometer simultaneously collects the spatial and spectral data. A process called binning sums the signal of all the pixels in the same column to increase the signal-to-noise (S/N). In conventional Raman spectroscopy, the x-axis of the CCD represents the wavelength, and the y-axis reflects the intensity. The spatial resolution is dependent on the laser spot size and the collection optics. These two factors, in turn, are limited by diffraction. The Gaussian laser beam diameter, d_l, is directly related to the focal length, f, of the lens and inversely related to the effective diameter of the lens, D. The relationship is shown below.[73]

$$d_l = 1.27\lambda\left(\frac{f}{D}\right) \qquad (1\text{-}1)$$

where f/D is also equal to $f/2NA$, d_l, is inversely related to the numerical aperture (NA) of the microscope objective. For microscopes, a larger NA value corresponds to a higher resolving power and a higher magnification.[73]

$$d_l = 1.27\lambda\left(\frac{f}{2NA}\right) \qquad (1\text{-}2)$$

In global imaging, the monochromatic radiation from the sample area scanned is scattered back into the microscope objective then filtered by, first, a Rayleigh band rejection filter and then a wavelength selector. The band filter rejects the scattered light produced from Rayleigh scattering. Afterwards, the filtered light goes through a wavelength selector and undergoes step scanning for a range of Raman shifts. A CCD image is then produced at each Raman shift. Raman global illumination imaging collects the spatial data along the sample at the selected Raman shift for both the x- and the y-axes. Thus, the result is a so-called data cube of the spectral intensity versus the three dimensional position and the Raman shift wavenumbers.[74]

The main advantage of the three Raman imaging techniques is the reduction in data collection time for a particular pixel dimension. The data collection time is shortest in Raman global imaging, however the spatial resolution received with line imaging is much improved because of the simultaneous detection available in line scan. Therefore, the user determines which imaging technique to choose based on whether better resolution or collection time is preferred.

In general, Raman scattering is very weak (~10^{-5} of the incident beam) and the low sensitivity obtained with Raman spectroscopy makes the technique inadequate of analyzing nanoparticles. Raman spectroscopy, while providing spatial resolution and resistance from water, unlike Fourier transform infrared spectroscopy, is very limited by low scattering cross sections that translate to weak signals for detection. The differential Raman cross sections $(d\sigma/d\Omega)_{NRS}$ are less than 10^{-29} cm^2sr^{-1}.[75] Generally, the cross-

sections are more than 10 orders of magnitude lower than that of infrared absorption and 12-14 orders below fluorescence cross sections. Therefore, the signal-to-noise (S/N) ratio of the surface Raman signal expected for one monolayer of absorbates is lower than the detection limit of a typical Raman spectrometer. Thus, low levels of detection cannot be achieved with normal Raman spectroscopy.[76,77] However, for the past two decades, Raman techniques have been improving in many fields particularly due to an increase in enhancement for molecules adsorbed on special metallic surfaces.[76] The development of an improved Raman spectroscopic technique called surface-enhanced Raman spectroscopy (SERS) allows for one to attain a Raman measurement with greater signal enhancement. In the following section, made will be introduction of the SERS method, as well as a brief discussion of the theories that explain its existence (i.e., classical and quantum mechanical theories). Following, the instrumentation of the method will generally be described.

1.5 Surface-enhanced Raman Spectroscopy

In 1974, Fleischman et al. reported the Raman spectrum of a monolayer of pyridine adsorbed on a silver electrode surface[77]; it was at this period that SERS was discovered. In 1977, the enhancement of Raman scattering of adsorbed species (~10^5 to 10^6 times stronger than the nonadsorbed species) was also observed by Jeanmaire and Van Duyne and Albrecht and Creighton, a technique called surface-enhanced Raman spectroscopy (SERS). Attainable with SERS are the nature of adsorbed molecules on specialized metal surfaces (e.g. silver nanorods, gold colloids) and the frequencies of bands associated with these molecules. Likewise, using this method attainable is information about the strength of the absorbate-surface interactions and the conformation

of the adsorbed molecules.[77] Many molecules adsorbed on SERS substrates ('rough' metal surfaces) exhibit Raman cross-sections several orders of magnitude greater than the corresponding quantity for an isolated molecule or from solution, this effect can be explained using two theories, classical or quantum mechanics.[78]

Surface enhanced Raman spectroscopy (SERS) is emerging as an important tool for numerous bioanalytical applications from identification of pathogenic organisms to the classification of microorganisms.[10,16,79,80] It stems from Raman spectroscopy, providing one with the ability to carryout whole-organism fingerprinting with high spatial resolution without the limitation of low signals for detection experienced with classical Raman spectroscopy.[81] The signal amplification results from the an electromagnetic field enhancement experienced by the molecules in close proximity to the roughened metallic surface of the SERS substrate. When an electromagnetic wave hits the molecule the radiation perturbs the electron cloud surrounding the molecule creating a separation of charge within the molecule (*i.e.,* induced dipole moment). The oscillating dipole moment acts like a source of electromagnetic radiation causing an intensified scattering of light.

As been studied in the literature, there are two effects that explain the SERS mechanism and estimate the power of the SERS signal. The electromagnetic enhancement theory was one proposed by David L. Jeanmaire and Richard P. Van Duyne in 1977. The theory is a result of excitation of surface plasmons on the surface of the substrate.[14] The other possible mechanism of the SERS effect is called the chemical enhancement mechanism (CE), which was also proposed in 1977 by M. Grant Albrecht and J. Alan Creighton. The CE mechanism explains that the SERS effect can be described by the formation of a bond, a charge-transfer (C-T) or bond formation of the

metal and absorbate. The attraction is not a stable chemical bond and is much weaker than covalent forces. It is a weak electron resonance and therefore the excitation energy of this resonance occurs very frequently in the visible region. The highest occupied molecular orbital (HOMO) and lowest unoccupied molecular orbital (LUMO) transition for the molecules requires more energy compared to the infrared and visible light involved in Raman experiments. A specific interaction of an absorbate with a nanoparticle's surface leads to a charge transfer from the absorbate into the empty level on the metal surface or from the occupied surface levels to the absorbate.[82-85] The bond formation can increase the molecular polarizability between the two, thereby the stronger the C-T bond the stronger the SERS spectrum. Since this theory relies on a formation of a bond between the absorbate and the surface, it therefore cannot explain the observed signal enhancement in all cases. For molecules without a lone pair of electrons in which the molecules can bond to the surface, a different mechanism exists that involves surface plasmons. The electromagnetic enhancement (EM) theory is one that can apply to even in cases where the specimen is only physisorbed to the SERS surface and thereby it is possible that the chemical mechanism most likely occurs in concert with the EM mechanism.[86]

In 1977, Van Duyne and Jeanmaire proposed the EM mechanism as an alternative explanation of the SERS effect. This enhancement occurs when an excitation source hits a metal surface causing the local electromagnetic field at the metal surface to slightly changed from that of the incident field, especially so when fine metal particles or roughened metal surfaces are involved. The light excitation at the surface of these metals excites conduction electrons and generates a surface plasma resonance (SPR). SPR

occurs because the electrons that are in motion create a strong EM field that form plasmons. Since plasmons have a natural, resonant frequency at which they oscillate best, if incoming light excites these plasmons into their resonant mode then we get an increase in the local EM field surrounding the metal. The applied field causes the roughness feature of the metal to be polarized and the electromagnetic field in the interior of the absorbate to increase greatly. Electromagnetic enhancement can also come from an enhancement factor of the polarizability in the following relationship

$$\mu=\alpha E \qquad (1\text{-}3)$$

where α is the molecular polarizability, E is the electric field and μ is the induced electric dipole moment (polarity). This is plausible because the intensity of Raman scattering is proportional to the square of the induced dipole moment and any enhancement of the dipole moment must be due to the enhancement of the α (molecular polarizability) or E (the electric field due to the incident radiation). Since the EM enhancement mechanism requires coupling of the incident radiation to the metal surface, scientists devote much theoretical and experimental effort to understanding surface plasmons that are created by the process.[87-90]

SPR is a collective excitation mode of the plasma localized near the surface of the metal. Plasmons can be produced electrons on corrugated surfaces of nanoparticles and explained by localized surface plasmon resonance (LSPR) spectroscopy of metallic nanoparticles. [7] LSPR is responsible for the electromagnetic-field enhancement that leads to SERS and other surface-enhanced spectroscopic processes. Researchers of this mechanism study the role of size, shape, material and local dielectric properties of metal

surfaces impacted by LSPR.[91-96] These studies generally provide a fundamental understanding of how surface plasmons are influenced by local structure and environment, they also suggest the usefulness of plasmons as a sensing modality. For the theory behind LSPR, we will should consider a spherical nanoparticle of radius *a* that is irradiated by z-polarized light of wavelength λ (where *a* is much smaller than the wavelength of light λ). The electric field appears static around the nanoparticle (Figure 1.3) allowing us to find the EM field distribution surrounding the nanoparticle by solving Maxwell's equations using a quasi-static approximation.[97,98] The resulting solution for the EM field outside the particle is given by

$$E_{out}(x,y,z) = E_0\hat{z} - \left[\frac{\varepsilon_{in} - \varepsilon_{out}}{(\varepsilon_{in} - 2\varepsilon_{out})}\right] a^3 E_0 \left[\frac{\hat{z}}{r^3} - \frac{3z}{r}(x\hat{\mathrm{x}} + y\hat{\mathrm{y}} + z\hat{\mathrm{z}})\right]. \qquad (1\text{-}4)$$

where ε_{out} is the dielectric constant of the external environment and ε_{in} is the dielectric constant of the metal nanoparticle. Since ε_{in} strongly depends on the wavelength, this first term determines the dielectric resonance condition for the particle. When ε_{in} is close to or equal to $-2\varepsilon_{out}$, the EM field is enhanced relative to the incident field. In regards to silver as the metal nanoparticle, this condition is met in the visible region of the spectrum, which has important implications for SERS. Consistent with experimental results, the size (*a*) and external dielectric constant (ε_{out}) also impact the EM field outside the particle.

The extinction spectrum of the metal nanoparticle can be calculated

$$E(\lambda) = \frac{24\pi^2 N a^3 \varepsilon_{out}^{3/2}}{\lambda \ln(10)} \left[\frac{\varepsilon_i(\lambda)}{(\varepsilon_r(\lambda) + \chi\varepsilon_{out})^2 + \varepsilon_i(\lambda)^2}\right] \qquad (1\text{-}5)$$

where ε_r and ε_i are the real and imaginary variables of the metal dielectric function, respectively. Important in this equation, is χ. This factor has a parallel relationship to the aspect factor and can have a value of 2 for the case of a sphere, and take on a value as high as 20 to account for particles with geometries with high aspect ratios.[99] This variable, however, can only be solved analytically for spheres and spheroids, and therefore must be approximated for all other geometries.[98,99] In this case the approximations can be solved using two methods, the discrete-dipole approximation method, modeled in the frequency domain, and the finite-difference time-domain method, evaluated in the time domain.[100-105]

In addition to modeling the extinction of particles, several equations illustrate how the LSPR are used for both sensing and spectroscopic experiments. For example, the LSPR extinction (or scattering) wavelength maximum, λ_{max}, is sensitive to the dielectric constant, as well as the refractive index n (since ε and n are related by $\varepsilon=n^2$). Therefore, changes in the presence of an adsorbed species, should cause a shirt in λ_{max}. This can be explained by the following relationship: [106,107]

$$\Delta\lambda_{max} = m\Delta n\left[1-\exp\left(-2d/l_d\right)\right]. \qquad (1\text{-}6)$$

In the equation above, m is the bulk refractive-index response of the nanoparticle(s); Δn is the change in refractive index induced by the adsorbate; d is the effective adsorbate layer thickness; and l_d is the characteristic EM-field-decay length (approximated as an exponential decay). As experiments have proven, when the thickness of the adsorbate increases, the intensity of the nanoparticle will shift to shorter wavelengths (i.e. higher

energy levels).[108] We can describe the enhancement factor for SERS using the following formula:

$$EF_{SERS}(\omega_\upsilon) = \frac{\left|E_{out}(\omega)^2 \middle\| E_{out}(\omega-\omega_\upsilon)^2\right|}{E_0^4} = \frac{\left[I_{SERS}(\omega)/N_{surf}\right]}{\left[I_{NRS}(\omega)/N_{vol}\right]}. \qquad (1\text{-}7)$$

The equation demonstrates how the Raman enhancement effect is influenced by the incident excitation, $E_{out}(\omega)$, and the resulting Stokes' shifted Raman, $E_{out}(\omega-\omega_\upsilon)$, EM fields. The experimental enhancement factor can be obtained using the right-hand side of the above equation—i.e., the SERS-enhanced Raman intensity, $I_{SERS}(\omega_\upsilon)$—normalized by the number of the molecules bound to the enhancing metallic substrate, N_{surf}, divided by the normal Roman intensity, $I_{NRS}(\omega_\upsilon)$, normalized by the number of molecules in the excitation volume, N_{vol}. This equation is important because it exemplifies the enhancing ability of substrates of various material, geometry, and LSPR wavelength.

Due to the enhancement factor contributed by both the electromagnetic field and the chemical adsorption, SERS has the capability of detecting on the single molecule level.[77] Unlike other detection methods, SERS does not require amplification steps, which is a quality that makes it an advanced biomedical sensing technique that can be rapidly applied to the detection of a variety of pathogens, especially viruses.[109-116] The potential of SERS as a sensitive detection technique for high levels of molecular specificity has be recognized for years.[117]

1.6 Oblique angle deposition of silver nanorods

Fabrication methods that result in highly ordered arrays of high aspect ratio nanostructures with control over surface morphology are highly desirable. High aspect

ratio Ag and Au SERS nanostructured substrates like nanorods and nanowires have been produced in the past using chemical and electrochemical methods like seeding growth,[118,119] electrochemical etching, and electroplating.[120-122] However, the data produced by these SERS active substrates are challenging to interpret because of contributions from plasmon coupling from aggregates or underlying films. Of recent interest has been the method of substrate preparation called nanosphere lithography, developed by Van Duyne et al. to fabricate increasingly complex periodic particle arrays comprised of Ag nanoparticles.[123] With this method the following optical properties of SERS active substrates were controllable: size, shape, inter particle spacing, nanoparticle—substrate interaction, etc. Similar optical properties can be investigated in the fabrication of nanoparticle arrays by DeJesus et al. using the method of electron-beam lithography (EBL) to produce substrates that demonstrate the strong dependence of particle size and array density on SERS performance.

Nonetheless, fabrication methods that result in highly ordered arrays with control over surface morphology are highly desirable. EBL has been used to produce SERS active nanorod arrays of varying aspect ratios by controlling the spacing between the nanoparticles.[124] However, this method suffers from many disadvantages like elaborate preparation protocols, issues of stability and aggregation, in the case of the chemical and electrolytic methods, while lithography is an expensive process that requires highly skilled operators and accessible instrumentation.

Oblique angle deposition (OAD) is a method that gets away from the disadvantages of the previously mentioned methods by producing SERS active substrates using a physical vapor deposition technique. This method involves positioning of a solid

substrate at a specific angle such that the vapor from the source is incident on the substrate close to the grazing angle (Figure 1.5).[48,125] Depositing metals at an angle results in the preferential growth of nanorods on the substrate in the direction of deposition.[14] This surface morphology occurs because of a shadowing effect where the initial metal nucleation sites are the places of growth of the nanostructues aligned in a specific direction.[126] The major advantages of this technique include the following: computer-enabled control over size, shape, and density of the nanostrctures all factors of temperature, deposition angle, and duration and rate of the deposition; the capability of using multiple metals during a deposition if a multiple pocketed crucible is available and if the metal can be evaporated; any standard thermal or electron beam evaporation system equipped with a holder capable of rotation in the polar direction can be utilized.[127] Ag nanorod substrates prepared by the OAD method (Figure 1.4) have been shown to provide SERS enhancement factor of ~ 10^8.[14]

Along with the sensitivity enhancement factor provided by SERS-AgNR substrates, another advantage of producing these substrates via the OAD method is that there is the possibility of rapidly (<60 sec) detection of various virus types in minute specimen volumes (0.75 ± 0.25 μL) without biochemical manipulation of the virus sample.[16] The high signal enhancement obtained from the AgNR-SERS substrates, as well as the small amount of analyte is need for detection, proves that SERS has the potential of being a reliable method for low level virus detection. With the high sensitive provided by the SERS-AgNR substrates, the selectivity possibilities of SERS assays[1] can be expressed with combing SERS with chemometrics.

1.7 Chemometrics.

Although, silver nanorod substrates provide a high level of sensitivity, they do not convey selectivity possibilities of SERS assays.[1] The selectivity of the SERS technique can be provided by multivariate statistical analysis of the spectral data.[17] Currently, chemometrics serves as this method of classification especially for the exploitation of data compression or reduction methods.[128] Chemometrics is a statistical method used in chemical data analysis. Statistical methodology has been suitable for applications in chemical problems for many years. Specifically, experimental design techniques have had a strong impact on understanding and improving industrial chemical processes.[129] Effective analytical techniques like spectroscopic methods allow one to obtain high dimensional data sets from which we may obtain valuable information using multivariate analyses.[130,131]

Quantitative chemometric strategies are suitable for analysis of complex mixtures because they allow fast and simultaneous determination of each component in a mixture without time-consuming separations and with minimum sample preparation.[132] Among these methods, PLS is a factorial multivariate calibration method that decomposes spectral data into loadings and scores, building the corresponding calibration methods from these new variables. [133,134] An alternative method of extracting relevant components for classification based on the PLS principle is of maximizing covariance using PLS-DA.[135,136] The fundamentals of PLS-DA consist in the application of a PLS regression model on variables which are indicators of the groups.[136] PLS-DA is mainly used to classify observations from the results of PLS regression on indicator variables. Both PLS and PLS-DA offer high selectivity of SERS data,[1] thus coupling these techniques with the

sensitivity and reproducibility of the SERS substrates provides one with close to optimal conditions for low level measles detection. In fact, in this section chemometric strategies will be introduced with the purpose of showing how PLS is the best method for determining the limit of detection of the measles vaccine strain (Edmonston). In following chapters, we will assign the actual measured spectra to categories in a training set using PLS and PLS-DA, however in the following section the methods of PLS and PLS-DA will be explained through the evolution of a few pre-existing chemometric techniques like MLR, HCA and PCA.

Classification is the technique of arranging samples into a group with similar characteristics. Most of the time, data sets contain samples that belong to several different groups or "classes." Classes can differ for many different reasons including variations in sample preparation and chemical composition (i.e aromatic, carbonyl, ester, etc.), or variations in process state. Many methods exist that help one to classify samples based on these measured responses. Methods that attempt to cluster data into groups or classes without using pre-established class memberships are called unsupervised pattern recognition (UPR), or cluster analysis. Classifying data in distinguishable groups (clusters) can be done in an unsupervised way, given that no information is known about the classes initially, using techniques like principal component analysis (PCA) and hierarchical cluster analysis (HCA). Clustering techniques are based on the assumption that samples that are close together in the measurement space are similar and therefore belong to the same class.[137] In this case the distance between samples can be expressed by simple Euclidean distance where d_{ij} between samples $\mathbf{x_i}$ and $\mathbf{x_j}$ is defined as

$$d_{ij} = \sqrt{(x_i - x_j)(x_i - x_j)^T} \quad (1\text{-}9)$$

which is just the square root of the sum of squared differences of the samples. Distance can be illustrated based on PCA scores instead of raw data; in doing so the data is noise-filtered therefore eliminating the deviations between samples contributed by instrumental noise. In this case, the normalized (by unit variance) distance, d_{ij}, between samples $\mathbf{x_i}$ and $\mathbf{x_j}$ with scores $\mathbf{t_i}$ and $\mathbf{t_j}$ is given by

$$d_{ij} = \sqrt{(t_i - t_j)\lambda^{-1}(t_i - t_j)^T} \quad (1\text{-}10)$$

in this case the principle component scores are normalized and the distance is weighted by the inverse of the eigenvalues, λ. The distance defined in equation 1-10 is one type of Mahalanobis distance, a distance that accounts for data sets having varying distances in their variation. Therefore, distance in some directions is weighted more than distance in other directions, as seen in Figure 1.6. Figure 1.6 illustrates a data set (stars) with lines representing contant Euclidean and Mahalanobis distances from the centroid. If the oval surrounding the stars represented a class then the data point shown as the sun would be outside the Mahalanobis line but inside the Euclidean distance line.

In cluster analysis, each sample is clustered based on principle components (PCs), orthogonal basis vectors that are used to model statistically significant variations in the dataset. This can best be described by the method of PCA (Figure 1.7). PCA builds linear multivariate models using PCs where each spectrum is assigned a score for each PC. Each spectrum can be plotted as a single point in a 2D PCA scores plot to reveal

clustering of similar spectra. PCs reduce the dimensionality of the sample matrix prior to clustering.

PCA is a chemometric tool used for data compression and information extraction. PCA finds groupings of variables, or factors, that illustrate major trends in a data matrix. If X is a data matrix with *m* row and *n* columns, and with each variable being a column and each sample a row, PCA decomposes X as the sum of *r* t_i and p_i, where *r* is the rank of the matrix X:[137]

$$X = t_1 p^{T_1} + t_2 p^{T_2} + ... + t_k p^{T_k} + ... + t_r p^{T_r} \qquad (1\text{-}11)$$

where rank is a number expressing the true underlying dimensionality of a matrix and the p_i factors are the loadings and the t_i the scores and the superscripted T_i symbolizes that the variable has been transposed‡;[137] or the expression can be expressed as the equivalent $X = TP^{T_1}$ (P^{T_1} is made up of the p^T as rows and **T** of the **t** as columns).[134] In the above equation, the data matrix is written as outer products of the loadings and scores vectors. Loadings contain information about the relationship of a set of variables while the scores contain information about how the samples relate to each other. Normally the model is truncated after *k* components and the remaining small variance factors are consolidated into a residual matrix E:[137]

$$X = t_1 p^{T_1} + t_2 p^{T_2} + ... + t_k p^{T_k} + E \qquad (1\text{-}12)$$

---

‡ a dataset will switch columns and rows to get pure spectra rather than pure variables.

Equation 1-11 can also be expressed as the matrix X of rank *r* as a sum of *r* matrices of rank 1:[134]

$$X = M_1 + M_2 + M_3 + ...+ M_r \qquad (1\text{-}13)$$

Here *r* must be less than or equal to the smaller dimension of X, *i.e.*, $r \leq \min\{m,n\}$. To illustrate what the t_i and p_i^T mean, an example for the two variables, in the two-dimensional plane, is given in Figure 1.8. For the illustrate of the two variables, Figure 1.8A shows how the principle component is the line of best fit for the data points that are shown in Figure 1.8B. Best fit meaning that the sum of squares of x_1 and x_2 residuals is minimized. This line is also the average of both regression lines. It goes from negative to positive infinity. The p_i^T is a 1x2 row vector. Its elements, p_1 and p_2 are the direction cosines, or the projections of a unit vector along the principle component on the axes of the plot. The scores vector, t_i, is a $nx1$ column vector. Its elements are the coordinates of the respective points on the principle component line (Figure 1.8B).[134] It is ideal to have an operator that places the columns of X onto a single dimension and an operator that projects the rows of X onto a single dimension (Figure 1.9). In this representation, each column of X is denoted by a scalar. Each row is represented by a scalar.

PCA relies on eigenvector decomposition of the covariance or correlation matrix of the process variables. For a data matrix X with *m* rows and *n* columns, the covariance matrix of X is expressed as

$$\text{cov}(X) = \frac{X^T x}{m-1} \qquad (1\text{-}14)$$

provided that the columns of X have been "mean-centered" (*i.e.,* the data has been shifted to the center of the data population see Figure 1.10) by subtracting off the original mean of each column. If the columns have been "auto-scaled" (*i.e.,* adjusted to zero mean and unit variance by dividing each column by its standard deviation), Equation 1-12 gives the correlation matrix of X. In the PCA decomposition, the p_i vectors are *eigenvectors* of the covariance matrix; that is, for each p_i

$$\mathrm{cov}(X)p_i = \lambda_i p_i \quad (1\text{-}15)$$

where λ_i is the *eigenvalue* associated with the eigenvector p_i. The t_i form an orthogonal set ($t_i^T t_j = 0$ for $i \neq j$), while the $\mathbf{p_i}$ are orthonormal ($p_i^T p_j = 0$ for $i \neq j$, $p_i^T p_j = 1$ for $i = j$). Note that for X and any t_i, p_i pair,

$$Xp_i = t_i \quad (1\text{-}16)$$

that is, the score vector t_i is the linear combination of the original X variables defined by p_i. To receive a more detailed description of the variables t_i, p_i please visit Adams 2004 and Wise 2006 [137,138].

PCA is shown graphically in a three-dimensional model in Figure 1.11, where the values of three variables are measured on a collection of samples. It is explicit that the all points (*i.e.* samples) lie in the plane and can be encased by an ellipse. The points vary more along the axis of the ellipse than in the other direction. The first PC describes the direction of the greatest variation in the dataset, which is the major axis of the ellipse. The second PC represents the second largest variation, which is the minor axis of the ellipse. A PCA model with two principle components adequately describes all the

variation in the measurements. Similar to PCA, the method of Hierarchical Clustering Analysis (HCA) uses PCs to illustrate the variation between classes. In this technique, the samples with the smallest distance are found and linked together using a dendogram.

In HCA, the samples with the closest chemical make-up cluster near one another and therefore the smallest distance occurs within these samples, which are linked together. The procedure is repeated for all samples and the results are displayed as a connection dendogram (Figure 1.12). For example, in a data set containing the points 1 through 7 (left image in Figure 1.12) point 4 is related most to point 5. In the dendogram this can be illustrated by the vertical line that connects the 4 to the 5. Point 6 is the nearest neighbor to the points 4 and 5. Therefore, on the dendogram point 6 is connected to the 4^{th} and 5^{th} points. The biggest limitation of PCA and HCA is that that they are two-dimensional techniques that cannot classify data that has a greater within-class variance than between-class variance. Therefore, multi-dimensional multivariate chemometric methods are better for more complex data sets.

Supervised pattern recognition techniques, methods that use pre-established class membership, are multivariate tools that are better suited to study complex data sets. Complex data sets like spectroscopic data have provided the means of attaining better estimates of chemical compositions. These measurements are indirect and rely on the ability to develop a model that relates the dataset of measured variables to the chemical composition of the system (or an unmeasured property of interest). One way of analyzing this type of data is through the development of regression models produced by multivariate regression tools like multiple linear regression (MLR).

MLR is a tool that is useful when one wants to know the relationship between a single outcome variable to two or more explanatory variables simultaneously. For example, MLR can be used to study the effects of explanatory variables (sometimes called independent variables), $x_1, x_2, \ldots, x_k$, on a response variable y. If we take a sample of *n* paintballs, and measure the value of each of the variables on every paintball. The MLR equation that estimates the relationships in the sample population is given by

$$Y = a + b_1 x_1 + b_2 x_2 + ... + b_k x_k \quad (1\text{-}17)$$

The goal of MLR is to create a linear, first-order relationship between the *m* variables $x_j (j = 1 - m)$ and for a variable *y*. Mathematically this can be expressed as follows

$$y = b_1 x_1 + b_2 x_2 + b_3 x_3 + ..b_m x_m + e \quad (1\text{-}18)$$

In the equation above, the x_j are the independent variables and *y* is the dependent variable, the b_j variables are sensitivities, and *e* is the error or residual. From MLR, the method of Principal Component Regression (PCR) was created—a regression analysis that uses PCA when estimating regression coefficients—which led to the invention of Partial Least Squares (PLS), a statistical method similar to PCR that finds a linear regression model by projecting the predicted variable and the measured variable in new space instead of finding hyperplanes of maximum variance between the response and independent variables.[139]

Today PLS is a good alternative to MLR and PCR methods because it is more robust. Robust meaning the model parameters do not change a lot when new calibration samples are withheld from the total samples.[134] A PLS model consists of two

components: a structural part that reflects the relationships between the latent variables and a measurement component (one that illustrates how the latent variables and their indicators—items, manifest variables, or observed measures—are related), and the weight relations that are used to estimate case values for the latent variables.[140] The first component of the PLS model, the unobservable variables, are estimated as exact linear combinations of their empirical indicators[141] PLS treats these estimated proxies as perfect substitutes for the latent variables. [142] The second component of PLS, the weights used to estimate case values, are estimated so that the resulting case values capture most of the variance of the independent variables that is useful for predicting the dependent variable.[143] This is based on the assumption that all measured variance of the variables in the model is useful variance that should be explained.[144] Using this weight component, it is possible to determine a value for each unobservable variable by calculating a weighted average of its indicators. This results in a model in which all unobservable variables are approximated by a set of case values that can be estimated by a set of simple ordinary least squares regressions. To summarize these ideas, first, the weight relations, which link the indicators (i.e. observable measures) to their respective unobservable variables, are estimated. Second, case values for each unobservable variable are calculated based on a weighted average of its indicators, using the weight relations as an input. Finally, these case values are used in a set of regression equations to determine the parameters for the structural relations.[141]

From the explanation of the PLS model, it is apparent that the most important part of a PLS analysis is the estimation of the weight relations. It would be easy to assume equal weights for all indicators, however this approach has two disadvantages:

First, there is no theoretical rationale for all indicators to have the same weighting. This is true because it can be assumed that the resulting parameter estimates of the structural model depend on the type of weighting used, at least as long as the number of indicators is not excessively large [145], the assumption of equal weights makes the results highly arbitrary. Second, such a procedure does not take into account the fact that some indicators may be more reliable than others and should receive higher weights.[146] Consequently, PLS uses more complex, two-step estimation process to determine the weights (ω_i): First, an outside approximation is made, in which case values for each latent variable (e.g. η_i) are estimated based on a weighted average of their respective indicators:

$$\eta_i' = \omega_i y_i + \omega_{i+1} y_{i+1} \qquad (1\text{-}17)$$

where η_2' is the average of the latent variables, ω is the weight and y is the endogenous (i.e. independent) variable. The weights used to calculate this aggregation are determined in a manner similar to a principle-components analysis for reflective or regression analysis for formative indicators.[147] Next, the inside approximation, improved case values are determined as a weighted average of neighboring latent variables:

$$\eta_i'' = \omega_i \eta_i' + w_{i+1}\xi_i + w_{i+2}\xi_{i+1} + w_{i+3}\xi_{i+2} \qquad (1\text{-}18)$$

where ξ is the latent exogenous (independent) variable. The latent exogenous variable is inversely related to the indicators of the exogenous variable (x) relative to the associated measurement error (δ) and the loadings of indicators of exogenous variable (λ_{xi}) factors, which are mathematically related as follows:

$$x_i = \lambda_{xi}\xi_i + \delta_i \qquad (1\text{-}19)$$

Likewise, the similar mathematical expression exists for the indicators of the endogenous variables (y) to its associated measurement error (ε) and the latent endogenous variables (η) and loadings of indicators of endogenous variable (λ_{yi}).

$$y_i = \lambda_{yi}\eta_i + \varepsilon_i \qquad (1\text{-}20)$$

For the case of the weighted variables, there are three different weighting schemes available (centroid, factor, and path weighting scheme[148]), but one can demonstrate that the choice between them has only a minor impact on the final results. Using the factor weighting scheme, the weight relations are modified (e.g. $\eta_i'' = \omega_i y_i + w_{i+1} y_{i+1}$) and the process of inside and outside approximation starts from the beginning again and is repeated until convergence of the case values is achieved.

PLS includes a dependent variable in the data compression and decomposition operations, *i.e.* both y and x data are actively used in the data analysis. Including these factors minimizes the potential of x variables having large error. Although, the concurrent use of x and y data makes the method more complex, the two loading vectors are required to provide orthogonality of the factors.[138] The x variables represent the two-dimensional data set also called the x-block, in the case of spectroscopy it signifies the spectral data of multiple samples. The y variables represent the y-block, which signifies the change in concentration of the data set. Once an x- and y-block are loaded into a PLS model, the relationship between the two can be expressed in a predicted concentration verses measured concentration (Figure 1.13). This regression model like the one shown in Figure 1.8 can allow one to test the linearity of the data set by analyzing parameters

like the correlation coefficient (r). In this example, the linearity between the measured and predicted terms (=95% linearity) was high. This demonstrates the ability of PLS models to express the linearity of spectroscopic data as in the study of Lyng et al. in quantitatively relating high-resolution magic angle proton magnetic resonance spectroscopic (HR ^{1}H MAS MRS) data to apoptotic cell density.[149]

The disadvantage of PLS models is the validation of these predictive models. The big question is whether a model is valid for a particular application.[150] Controversial in model validation is simultaneously testing the y-intercept (at zero) and the slope (at unity) when regressing outputs of a given predictive model on real-system values.[151] The debate about the validity of this test has centered mainly on possible bias in the estimated slope and intercept or on autocorrelated errors in which one variable can be wrongly regressed over the other.[152,153] The validity of this test stems from its conceptual formulation. When outputs of a predictive model agree completely with actual-system values, their corresponding linear regression will have an intercept of zero and a slope of unity. Therefore, the test is evaluating the degree of relationship between actual-world data and model input.[154] Nonetheless, PLS seems to be an integral tool in the analysis of data where univariate techniques like simple Beer-Lambert regression curves fail. PLS is helpful because it is a multivariate tool that can be used to quickly analyze complex mixtures since the simultaneous determination of each component in a mixture can be performed without time-consuming separations and with minimum sample preparation. For this reason it can be used in this study of the measles virus in clinical samples by providing a relationship between the relative intensity of spectral data to the change in viral concentration.

An alternative method of extracting relevant components for classification based on the PLS principle is of maximizing covariance using PLS-DA.[135,136] The fundamentals of PLS-DA consist in the application of a PLS regression model on variables which are indicators of the groups.[136] PLS-DA is mainly used to classify observations from the results of PLS regression on indicator variables. PLS-DA models focus on the variation between classes rather than the variation within the class. PLS-DA searches for factors, also called latent variables, to maximize the variations in the sample data from the x-block (data set) that can be used to predict the class from the y-block. Unlike with PLS, in PLS-DA the y-block is made of *y* variables, enough for each class, that indicate if the samples are in one of the classes by setting the value to 1 if it is in the class and 0 if it is not. A 1 indicates a sample belongs to a class, and a 0 indicates that it does not. The model, of course, will not predict either a 1 or 0 perfectly, so a limit must be set, called the threshold, above which the sample is estimated as a 1 and below which it is estimated as a 0. A threshold value is also calculated for each class prediction model. In Figure 1.14, the circled data, points belonging to Class 1, indicate that the PLS-DA model can confidently classify Class 1 data from the remainder of the data set since the points all lie above the threshold and are near 1 on the y-axis. The primary goal of PLS-DA is to give a calibration model that maximizes the sensitivity and specificity of the training set, where sensitivity is defined as the The sensitivity is defined as the number of predicted samples in a class divided by the actual number of samples in the class and specificity is given as the number of samples predicted not in the class divided by the actual number of samples not in the class. A calibration model with high sensitivity and specificity will most likely predict the class effectively.

In the past, the use of PLS-DA, SERS has been deemed a qualitative methodology. This is the case of the qualitative analysis performed by Hoang et al. in 2005 when four genotypes of the measles virus was classified when applying SERS spectral data to a PLS-DA model. However, SERS has never been used as a quantitative methodology, however it is believed that the application of SERS spectral data to PLS models can provide quantitative data. Using PLS, one can create linear regression curves that will enable them to obtain measured versus predicted measurements for various concentrations of viral samples. The predicted values are most important for analyzing the limit of detection (LOD) of viral samples because they can for lower levels of detection of a particular assay. Since viral shedding of an infected host can be anywhere from 1 to about 10,000 pfu/ml, it is beneficial to have a detection technique that can detect samples at that level. Since Ag nanorod-SERS is an extremely sensitive assay, it is believed that the technique can be used with PLS to determine the limit of detection of measles samples.

1.8 The importance of finding the limit of detection

Current bio-analytical methods show an interest in trace level detection. Such methods are central to public health, medical, and environmental control sectors. The sensitivity of these analytical tools is of importance in such diverse fields as diagnosis of infectious diseases; trace detection of DNA in forensics; bacterial contamination in public water supplies; and viral infection of blood in transfusion services.[155]

With the increased demand for rapid trace detection and high throughput methods, modern bio-analytical techniques are being challenged on their capabilities of analytical

sensitivity. Sensitivity can described as the smallest concentration of target analyte that can be detected and distinguished from a zero result (background).[156] The sensitivity of an assay is dependent upon factors including sampling procedures, presence of competitors and inhibitors, detection methods and other features, which may be unique to different assays.[157]

The sensitivity of a method is associated with the lower limit of applicability of that method.[158] In regards to chemicals, the minimum detectable value frequently refers to the minimum detectable net concentration or amount. The minimum detectable values help one determine the "fitness for purpose" of a certain assay (i.e. measurement process). This value can thus be analyte and assay specific, as it also refers to predicting the detectable value based on the capability of a process.

One of the best reasons for the desire to determine the limit of detection (LOD) is to identify where the method performance becomes insufficient for acceptable detection of the analyte, defining the problematic areas that subsequent analytical measurements should stay away from. The evaluation of the LOD of an assay is essential for trace detection methods, particularly where the result will be used for public health applications.

Finding the LOD of measles viral strains is desired because of the prevalence of cases where vaccinated individuals and ones who have been infected have low levels of viral shedding. This is a limitation even for sensitive viral detection methods like RT-PCR. Likewise, serologic assays for the detection of IgM, in cases with previously vaccinated populations, provide low sensitivity. In previously vaccinated persons who

have become infected, the timing of the IgM reponse may be altered or the response absent or undetectable.[1] Since the laboratory surveillance of the measles virus remains a controversial issue because of the false-positive results[2-4] and lower sensitivity[66] provided by conventional techniques, a more reliable and more sensitive method of detection for low-level samples is desired. The use of SERS with multivariate analytical tools seems to offer the possibility of low-level measles virus detection. The method of SERS, an extension to the vibrational spectroscopic technique Raman spectroscopy, will be discussed later to show how the method can be used to analyze minute volumes of samples like the measles virus in clinical samples. The validation of MV RNA present in the measles samples will be performed via Quantitative Reverse Transcription-Polymerase Chain Reaction (qRT-PCR), or Real Time PCR, which will be further discussed in the next section.

1.9 Real-time Polymerase Chain Reaction.

Polymerase chain reaction (PCR) is a method used to amplify one or more copies of a segment of DNA several orders of magnitude using specific genome- and antigenome-sense primers, usually separated by 200 to 400 nucleotides on the genome of interest for diagnostic reasons. The size of the DNA product is defined by the location of the two primers on the virus genome and non-specific DNA products can sometimes be produced and care is needed when interpreting these results. The genome of all morbilliviruses consists of a single strand of negative sense RNA and therefore cannot be amplified directly by PCR but must first be copied into DNA by reverse transcription in a two-step reaction, reverse-transcription/ polymerase chain reaction (RT-PCR).[60]

Therefore, PCR is a time consuming step. Additionally, the process may be constrained by the need for an adequate amount of input nucleic acids for quantization purposeses.[159]

For the case of this study, quantitative Real Time -PCR (qRT-PCR) will be used to analyze the measles samples. This technique can be performed in a single 96-well plate due to the availability of thermostable DNA polymerases derived from thermophillic bacteria. Within the well plate, samples of the known MV concentration (series of ten-fold dilutions), non-infected samples containing only the reagents and the other MV samples (analyte). The process is done through thermal cycling, a series of heating and cooling the DNA. The cycle begins by heating the DNA to high temperature (94ºC) so as to dissociate the DNA duplex, and then cooling to allow annealing of the primers (37ºC to 50ºC) and finally heating to the optimum temperature (72ºC) for the polymerase to copy new DNA. The cycles are repeated 25 to 35 times (25 cycles is said to increase the initial DNA up to 10^7 times) to produce quantitative data that can be analyzed on a computer program. Applied Biosystems makes a software program that allows one to obtain an amplification plot of the cyclic process. From the amplification plot, one can chose the fluorescence threshold, a constant value amongst the different cycles where the amount of amplified DNA is significant enough to provide accurate quantitative data. The cycle threshold (Ct) is equal to the fluorescence threshold in each cycle, the point where the cycle number (x axis) and rate of change of the relative fluorescence units (y axis) intersect. A linear regression plot of the Ct values verses the RNA quantity (dilution concentration defined by the known samples) is plotted for each sample thereby allowing one to determine the RNA concentration of the unknown samples.

In determining the RNA concentration of the unknown samples we can verify the presence of MV in the measles samples that were purified and applied to our Ag-SERS substrates for viral detection. Therefore, it is assumed that any classification or regression that is achieved through chemometric techniques is valid.

1.10 Summary of Presented Work

Chapter II describes the use of SERS as an identification technique for measles detection. Presented is qualitative data about individual MV strains A1, H, and D4 using Ag-SERS substrates, in conjunction with Partial Least Squares- Discriminant Analysis (PLS-DA), to demonstrate the sensitivity of differentiating between different strains using the SERS method.

Chapter III demonstrates the use of SERS for low-level measles detection. Presented is quantitative data was acquired about on MV strain using Ag-SERS substrates and PLS regression curves to test the possibility of using SERS for low-level virus detection and to determine the limit of detection of MV samples.

Chapter IV includes conclusions on the studies summarized in previous chapters as well as includes area for future research on the quantitative study of the measles virus.

1.11 References

1. Bottomley, L.; Zhao, Y.; Tripp, R.; Dluhy, R., Georgia Research Alliance FY2009 Collaboration Planning Grant. University of Georgia, Georgia Institute of Technology, CDC MMR and Herpesvirus Branch: Athens, Atlanta, 2009; p 21.

2. (a) Riddell, M. A.; Mossa, M. J.; Hauer, D.; Monzec, M.; Griffin, D. E., Slow clearance of measles virus RNA after acute infection. *J of Clin Virol* **2007,** *39*, 312-317; (b) Mancuso, J.; Krauss, M.; Audet, S.; Beeler, J., ELISA underestimates measles antibody seroprevalence in US military recruits. *Vaccine* **2008,** *26* (38), 4877-4878; (c) Jenkerson, S.; Beller, M.; Middaugh, J.; Erdman, D., False positive rubeola IgM tests [letter]. *N Engl J Med* **1995,** *332*, 1103-4.

3. Rota, P.; Bellini, W., Update on the global distribution of genotypes of wild type measles viruses. *J Infect Dis* **2003,** *187 Suppl 1* (10 (2)), S270-6.

4. Carey, P. R., *Biochemical applications of Raman and resonance Raman spectroscopies*. Academic Press: New York, 1982; p 262.

5. (a) Willets, K.; Duyne, R. P. V., *Ann. Rev. Phys. Chem.* **2007,** *58*, 267-297; (b) Aroca, R., in Surface-Enhanced Vibrational Spectroscopy. In *An associated database of almost 5800 references is available at* www.spectroscopynow.com [Online] Wiley: Chichester, 2006; (c) Kneipp, K.; Kneipp, H., *Surface-enhanced Raman Scattering*. Springer-Verlag: Berlin, 2006; p 464.

6. Shanmukh, S.; Jones, L.; Zhao, Y.-P.; Driskell, J. D.; Tripp, R.; Dluhy, R. A., Identification and classification of repiratory syncytial virus (RSV) strains by surface-enhanced Raman Spectroscopy and mulitvariate statistical techniques. *Anal. Bioanal Chem* **2008,** *390*, 1551-1555.

7. Bao, P.-D.; Huang, T.-Q.; Liu, X.-M.; Wu, T.-Q., Surface-enhanced Raman spectroscopy of insect nuclear polyhedrosis virus. *J. Raman Spectrosc* **2001,** *32*, 227.

8. Driskell, J.; Kwarta, K. M.; Lipert, R. J.; Porter, M. D., Low-level detection of viral pathogens by a surface-enhanced Raman scattering based immunoassay. *Anal. Chem* **2005,** *77*, 6147.

9. Abelmann, L.; Lodder, C., Oblique evaporation and surface diffusion. *Thin Solid Films* **1997,** *305*, 1-21.

10. (a) Driskell, J.; Shanmukh, S.; Liu, Y.; Chaney, S. B.; Tang, X.-J.; Zhao, Y.-P.; Dluhy, R. A., The Use of Aligned Silver Nanorod Arrays Prepared by Oblique Angle Deposition as Surface Enhanced Raman Scattering Substrates. *J. Phys. Chem. C* **2008,** *112*, 895-901; (b) Chaney, S. B.; Shanmukh, S.; Dluhy, R. A.; Zhao, Y.-P., Aligned silver nanorod arrays produce high sensitivity surface Raman spectroscopy substrates. *Appl. Phys. Lett.* **2005,** *87* (3), 31908.

11. Shanmukh, S.; Jones, L.; Driskell, J.; Zhao, Y. P.; Dluhy, R.; Tripp, R., Rapid and sensitive detection of respiratory virus molecular signatres using a silver nanorod array SERS substrate. *Nano Lett.* **2006,** *6* (11), 2630-2636.

12. Brereton, R. G., *Chemometrics: Data Analysis for the Laboratory and Chemical Plant.* . John Wiley & Sons Ltd.: Chichester, 2003; p 489.

13. Hoang, V. Detection and Classification of Measles Virus By Surface-Enhanced Raman Scattering (SERS) Spectroscopy and Fourier Transform Infrared (FTIR) Spectroscopy. Univ of GA, Athens, 2008.

14. Fraser, K., *Measles virus and its biology*. Academic Press: London, New York, 1978; p 249.

15. Panum, P., Observations made during the epidemic of measles on the Faroe Islands in the year 1846. *Medical Classics* **1938,** *3*, 829-886.

16. (a) Cherry, J.; Feigin, R. D.; P.G. Shackelford; Hinthorn, D. R.; Schmidt, R. R., A clinical and serologic study of 103 children with measles vaccine failure. *J. Pediatri* **1973,** *82*, 802-808; (b) Edmonson, M. B.; Addiss, D. G.; McPherson, J. T.; Berg, J. L.; Circo, S. R.; Davis, J. P., Mild measles and secondary vaccine failure during a sustained outbreak in a highly vaccinated population. *JAMA* **1990,** *263*, 2467-2471; (c) Mathias, R. G.; Meekison, W. G.; Arcand, T. A.; Schechter, M. T., The role of secondary vaccine failure in measles outbreaks. *Am. J. Public Health* **1989,** *79*, 475-478; (d) Ozanne, G.; d'Halewyn, M. A., Preformance and reliability of the Enzygnost Measles enzyme-linked immmunosorbent assay for detection of measles virus-specific immunoglobulin M antibody during a large measles epidemic. *J. Clin. Microbiol.* **1992,** *30*, 564-569.

17. McNeill, W., *Plagues and Peoples*. Anchor Press/Doubleday: Garden City, New York, 1976.

18. Rhazes, A.-B., *Treatise on the Smallpox and Measles*. J Brindley: London, 1748.

19. Rolleston, J., *The History of the Acute Exanthemata*. William Heinemann: London, 1937.

20. Black, F., Why did they die? *Science* **1975,** *258*, 1739-1740.

21. Lucas, J., An account of unknown symptoms succeeding the measles; wth additional remarks on the infection of measles and smallpox. *London Med J* **1790,** *11*, 325-331.

22. Von Pirquest, C., Verhalten der kutanen tuberkulin-reaktion wahrend der Masern. *Deutsch Med Wochesnschr* **1908,** *35*, 1297-1300.

23. Tellez-Nagel, I., Subacute sclerosing leukoencephalitis: ultrastructure of intranuclear and intracytoplasmic inclusions. *Science* **1966,** *154*, 899-901.

24. Connolly, J.; Allen, I.; Hurwitz, L., et al., Measles virus antibody and antigen in subacute sclerosing panencephalitis. *Lancet* **1967,** *1*, 542-544.

25. Ender, J.; Peebles, T., Propagation in tissue cultures of cytopathic agents from patients agents from patients with measles. *Proc. Soc. Exp. Biol. Med.* **1954,** *86*, 277-286.

26. Smaron, M.; Saxon, E.; Wood, L., et al., Diagnosis of measles by fluorescent antibody and culture of nasopharyngeal secreations. *J Virol Methods* **1991,** *33*, 223-229.

27. Kobune, F.; Sakata, H.; Sugiura, A., Marmoset lymphoblastoid cells as a sensitive host for isolation of measles virus. *J Virol* **1990,** *1990* (64).

28. Ono, N.; Tatsuo, H.; Hidaka, Y., et al. , Measles viruses on throat swabs from measles patients use signaling lymphocytic activation molecule (CDw150) but not CD46 as a cellular receptor. *J Virol* **2001,** *75*, 4399-4401.

29. Norrby, E.; Enders-Ruckle, G.; ter Meulen, V., differences in teh appearance of antibodies to structural compoents of measles virus after immunization with inactivated and live virus. *J. Infect Dis* **1975,** *232*, 262-269.

30. Albrecht, P.; Herrmann, K.; Burns, G., Role of virus strain in conventional and enhanced measles plaque neutralization test. *J. Virol Methods* **1981,** *3*, 251-260.

31. Knipe, D. M., Measles Virus. In *Fields' Virology*, 5 ed.; Howley, P. M.; Griffin, D. E.; Lamb, R.; Martin, M., Eds. Lippincott Williams & Wilkins: Philadelphia, 2007; Vol. 1.

32. Longhi, S., Nucleocapsid Structure and Function. In *Current Topics in Microbiology and Immunology* Springer Berlin Heidelberg: 2009; Vol. 329, pp 103-128.

33. Klingele, M.; MHartter, H.; Adu, F., et al., Resistance of recent mealses virus wild-type isolates to antibody-mediated neutralization by vaccinees with antibody *J Med Virol* **2000,** *62*, 91-98.

34. (a) Rima, B.; Earle, J.; Baczko, K., et al. , Sequence divergence of measles virus haemagglutinin during natural evolution and adaptation to cell culture. *J. Gen. Virol* **1997,** *78*, 97-106; (b) Rota, J.; Hummel, K.; Rota, P., et al., Genetic variability of the glycoprotein genes of current wild-type measles isolates. *Virology* **1992,** *188*, 135-142.

35. (a) Giraudon, P.; Jacquier, M.; Wild, T., Antigenic analysis of African measles virus field isolates: identification and location of one conserved and two variable epitope sites on the NP protein. *Virus Res* **1988,** *18*, 137-152; (b) Sheshberadaran, H.; Norrby, E., Characterization of epitopes on the measles virus hemagglutinin. *Virology* **1986,** *152*, 58-65; (c) Tamin, A.; Rota, P.; Wang, Z.-D., et al, Antigenic analysis of current wild type and vaccine strains of measles virus. *J Infect Dis* **1994,** *170*, 795-801.

36. Buckland, R.; Giraudon, P.; Wild, F., Expression of measles virus nucleoprotiein in *Escherichia coli*: Use of deletion mutants to locate the antigenic sites. *J Gen Virol* **1989,** *70*, 435-441.

37. Robbie, K.; Brett, M., *J. Vac. Sci. Technol. A* **1997,** *15*, 1460.

38. Riddell, M.; Rota, J.; Rota, P., Review of the temporal and geographical distibution of measles virus genotypes in the prevaccine and postvaccine eras. . *J. Virol* **2005,** *2*, 87.

39. WHO, Nomenclature for describing the genetic characteristics of wild-type measles (update). . *Part I. World Health Organization Weekely Epidemiological Record* **2001,** *76*, 242-247.

40. (a) Mulders, M.; Truong, A.; Muller, C., Monitoring of measles elimination using molecular epidemiology. *Vaccine* **2001,** *19*, 2245-2249; (b) Rota, J.; Bellini, W.; Rota, P., *In: Thompson RCA*. Molecular epidemiology of infectious diseases ed.; Kluwer Academic/ Lippincott Raven Publishers: London, 2000; Vol. 168, p 80.25; (c) Bellini, W.; Rota, P., Genetic diversity of wild-type measles viruses: implications for global measles elimination programs. *Emerg Infect Dis* **1998,** *4*, 1-7; (d) Rota, J.; Heath, J.; Rota, P., Molecular epidemiology of measles virus: identification of pathways of transmission and the implicaitons for measles elimination. *J Infect Dis* **1996,** *173*, 32-37; (e) Rima, B.; JAP, E.; Baczko, K., Measles virus strain variations. *Curr top Microbiol Immnol* **1995,** *191*, 65-84; (f) Rota, P.; Rota, J.; Bellini, W., Molecular epidemiology of measles virus. *Semin Virol* **1995,** *6*, 379-386.

41. Clements, C.; Strassburg, M.; Cutts, F., The epidemiology of measles. *World Health Stat Q* **1992,** *45*, 285-91.

42. Venczel, L.; Rota, J.; Dietz, V.; Morris-Glasgow, V.; Siqueira, M.; Quirogz, E.; Rey, G.; Quadros, C. d., The Measles Laboratory Network in the Region of the Americas. *J Infect Dis* **2003,** *187 (Suppl 1)*, S140-S145.

43. Pan American Health Organization, Measles eradication: field guide. PAHO: Washington, DC, 1999; p 41 (PAHO technical paper).

44. Anderson, J.; Barrett, T.; Scott, G. R., *Manual on the diagnosis of rinderpest*.

45. Bernd Kochanowski, U. R., *Quantitative PCR Protocols*. Humana Press: New Jersey, 1999.

46. Morfina, F.; Beguin, M.; Lina, B.; Thouvenot, D., Detection of measles vaccine in the throat of a vaccinated child. *Vaccine* **2002,** *20* (11-12), 1541-1543.

47. (a) Helfand, R.; Kebede, S.; Alexander, J., Comparative detection of measles-specfic IgM in oral fluid and serum from children by an antibody-capture IgM EIA. *J. Infect Dis* **1996,** *173*, 1470-4; (b) Lieven, A.; Burunell, P., Specific immunoglobulin M enzyme-linked immunosorbent assay for confirming the diagnosis of measles. *J. Clin. Microbiol.* **1986,** *24*, 391-4; (c) Onzanne, G.; Halewyn, M., Performance and reliability of the Enzygnost measles enzyme-linked immuno-sorbent assay for detection of measles virus-specific immunoglobulin M antibody during a large measles epidemic. *J. Clin. Microbiol.* **1992,** *30*, 564-9.

48. Helfand, R.; Heath, J.; Anderson, L., Diagnosis of measles with an IgM capture EIA: the optimal timing of specimen collection after rash onset. *J. Infect Dis* **1997,** *175* (1), 195-9.

49. Scheld, W. M., *Infections of the Central Nervous Systems* 3ed.; Lippincott Williams & Wilkins: Philadelphia, 2004.

50. Dietz, V.; Rota, J.; Izurieta, H.; Carrasco, P.; Bellini, W., The laboratory confirmation of suspected measles cases in settings of low measles transmisison: conclusions from the experience in teh Americas. *Bull World Health Organ* **2004,** *82*, 852.

51. (a) Pelletier, M. J., Raman Monochromators and Polychromators. In *Handbook of Vibrational Spectroscopy*, John Wiley & Sons: Chichester, 2002; pp 467- 481; (b) McCreery, R. L., Dispersive Raman Spectrometer. In *Raman Spectroscopy for Chemical Analysis*, John Wiley & Sons: New York, 2000; pp 155-171.

52. Ingle, J. D.; Crouch, S. R., *Spectrochemical Analysis*. Prentice Hall: Englewood Cliffs, NJ, 1988.

53. Pommier, C. J.; Walton, L. K.; Ridder, T. D.; Denton, M. B., Array Detectors for Raman Spectroscopy. In *Handbook of Vibrational Spectroscopy*, Ingle, J. D.; Crouch, S. R., Eds. Chichester, 2002; Vol. 1, pp 507-521.

54. Baldwin, K. J.; Batchelder, D. N.; Webster, S., Raman Microscopy: Confocal and Scanning Near Field. In *Handbook of Raman Spectroscopy: From the Research Laboratory to the Process Line*, Dekker, M., Ed. I.R. Lewis H.G.M. Edwards: New York, 2001.

55. Treado, P. J.; Nelson, M. P., Raman Imaging. In *Handbook of Vibrational Spectroscopy*, John Wiley & Sons: 2002.

56. Tian, Z.; Ren, B.; Wu, D., Surface-Enhanced Raman Scattering: From Noble to Transition Metals and from Rough Surfaces to Ordered Nanostructures. *J. Phys. Chem. B* **2002,** *106* (37), 9463-9483.

57. (a) Vo-Dihn, T., Surface-enhanced Raman spectroscopy using metallic nanostructures. *Trac-Trends* **1998,** *17*, 557-582; (b) Ferraro, J. R.; Nakamoto, K.; Brown, C. W., *Introductory Raman Spectroscopy*. 2 ed.; Academic Press: 2003.

58. Kneipp, K.; Kneipp, H.; Itzkan, I.; Dasari, R. R.; Feld, M. S., Surface-enhanced Raman scattering and biophysics. *J. Phys. : Condens. Matter* **2002,** *14*, R597-R624.

59. (a) Patel, I.; Premarsiri, W.; Moir, D.; Ziegler, L., Barcoding bacterial cells: a SERS-based methodology for pathogen identification *J. Raman Spectrosc* **2008,** *39*, 1660-1672; (b) Driskell, J.; Shanmukhy, S.; Liu, Y.; Hennigan, S.; Jones, L., Infectious agent detection with SERS-active silver nanorod arrays prepared by oblique angle deposition. *IEEE Sensors Journal* **2008,** *8*, 863-870.

60. Driskell, J. e. a., Rapid and Sensitive Detection of Rotavirus Molecular Signatures Using Surface Enhanced Raman Spectrscopy. *PLoS ONE* **2010,** *5* (4), 1-9.

61. (a) Michaels, A. M.; Nirmal, M.; Brus, L. E., Surface-enhanced Raman spectroscopy of individual rhodamine 6G molecules on large Ag nanocrystals. *J. Am. Chem. Soc.* **1999,** *121*, 9932-9939; (b) Ethchegoin, P. e. a., A novel amplification mechanism for surface enhanced Raman scattering. *Chem Phys Lett* **366,** *366*, 115-121; (c) Otto, A.; Mrozek, I.; Grabhorn, H.; Akemann, W., Surface-enhanced Raman scattering. *J. Phys. : Condens. Matter* **1992,** *4*, 1143-1212; (d) Otto, A., On the electronic contribution to single molecule surface enhanced Raman spectroscopy. *Indian J. Phys.* **2003,** *77B*, 63-73.

62. Hossain, M. K.; Ozaki, Y., Surface-enhanced Raman scattering: facts and inline trends. *Current Science* **2009,** *97* (2), 192-201.

63. (a) Zeman, E. J.; Schatz, G. C., An accurate electromagnetic theory study of surface enhancement factors for silver, gold, copper, lithium, sodium, aluminum, gallium, indium, zinc, and cadmium. *J. Phys. Chem.* **1987,** *91*, 634-643; (b) Moskovitis, M., Surface roughness and the enhanced intensity of Raman scattering by molecules adsorbed on metals. *J. Chem. Phys.* **1978,** *69*, 4159-4161; (c) Haynes, C.; Van Duyne, R., Nanosphere lithography: a versatile nanofabrication tool for studies of size-dependent nanoparticle optics. *J. Phys. Chem. B.* **105,** *105*, 5599-611; (d) Sherry, L.; Chang, S.; Shatz, G.; van Duyne, R. P.; Wiley, B.; Xia, Y., Localized surface plasmon resonance spectroscopy of single silver nanocubes. *Nano Lett.* **2005,** *5*, 2034-38.

64. (a) McFarland, A.; van Duyne, R. P., Single silver nanoparticles as real-time optical sensors with zeptomole sensitivity. *Nano Lett.* **2003,** *3*, 1057-62; (b) Haes, A.;

Haynes, C.; McFarland, A.; Zou, S.; Schatz, G. C.; van Duyne, R. P., Plasmonic materials for surface-enhanced sensing and spectroscopy. *MRS Bull.* **2005,** *30*, 368-75; (c) Haes, A.; van Duyne, R. P., A unified view of propagating and localized surface plasmon resonance biosensors. *Anal Bioanal Chem* **2004,** *379*, 920-30; (d) Miller, M.; Lazarides, A., Sensitivity of metal nanoparticles surface plasmon resonance to the dielectric environment. *J. Phys. Chem. B* **2005,** *109*, 21556-65; (e) Mock, J.; Barbic, M.; Smith, M.; Schultz, D.; Schultz, S., Shape effects in plasmon resonance of individual colloidal silver nanoparticles. *J. Chem. Phys.* **2002,** *116*, 6755-59; (f) Haynes, C.; McFarland, A.; Smith, M.; Hulteen, J.; van Duyne, R. P., Angle-resolved nanosphere lithography: manipulation of nanoparticle size, shape, and interparticle spacing. *J. Phys. Chem. B* **2002,** *106*, 1898-902.

65. (a) Schatz, G. C.; Young, M. A.; van Duyne, R. P., Electromagnetic mechanism of SERS. . In *Surface-Enhanced Raman Scattering: Physics and Applications*, Kneipp, K.; Kneipp, H.; Moskovitis, M., Eds. Springer-Verlag: Berlin, 2006; (b) Kelly, K.; Coronado, E.; Zhao, L.; Schatz, G., The optical properties of metal nanoparticles: the influence of size, shape, and dielectric environment. *J. Chem. Phys. B.* **2003,** *107*, 668-77.

66. Link, S.; El-Sayed, M. A., Spectral properties and relaxation dynamics of surface plasmon electronic oscillations in gold and silver nano-dots and nano-rods. *J. Phys. Chem. B* **1999,** *103*, 8410-26.

67. (a) Draine, B.; Flatau, P., Discrete-dipole approximation for scattering calculations. *J. Opt. Soc. Amer* **1994,** *11*, 1491-99; (b) Jensen, T.; Kelly, K.; Lazarides, A.; Schatz, G. C., Electrodynamics of noble metal nanoparticles and nanoparticle

clusters. *J. Cluster Sci* **1999,** *10*, 295-317; (c) Yang, W.; Schatz, G. C.; van Duyne, R. P., Discrete dipole approximation for calculating extinction and Raman intensities for small particles with arbitrary shapes. *J. Chem. Phys.* **1995,** *103*, 869-75; (d) Novotny, L.; Bian, R.; Xie, X., Theory of nanometric optical tweezers. *Phys. Rev. Lett.* **1997,** *79*, 645-48; (e) Bian, R.; Dunn, R.; Xie, X.; Leung, P., Single molecule emission characteristics in near-field microscopy. *Phys. Rev. Lett.* **1995,** *75*, 4772-75; (f) Taflove, A., *Computational Electrodynamics: The Finite-Difference Time Domain Method*. Artech House: Boston 1995.

68. (a) Jung, L.; Campbell, C.; Chinowsky, T.; Mar, M.; Yee, S., Quantitative interpretation of the response of surface plasmon resonance sensors to adsorbed films. *Langmuir* **1998,** *14*, 36-48; (b) Haes, A.; van Duyne, R. P., A nanoscale optical biosensor: sensitivity and selectivity of an approach based on the localized surface plasmon resonance of triangular silver nanoparticles. *J. Am. Chem. Soc.* **2002,** *124*, 10596-604.

69. Zhang, X.; Hicks, E.; Zhao, J.; Schatz, G. C.; van Duyne, R. P., Electrochemical tuning of silver nanoparticles fabricated by nanosphere lithography. *Nano Lett.* **2005,** *5*, 1503-7.

70. (a) Green, M.; Liu, F.; Cohen, L.; Kollensperger, P.; Cass, T., SERS platforms for high density DNA arrays. *Faraday* **2006,** *132*, 269-280; (b) Kattumuri, V.; Chandrasekhar, M.; Guha, S., Agarose-stabilized gold nanoparticles for surface-ehanced Raman spectroscopic detection of DNA nucleosides. *Appl. Phys. Lett.* **2006,** *88* (15); (c) Kneipp, K.; Flemming, J., *J. Mol. Struct.* **1986,** *145*, 173-179; (d) Koglin, E.; Sequaris, J. M.; Valenta, P., *J. Mol. Struct.* **1982,** *79*, 185-189; (e) Nabiev, I.; Sokolov, K.; Voloshin,

O., *J. Raman Spectroscopy* **1982,** *21*, 333-336; (f) Otto, C.; van de Tweel, T.; de Mul, F.; Greve, J., Surface-enhanced Raman spectroscopy of DNA bases. *J. Raman Spectroscopy* **1986,** *17* (3), 289-298; (g) Thornton, J.; Force, R., *Appl. Spec.* **1991,** *45*, 1522-1526; (h) Suh, J.; Moskovits, M., *J. Am. Chem. Soc.* **1986,** *108*, 4711-4718.

71. Vo-Dinh, T.; Hiromoto, M.; Begun, G.; Moody, R., *Anal Chem* **1984,** *56*.

72. (a) Nikoobakht, B.; El-Sayed, M., *J. Phys. Chem. A* **2003,** *107*, 3372; (b) Tao, A.; Kim, F.; Hess, C.; Goldberger, J.; He, R.; Sun, Y.; Xia, Y.; Yang, P., *Nano Lett.* **2004,** *3* (1229).

73. (a) Sauer, G.; Brehm, G.; Schneider, S.; Graener, H.; Seifert, G.; Nielsch, K.; Choi, J.; Goring, P.; Gosele, U.; Micleas, P.; Wehrspohn, R., *J. Appl. Phys* **2005,** *97*, 024308; (b) Moskovits, M.; Jeong, D., *Chem. Phys. Lett.* **2004,** *397*, 91; (c) Yao, J.; Pan, G.; Xue, K.; Wu, D.; Ren, B.; Sun, D.; Tang, J.; Xu, X.; Tian, Z., *Pur Appl. Chem.* **2000,** *72*, 221.

74. Haynes, C.; Van Duyne, R., *J. Phys. Chem. B* **2001,** *105*, 5599.

75. Felidj, N.; Aubard, J.; Levi, G.; Krenn, J.; Hohenau, A.; Schider, G.; Leitner, A.; Aussenegg, F., *Appl. Phys. Lett.* **2003,** *82*, 3095.

76. Robbie, K.; Sit, J.; Brett, M., *J. Vac. Sci. Technol. A* **1998,** *16* (1115).

77. Abelmann, L.; Lodder, C., *Thin Solid Films* **1997,** *305*, 1.

78. Zhao, Y.-P.; Ye, D.-X.; Wang, G.-C.; Lu, T.-M., *Nano Lett.* **2002,** *2*, 351.

79. Kemsley, E.; Ruault, S.; Wilson, R., Discrimination between Coffea arabica and Coffea canephora variant robusta beans using infrared spectroscopy *Food Chem.* **1995,** *54*, 321-326.

80. Frank, I. E.; Friedman, J. H., A Statistical View of Some Chemometrics Regression Tools. *Technometrics* **1993,** *35* (2), 109.

81. (a) Chevallier, S.; Bertrand, D.; Kohler, A.; Courcoux, P., Application of PLS-DA in multivariate image analysis. *J. Chemom.* **2006,** *20*, 221-229; (b) Tran, T.; Wehrens, R.; Buydens, L., Clustering multispectral images: a tutorial. *Chemometrics Intell. Lab. Syst.* **2005,** *77*, 3-17.

82. Maggio, R.; Cerretani, L.; Chiavaro, E.; Kaufman, T.; Bendini, A., A Novel Chemometric Strategy for the Estimation of Extra Virgin Olive Oil Adulteration With Edible Oils. *Food Control* **2010,** *21* (6), 890-895.

83. (a) Martens, H.; Naes, T., *Multivariate calibration* Wiley: Chichester, 1989; (b) Geladi, P.; Kowalski, B. R., Partial Least-Squares Regression: A Tutorial. *Anal Chimica Acta* **1986,** *185*, 1-17.

84. (a) Nocairi, H.; Qannari, E.; Vigneau, E.; Bertrand, D., Discrimination on latent components with respect to patterns. Application to multicollinear data. *Comput. Stat. Data Anal.* **2005,** *48*, 139-147; (b) Baker, M.; Rayens, W., Partial least squares for discrimination. *J. Chemom.* **2003,** *17*, 166-173.

85. Wise, B. M.; Shaver, J. M.; Gallagher, N. B.; Windig, W.; Bro, R.; Koch, R. S., PLS Manual Toolbox 4.0 to use with MatLab. Eigenvector Research, Inc.: 2006.

86. Adams, M., *Chemometrics in analytical spectroscopy*. 2 ed.; The Royal Society of Chemistry: Cambridege, 2004.

87. Kramer, R., *Chemometric Techniques for Quantitative Analysis* 1ed.; CRC Press: New York, 1998.

88. Chin, W. W.; Newsted, P. R., Structural equation modelling analysis with small samples using partial least squares. . In *Statistical strategies for small sample research*, Hoyle, R. H., Ed. Sage: Thousand Oaks, CA, 1999; pp 307–341.

89. Fornell, C.; Bookstein, F. L., Two structural equation models: LISREL and PLS applied to

consumer exit-voice theory. *Journal of Marketing Research* **1982,** *19*, 440–45.

90. Dijkstra, T., Some comments on maximum likelihood and partial least squares methods. *Journal of Econometrics* **1983,** *22,* , 67-90.

91. Garthwaite, P. H., An interpretation of partial least squares. *Journal of the American Statistical Association* **1994,** *89* (425), 122–127.

92. Chin, W. W.; Marcolin, B. L.; Newsted, P. R., A partial least squares latent variable modelling approach for measuring interaction effects: Results from a Monte Carlo simulation study and voice mail emotion/adoption study. In *The 17th International Conference on Information Systems,*, Cleveland, OH, 1996.

93. McDonald, R. P., Path analysis with composite variables. *Multivariate Behavioral Research* **1996,** *31*, 239–270.

94. Chin, W. W.; Marcolin, B. L.; Newsted, P. R., A partial least squares latent variable modelling

approach for measuring interaction effects: Results from a Monte Carlo simulation study and an

electronic-mail emotion/adoption study. . *Information Systems Research* **2003,** *14*, 189–217.

95. Cassel, C. M.; Hackl, P.; Westlund, A. H., Robustness of partial least-squares method for estimating

latent variable quality structures. *Journal of Applied Statistics* **1999,** *26*, 435–446.

96. Lohmöller, J.-B., *Latent variable path modelling with partial least squares*. Physica Verlag: Heidelberg, Germany, 1989.

97. Lyng et al., *BMC Cancer* **2007,** *7* (11).

98. Haenlein, M.; Kaplan, A. M., A Begineer's Guide to Partial Least Squares Analysis. *Understanding Statistics* **2004,** *3* (4), 283-297.

99. Blackie, M. J.; Dent, J. B., *Systems Simulation in Agriculture*. Elsevier Science & Technology: London, 1979.

100. (a) Harrison, S., Regression of a model on real-system output: an invalid test of model validity. *Agric. Syst.* **1990,** *34*, 183-190; (b) Mayer, D.; Stuart, M.; Swain, A., Regressoin of real-world data on model output: an appropriate overall test of validity. *Agric. Syst.* **1994,** *45*, 93-104.

101. Analla, M., Model Validation Through the Linear Regression Fit to Actual Versus Predicted Values. *Agric. Syst.* **1998,** *57*, 115-119.

102. Burns, M.; Valdivia, H., Modelling the limit of dectection in real-time quantitative PCR. *Eur Food Res Technol* **2008,** *226*, 1513-1524.

103. Saunders, G.; Parkes, H., (eds), *Analytical molecular biology: quality and validation*. RSC: Cambridge, 1999.

104. Foy, C.; Parkes, H., Emerging homogenous DNA-based technologies in the clinical laboratory. *Clin Chem* **2001,** *47*, 990-1000.

105. McNaught, A.; Wilkinson, A., *Compendium of chemical terminology--IUPAC Recommendations*. Blackwell: Amsterdam, 1997.

106. Kochanowski, B.; Reischl, U., *Quantitative PCR Protocols*. Humana Press: New Jersey, 1999.

107. Takeda, M., Measles virus breaks through epithelial cell barriers to achieve transmission. *The Journal of Clinical Investigation* **2008,** *118* (7), 2386-9.

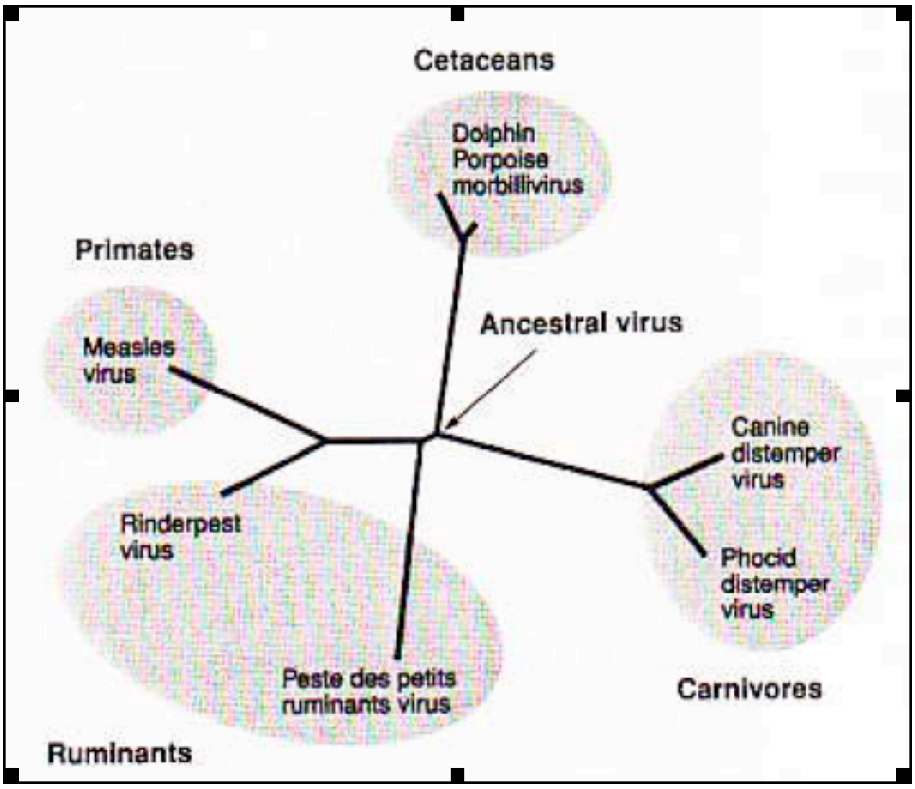

Figure 1.1 Genetic relationships between morbilliviruses based on comparison of the nucleotide sequences of the N genes. The branch lengths are proportional to the mutational differences between the viruses and the hypothetical common ancestor that existed at the nodes in the tree.[39]

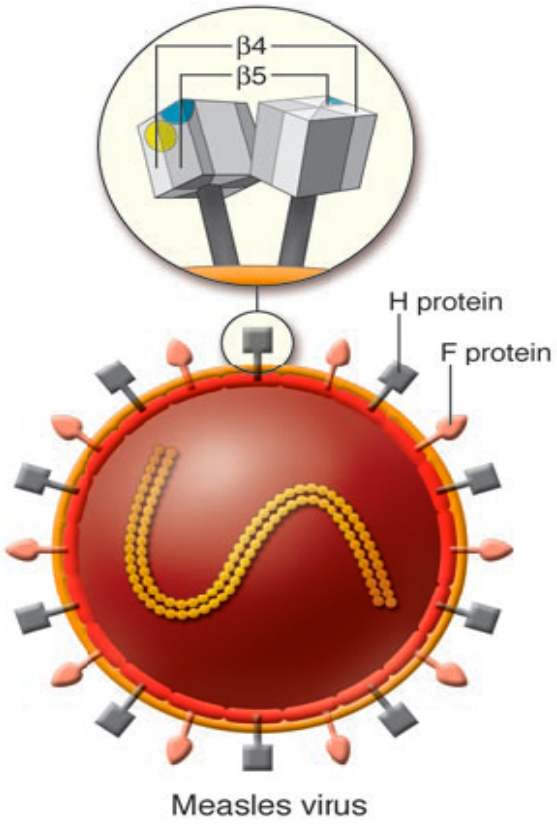

Figure 1.2 Schematic of the MV particle (diameter ~120-250nm) and its receptor-binding H protein. MV is an enveloped virus and possesses 2 types of glycoprotein spikes, designated H and F proteins. The F protein mediates membrane fusion between the viral envelope and the host cell plasma membrane, while the H protein that forms homodimers on the viral envelope is responsible for binding of virus to receptors on target cells. The head domain of the H protein exhibits a six-bladed b-propeller fold.[160]

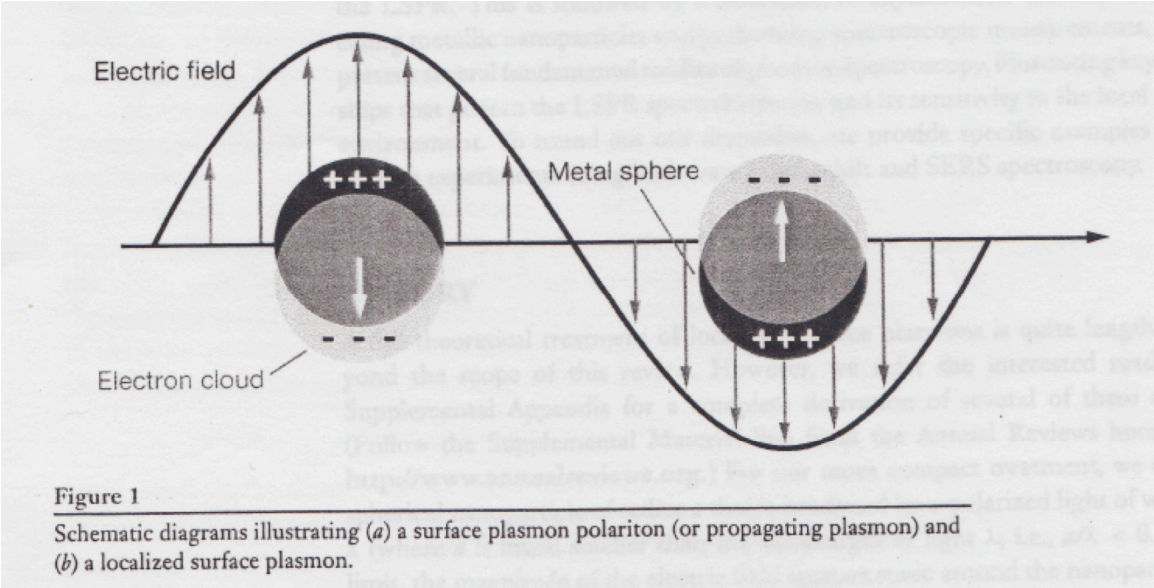

Figure 1

Schematic diagrams illustrating (*a*) a surface plasmon polariton (or propagating plasmon) and (*b*) a localized surface plasmon.

Figure 1.3 Schematic diagrams illustrating a localized surface plasmon. The metal sphere is surrounded by an electron cloud (surface plasmons) all within an electric field.[90]

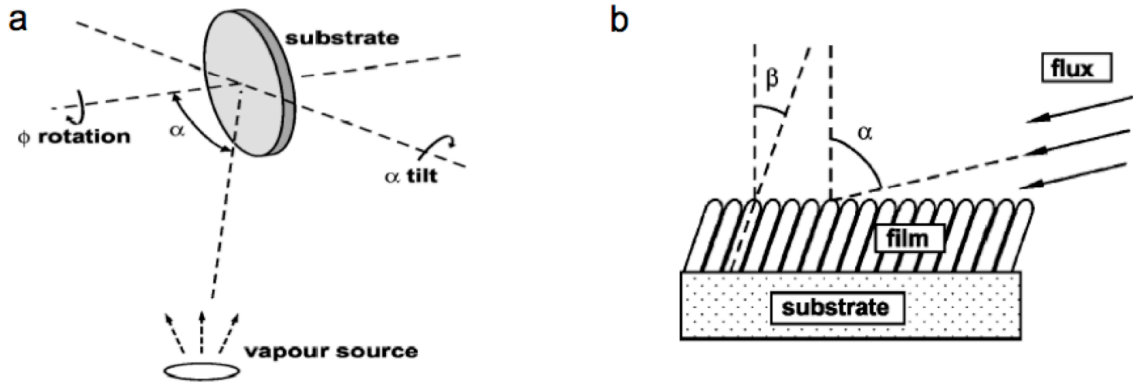

Figure 1.4 The method of Oblique Angle Deposition for the creation of silver nanorods array substrates involves (a) positioning of a solid substrate at a specific angle, θ, such that the vapor from the source is incident on the substrate close to the grazing angle, α. The method creates silver rods that are at an angle, β, normal to the substrate surface and where the flux angle, α, or the angle of the plume that impacts the surface is nearly 86°.[13]

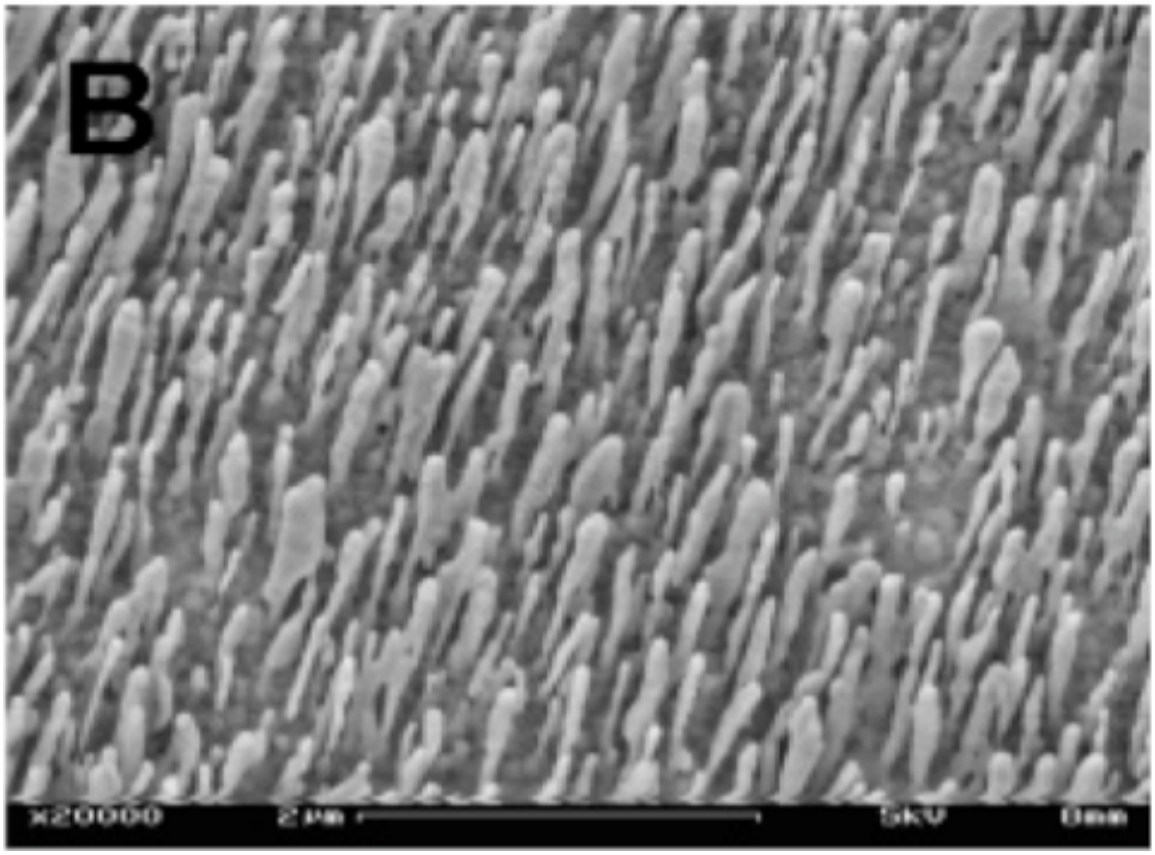

Figure 1.5 Representing a scanning electron micrograph of the Ag nanorod arrays deposited with average lengths of 860 ± 5 nm, a typical SERS substrate used for virus detection. [15]

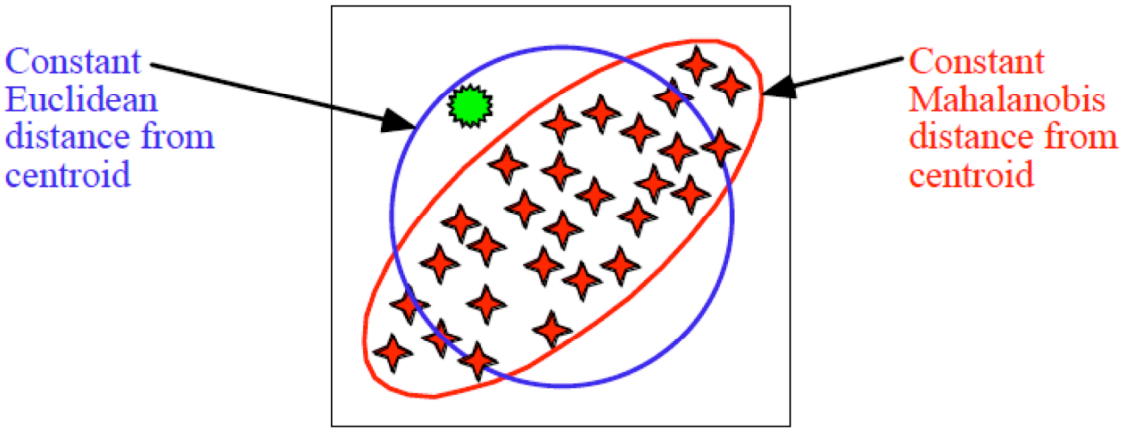

Figure 1.6 Contrast between Mahalanobis and Euclidean distance measures. This illustration shows a data set (the stars) with lines representing constant Euclidean and Mahalanobis distances from the centroid. If these lines represented class boundaries, the data point shown as the sun would be clearly outside the Mahalanobis line, but would be inside a Euclidean distance line (especially if it were expanded to encompass all the data points). [137]

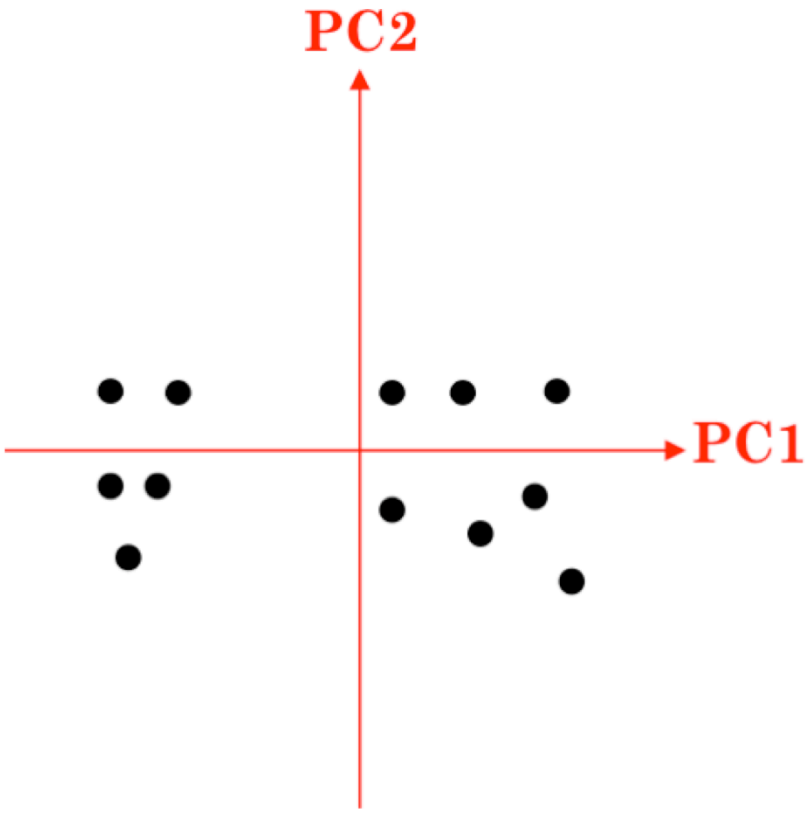

Figure 1.7 A PCA model expressed as orthogonal basis vectors called principle components where the spectra of a data set is repressed by a point in the PCA model.

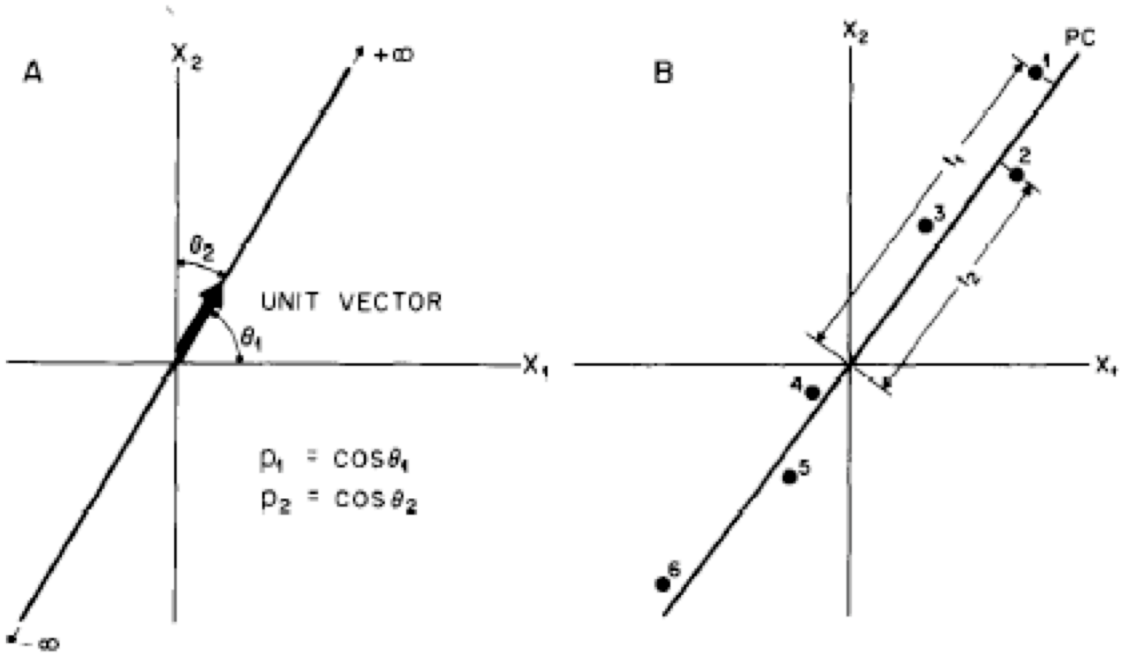

Figure 1.8 A principle component in the form of two variables: (A) loadings are the angle cosines of the direction vector; (B) scores are the projections of the sample points (1-6) on the principal component direction. Note that the data are mean-centered.[134]

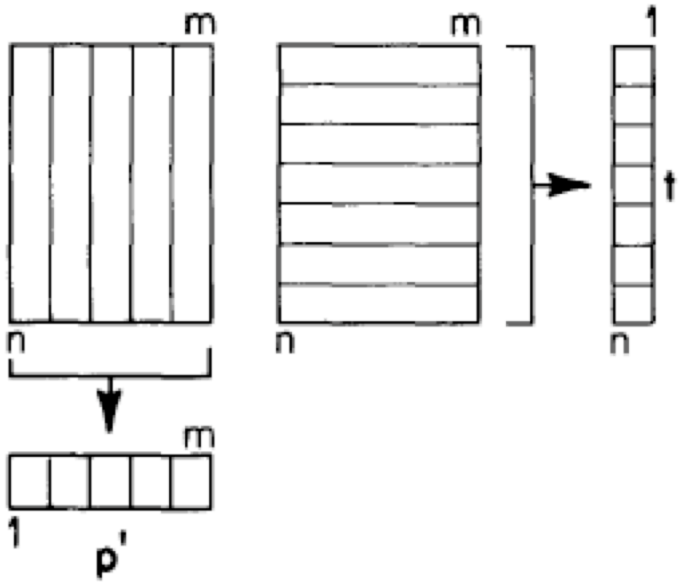

Figure 1.9 Scores and loadings are obtained by projecting X into vectors. Each column of X, loadings, are projected into an element of the vector p, whereas the scores, each row of X, is projected into an element of the vector t.[134]

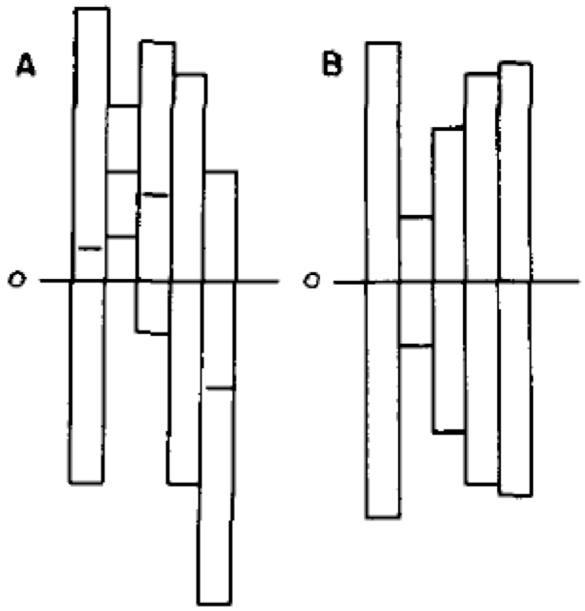

Figure 1.10 Data preprocessing. The data for each variable are represented by a variance bar and its center. (A) Most raw data look like this. (B) The result after mean-centering only. [134]

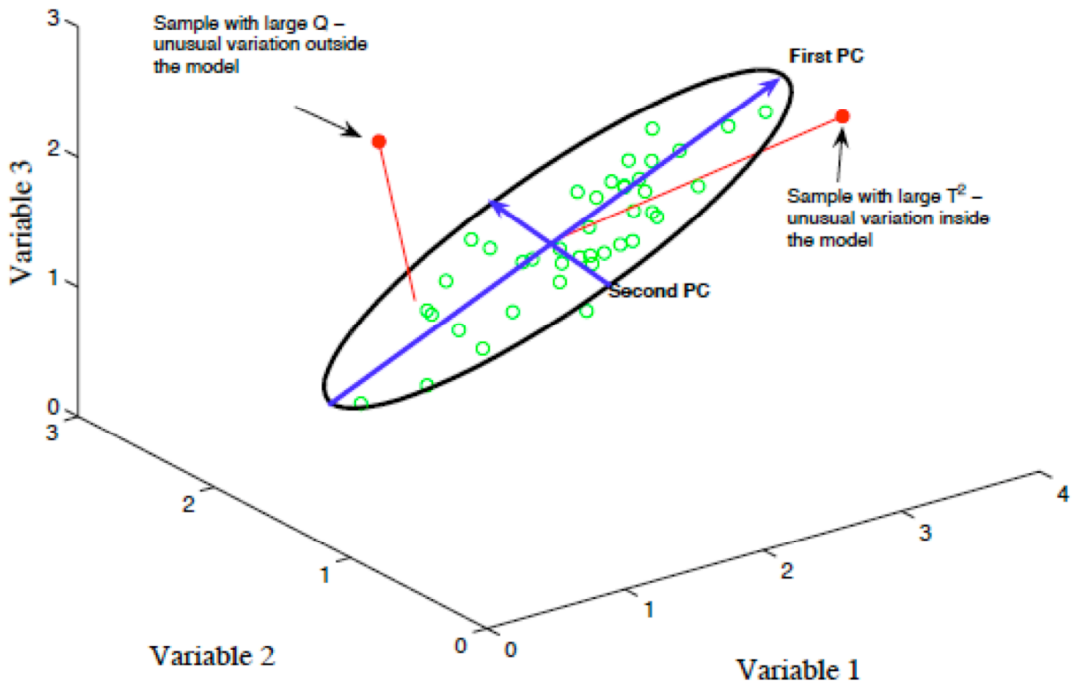

Figure 1.11 Graphical representation of Principal Components Analysis. Shown here are the values of three variables measured on a collection of samples. When plotted in three dimensions, it is apparent that the samples all lie on a plane and can be enclosed by an 101 ellipse. It is also apparent that the samples vary more along one axis of the ellipse than along the other. The first PC describes the direction of the greatest variation in the data set, which is the major axis of the ellipse. The second PC describes the direction of second greatest variation, which is the minor axis of the ellipse. In this case, a PCA model (the scores and loadings vectors and associated eigenvalues) with two principal components adequately describes all the variation in the measurements. [137]

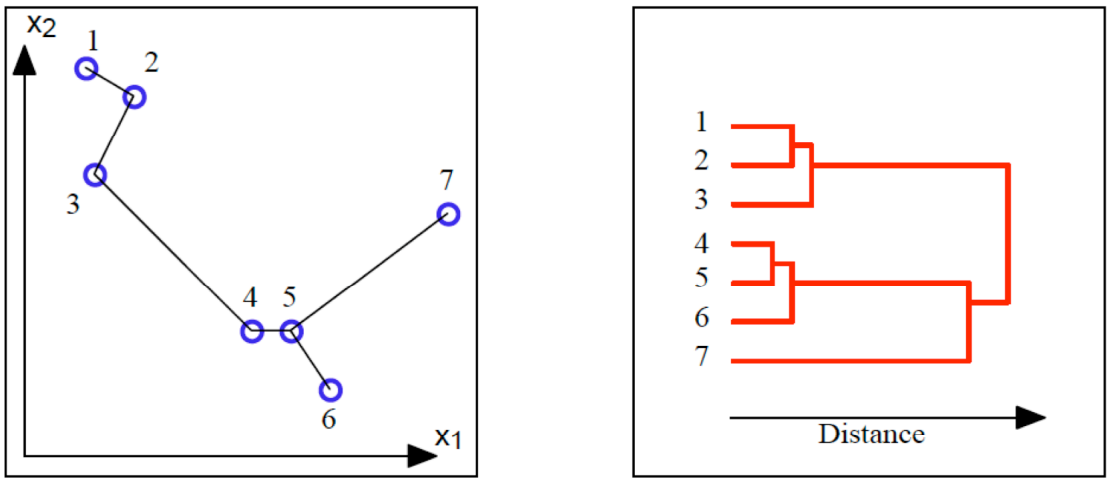

Figure 1.12 Example of linking in cluster analysis and resulting dendogram. Here the group of samples (with two measured parameters x_1 and x_2) are linked together, starting with the closest two, numbers 4 and 5, followed by the next closest samples, 1 and 2. Sample 6 is then linked to sample 5, which is already linked to sample 4, and so on. The results are shown in the dendogram at right. The vertical bars indicate which samples or groups are linked, while the horizontal position of the bar indicates the length of the link, *i.e.*, the distance between the linked samples or groups.[137]

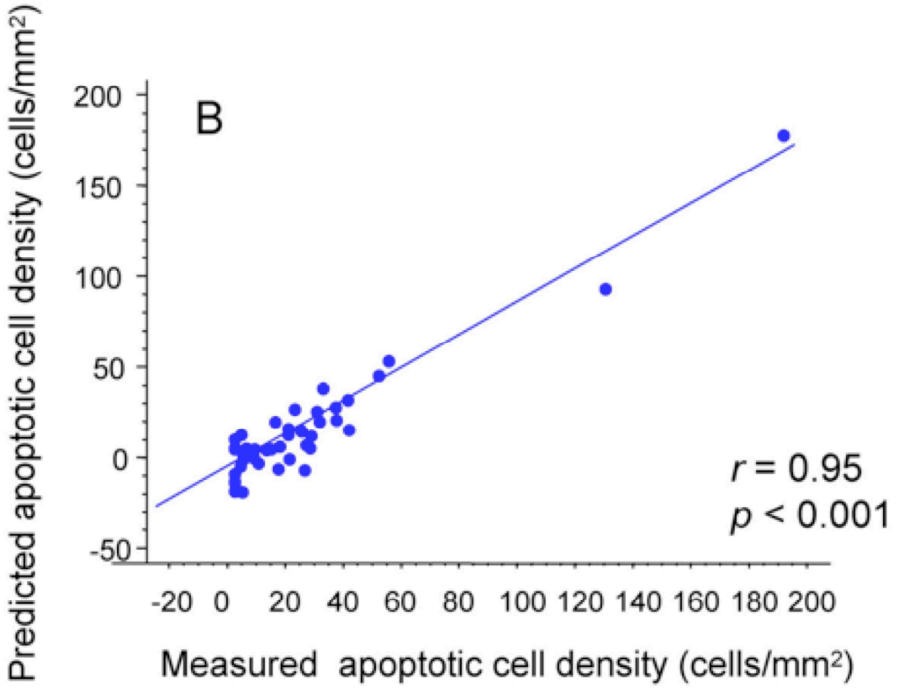

Figure 1.13 An example of a calibration plot created in PLS. The plot demonstrates the ability of PLS to measure the linearity of the actual (y-measured) and predicted (y-predicted) apopotic cell density predicted *versus* measured apoptotic cell density . Each point represents the data of a single biopsy. Shown are the Pearson correlation coefficient (r) and *p*-value are marked (p). [137]

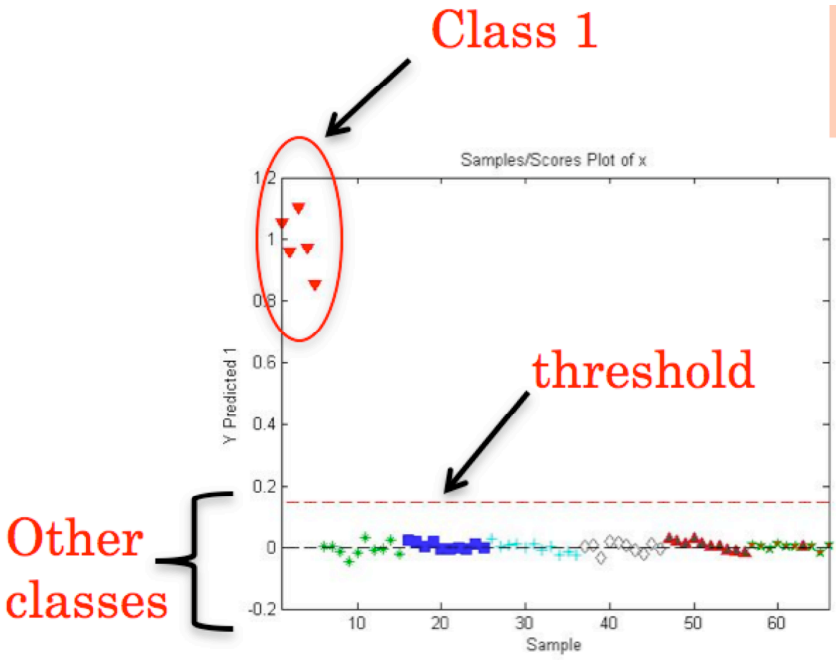

Figure 1.14 A PLS-DA model demonstrating that the circled data belongs to Class 1 because it is clustered above the threshold and near 1.

Chapter 2

Surface-enhanced Raman Spectroscopy: A qualitative tool for measles virus identification[1]

[1] Lynch, T., R.A. Dluhy, P. Rota, Y. Zhao, and R. Tripp. To be submitted to *Applied Spectroscopy.*

2.1 Abstract

Measles is a very contagious disease known by a prodromal illness of fever, cough, and conjunctivitis followed by the appearance of a generalized maculopapular rash. Traditionally, the measles virus (MV) can be detected using tests such as polymerase chain reaction (PCR), enzyme-linked immunosorbent assay (ELISA), and immunofluorescent antibody (IFA) assay. However, these techniques might not be reliable for low limits of detection, seldom cannot provide conclusive information and, in most cases, are not time efficient. The difficulties in MV detection have driven the search for new methods that overcome the limitations associated with conventional techniques. Surface-enhanced Raman spectroscopy (SERS) demonstrates a quick, label-free spectroscopic method that is desirable for determining the detection limit of viral samples. Silver (Ag) nanorods SERS substrates, prepared by the oblique angle deposition method, were created for the detection of three measles genotypes: D, A, and H1. The chemometric analysis method Partial Least Squares Discriminant Analysis (PLS-DA) was used to provide specificity of the SERS-Ag nanorods assay, specifically by classifying all analyzed MV genotypes with 100% specificity.

2.2 Introduction

The measles virus (MV) is a RNA type monotypic[§] virus that belongs to the *Paramyxoviridae* family and *Morbillivirus* genus. The virus is extremely contagious and is spread between hosts via the respiratory system. During the initial, an infected host will develop antibodies against the viral nucleocapsid (N) and the virulent transmembrane proteins, hemagglutinin (H) and fusion (F) proteins. The immune system will then try to prevent viral replication by removing the pathogens. The infection normally occurs once in a lifetime, as the host develops immunity. Attaining the measles vaccine will also enable lifetime immunity. However, the measles mortality rate remains significant, especially in underdeveloped countries, partially due to the lack of modern technologies and good health-care. In order to control the spread of the virus, initiatives have been implemented like the supplementary immunization activities (SIAs) implemented by the World Health Organization (WHO) and United Nations Children's Fund (UNICEF). However, with MV undergoing numerous mutations over time, the creation of vaccinations for the various genotypes presents a challenge for measles surveillance. Therefore it is important that a technique be available which enables one to distinguish viral strains.

The preliminary diagnosis of the measles is the review of the exposure history of the host, including a physical exam that focuses on the presence of symptoms like rash and fever.[18] Laboratory surveillance for measles is based on detection of virus-specific antibodies and detection of viral proteins or viral RNA.[1] Detection of virus-specific antibodies such as immunoglobin M (IgM) occurs using serologic methods like

[§] Being a single species representative in a genus

immunofluorescent antibody (IFA) and enzyme-linked immunosorbent assays (ELISA or EIA) by documentation of IgG seroconversion or four-fold rise in IgG EIA titer between acute- and convalescent-phase sera, and by isolation of MV or deletion of MV RNA from a clinical specimen. Serologic methods, however, are not measles specific, meaning they cannot distinguish between wild-type infections and vaccine-associated cases because they merely measure levels of antibodies (IgG or IgM) that can be attributed to a number of infections. Additionally, these tests are not time-efficient, have low sensitivity, poor detection limit, and frequently lead to false negatives.[2-4]

Highly viral detection sensitive methods like reverse transcription-polymerase chain reaction (RT-PCR) are utilized for the detection of MV RNA in a variety of clinical samples. RT-PCR is a technique carried out through the detection of viral RNA via nucleic acid extraction and amplification. Although this method has served as a valuable, alternative procedure for cases in which serologic testing results are inconclusive, inconsistent, or unavailable[1], it does not have the capacity to detect low levels of viral sample. Low levels of virus typically found in a clinical samples limit the sensitivity of this viral antigen detection method. For example, previously vaccinated individuals who experience the reoccurrence of a measles outbreak have decreased amount of viral shedding, thereby low levels of RNA cannot be detected by RT-PCR. In addition to its limitations with sensitivity, RT-PCR viral RNA or viral isolation samples are often inadequate because of improper collection, storage, and processing and transportation.[5] Sample preparation alone is a lengthy and requires much precision to produce consistent and conclusive results. Likewise, it takes hours to obtain results. Finding a method that increases the reliability and speed of viral detection assays is advantageous in the future

of measles surveillance and to establish a basis for further studies concerning virus discrimination.

Surface-enhanced Raman spectroscopy (SERS) serves as an alternative for viral detection enabling one to quickly obtain viral information with low sample preparation and high sensitivity and specificity. The signal enhancement of SERS, compared to classical Raman spectroscopy, is on average on the order of 10^5 to 10^6, with the maximum at 10^{14}, which allow for the analysis of single-molecule detection. SERS is also a highly sensitive method due to the fact that the detected SERS vibrational frequencies correspond directly to the various molecules bound to the surface of the substrate. In previous studies, Shanmukh et al. discovered that SERS silver (Ag) nanorods substrates could be used to effectively identify different strains of respiratory syncytial virus (RSV) in cell culture media at samples volumes of 0.5 to 1.0 μL.[10] Likewise, Hoang et al. used Ag nanorods substrates to classify three various MV genotype strains with nearly 100% sensitivity. The majority of enhancing materials used in past SERS studies have provided sufficient enhancement, provided the analyte could be brought to the enhancing surface. The choice between enhancing materials not only lies in the surface chemistry but also ease of use for a particular application as in the electromagnetic properties of the enhancing substrate.

SERS substrate fabrication methods that result in highly ordered arrays of high aspect ratio nanostructures with control over surface morphology are highly desirable. High aspect ratio Ag and Au SERS nanostructured substrates, like nanorods and nanowires, have been produced in the past using chemical and electrochemical methods like seeding growth,[118,119] electrochemical etching, electroplating, and thermal

evaporation.[120-122] However, the data produced by these SERS active substrates are challenging to interpret because of contributions from plasmon coupling from aggregates or underlying films. Oblique angle deposition (OAD) is a method that gets away from the disadvantages of other SERS substrate fabrication methods producing SERS active substrates using a physical vapor deposition technique. This method involves positioning of a solid substrate at a specific angle such that the vapor from the source is incident on the substrate close to the grazing angle.[48,125] Depositing metals at an angle results in the preferential growth of nanorods on the substrate in the direction of deposition.[14] This surface morphology occurs because of a shadowing effect where the initial metal nucleation sites are the places of growth of the nanostructues aligned in a specific direction.[126] The major advantages of this technique include the following: computer-enabled control over size, shape, and density of the nanostrctures all factors of temperature, deposition angle, and duration and rate of the deposition; the capability of using multiple metals during a deposition if a multiple pocketed crucible is available and if the metal can be evaporated; any standard thermal or electron beam evaporation system equipped with a holder capable of rotation in the polar direction can be utilized.[127]

Ag nanorod substrates prepared by the OAD method have been shown to provide SERS enhancement factor of ~ 10^8. In this chapter, discussed will be the capabilities of using SERS to detect three MV strains: D4, H1, and A. The specificity of the SERS assay will be reflected by the additional use of chemometric methods like Hierarchical Cluster Analysis (HCA), Partial Least Squares Discriminant Analysis (PLS-DA), and Principle Component Analysis (PCA). These methods allow one to view inconsistencies between spectra of different strains, with the differences between individual strains themselves

being greater than the variance due to inconsistencies in sample preparation and substrate morphology.[10]

2.3 Methods

Measles samples had to be diluted to ensure that SERS could be done on the chosen nanomaterials. If the samples were too thick an unknown scattering effect would be carried out and spectroscopic data unrepresentative of the MV samples would be obtained. PLS is a multivariate calibration method that decomposes spectral data into loadings and scores. Using this technique, regression curves can be created. These PLS models were used to show the dilution to spectral intensity relationship of various measles virus. This was specifically used to determined what dilution factor was suitable for analyzing further samples of MV.

SERS substrate preparation. The silver nanorod used in this study were created using the OAD method using a custom-designed electron-beam evaporation system (Torr International, New Windsor, NY) that has been described previously.[161] Before the deposition, glass substrates were cleaned using a heated Piranha solution (1:4 ratio hydrogen peroxide to sulfuric acid, respectively). The metal used for the evaporation was Ag pellets (Alfa Aesar, Ward Hill, MA, 99.999%). The metal film layers were monitored using a quartz crystal microbalance positioned at normal incidence to the vapor source. For this study two types of substrates were produced, 1x1 cm chips and 3x1 in slides. The 1x1 cm chips were prepared from larger 3x1 in glass slides and cut to size using a metal scriber. In each case, the glass pieces were mounted side-by-side onto the substrate holder for OAD. On the substrates, three layers of metal were deposited: 20 nm Ti, 500 nm Ag, and 2,000 nm Ag (when the vapor incident angle was tuned to 86°) when the

background pressure was approximately 4 x 10^{-6} Torr. Previous studies using scanning electron microscope (SEM) images were used to analyze Ag nanorod surfaces. Driskell et al. determined that average overall rod length of the nanorod substrates to be 868 ± 95 nm, while the diameter of the nanorods were 99 ± 29 nm. The density of the nanorods was calculated to be 13.3 ± 0.5 rods/μm^{-2} with an average tilt angle of 71.3 ° ± 4.0 °.

Measles virus propagation. The following measles viruses were used in the analyses: measles virus (MV) strains H1, A, and D4. Viral strains all are clarified cell culture supernatants from Vero/hSLAM cells in Dulbecco's Modified Eagles Medium (DMEM; GIBCO BRL Laboratories, Grand Island, NY) without antibiotics or fetal bovine serum (FBS; Hyclone Laboratories, Salt Lake City, UT). Measles were harvested in serum-free DMEM followed by two freeze—thaws (-70 °C/4 °C), after which the contents were collected and vortex for 1 min. The virus titers were approximated 10^6 PFU/mL, determined by immunostaining plaque array (CDC MMR Laboritories, Atlanta, GA). The control for these studies was uninfected Vero cell lysate cleared.

Sample prepation. Serial dilutions in the cellular media were performed ranging from 1:10 to 1:1000. To prevent the formation of a thick cellular layer on the surface of the Ag nanorods, MV samples were diluted in HyPure™ Molecular Biology Grade Water (Thermo Scientific, Waltham, MA) before they were placed on Ag nanorod substrates and SERS spectral collections were made.

SERS measurement. SERS spectra were collected using a Renishaw inVia confocal Raman microscope system (Hoffman Estates, IL) with a 785 nm near-infrared diode laser as the excitation source. Attenuated light, from a high power (300 ± 30 mW) laser, was set to ~7mW at the sample surface using a series of neutral density filters. The

laser spot was focused into a ~115 μm x 11 μm spot using a 5 x objective. SERS spectra were collected from 400 to 800 cm^{-1} in the ExtendedScan mode using six coadded 10 s collection times. A 3.0-μL aliquot of the sample (i.e., intact virus or cell lysate control media) was applied to the Ag nanorod array substrate and allowed to dry overnight at room temperature prior to spectrum acquisition.

Data analysis. It is important for SERS to have the ability to differentiate between various strains (i.e. genotypes) of the MV since the virus has the capability of mutating, which is the common instigator of reoccurring outbreaks. Secondly, most genotypes differ in nucleotide sequence by as little as 2.5%. We analyzed the H1, A, and D4 genotypes by first diluting the viruses in molecular grade water (solvent). After the spectral data was collected, PLS-DA was utilized as a classification method, which maximizes the sensitivity and the specificity of the data set. Using this technique, it was possible to classify the genotypes of MV (into their respective classes) based on their genetic differences.

2.4 Results

Using PLS-DA to find the dilution factor. In previous studies, molecular samples have been diluted in a solvent to prevent the aggregation of a film created by cellular debris on Ag nanorods substrates. In Figure 2.1, the thick layer caused by depositing the MV sample "as is" onto the bare Ag nanorods substrate has been known to decrease SERS enhancement and lower spot to spot reproducibility. Therefore, it was necessary to find the dilution factor for MV samples. The cell lysate media was diluted in water using ten-fold dilutions from 1:10 to 1:1000. Approximately 1μL of the diluted samples were individually deposited onto Ag nanorod substrates and SERS spectra were collected. The spectral data was initially interpreted by visually examining SERS spectra (Figure 2.2).

However, no quantitative data could be inferred from analyzing the raw spectra, specifically no linear relationship could be made between any individual bands with respect to the amount the lysate media was diluted into the solvent (not shown). Therefore, Partial Least Squares (PLS) was used to create a y-measured versus y-predicted linear regression curve of the dilution factors (Figure 2.3). Three classes (denoting the three dilution factors of the lysate media—1:10, 1:100, and 1:1000) are show in Figure 2.3 with the green line denoting a completely linear fit (R^2=1.0) and the red line expressing the actual fit of the curve (R^2=0.719). The 1:10 class appeared to have the least variance from looking at the logarithmic plot. The averages for the y-measured versus y-predicted data for each class were calculated, as well as the standard deviation (SD) and relative standard deviation (RSD), and then displayed in Table 2.1. In this table one can see that the 1:100 class had the lowest SD and the 1:1000 class had the highest. The RSD, however, is a better measurement of the variance when comparing the uncertainty between different measurements of varying absolute magnitude.[152,162] RSD is the absolute value of the standard deviation expressed as a percentage of the mean ($RSD=100(s/\bar{x})$). It is a statistical measure of the reliability of an assay. Therefore, the 1:10 dilution factor was chosen as ideal for so-called thinning out viral and cell lysate media for future studies.

Differentiating SERS data of three MV strains (D4, A and H1). The need for measles surveillance includes the monitoring viral mutations over time and in different regions of the world.[59] Consequently, it is important to be able to detect slight genetic differences in viral samples. SERS was used to gather spectral data about three MV genotypes at which chemometric analysis was later used to classify the samples based on

their genetic differences. Initially, the SERS spectra of the genotypes were visually analyzed (Figure 2.4-2.6). A comparison between the spectra of measles samples with literature references of Raman band assignments of proteins, peptides, and nucleic acid bases as references, the prominent bands were assigned to components of the virus and the cell culture media.[163] For example, the Raman shifts detected at 1650 and 1230-1295 cm^{-1} were assigned to amide (I and III), 1061 cm^{-1} C-N and C-C stretching, 1606 and 620 cm^{-1} phenylalanine, 1440-1460 C-H deformation, 1290 cm^{-1} CH_2 deformation, 850 cm^{-1} "buried" tyrosin, 785 cm^{-1} cytosine and uracil ring/stretching, 720 cm^{-1} adenine, and 620 cm^{-1} guanine, respectively (Table 2.2).[163]

The differentiation of viral genotypes using their SERS spectra requires that the inconsistency between spectra of the individual strains themselves be greater than the variance due to inconsistencies in sample preparation and substrate morphology.[10] The spectra of the D4, A, and H1 gentypes of MV are shown in Figures 2.4 to 2.6, which have been baseline corrected. There were observable variations in the spectral data of the virus samples, the cell lysate media control, and the solvent (Figure 2.4-2.7). These spectral variations included the appearance or disappearance of bands and changes in bandshape. For example, the 1000 cm^{-1} band for C-C stretching and/or phenylalanine appeared in all spectra but was most prominent in the spectra of the media control (Figure 2.2). The amide I and III protein bands around 1650 and 1230 cm^{-1} only appeared in the sample spectra, and not in the solvent spectrum. The presence of different ratios of amino acids and nucleic acid bases in the viral samples may have given rise to the changes in band intensities among spectra; this is the case for the spectra of the three genotypes that had varying band intensities for the nucleotides adenine, cytosine, uracil and guanine at 720,

785, and 665 cm^{-1}, respectively. It is not expected to obtain high intensities for the nucleotides since measles virus nucleocaspids contain on average 5% RNA[164] but around six higher molecular weight polypeptides (40-80 daltons)[165].

Visually, it is difficult to differentiate amongst the spectra of the genotypes and cell media control because of fluctuations of some spectral variations. These variations did not give a distinct classification of samples. Therefore, chemometric analysis was applied to provide a consistent and visually clear model for separation of genotypes base on detectable statistical variations in the data. Used was Partial Least Squares Discriminant Analysis (PLS-DA), a chemometric method used to cluster data based on genetic similarities. In PLS-DA analysis, y-predicted versus samples scores plot illustrated the capability of separating measles genotypes (classes) (n=4) based on their spectral data (Fig. 2.8-2.10). This was assumed based on the red dash line represented the threshold for the prediction model. The threshold value defined the cut-off point for the class assignment. Samples that belonged to the A genotype class had a calculated y-predicted value that clustered above the 0.73 threshold (Figure 2.8). Whereas, the D4 and H1 classes had values approximately close to 0 since samples with y-predicted values below that threshold were identified as not belonging to the A genotype class. According to the y-predicted plot, all the samples from the A genotype class were correctly identified by PLS-DA. Likewise, for classes D4 and H1 this was also accurate in Figures 2.9 to 2.10. A PLS-DA model was tested by Venetian blinds cross-validation (CV), using 9 data splits. The model was able to predict the class with 100% sensitivity and specificity, meaning that all samples were correctly predicted as in-the-class when chosen to be and vice versa (Table 2.3).

2.5 Discussion

The results from this study show that SERS has the ability to provide a rapid and reliable means of detecting very low levels of viruses, which is the leading death of children to-date. Current viral diagnostic methods are not time efficient and lack the sensitivity of SERS. Advances in nanofabrication allow for the development of biosensing devices like Ag nanorods that allow for rapid, reproducible and sensitive detection of infectious diseases. Ag nanorods substrates were successfully used to detect the presence of amino acids and nucleotides in infectious and cell control media samples with great signal-to-noise such as the bands at 1650 and 1230-1295 cm^{-1} for amide I and III, 1606 and 620 cm^{-1} phenylalanine, 850 cm^{-1} "buried" tyrosin, 785 cm^{-1} cytosine and uracil ring/stretching, 720 cm^{-1} adenine, and 620 cm^{-1} guanine, respectively.[163] The viral and cell control media samples could confidently be differentiated from the background and solvent spectra as well; amino acids and/or polypeptides that comprise the measles virus were not identified in the spectra of the background nor solvent. Additionally, the ability of Ag nanorods to differentiate between measles genotypes, which have minute genetic variations (~5-7% sequence diversity), with 100% sensitivity can contribute to low-level detection of measles. Likewise, chemometric analysis increases the benefits of the SERS-Ag nanorods assay in providing a method that can differentiate amongst measles genotypes with 100% specificity.

2.6 Acknowledgements

The research was funded by the Faculty in Infectious Disease at the UGA and Centers for Disease Control and Prevention (UGA/CDC FID) Seed Grant. The author thanks Paul Rota, Marcus Collins, and the Centers for Disease Control (CDC) for

supplying the measles samples and Yiping Zhao for the use of the e-beam evaporator.

2.7 References

(1) Hoang, V., Univ of GA, 2008.

(2) Bottomley, L.; Zhao, Y.; Tripp, R.; Dluhy, R.; University of Georgia, Georgia Institute of Technology, CDC MMR and Herpesvirus Branch: Athens, Atlanta, 2009, p 21.

(3) Riddell, M. A.; Mossa, M. J.; Hauer, D.; Monzec, M.; Griffin, D. E. *J of Clin Virol* **2007**, *39*, 312.

(4) Mancuso, J.; Krauss, M.; Audet, S.; Beeler, J. *Vaccine* **2008**, *26*, 4877.

(5) Jenkerson, S.; Beller, M.; Middaugh, J.; Erdman, D. *N Engl J Med* **1995**, *332*, 1103.

(6) Rota, P.; Bellini, W. *J Infect Dis* **2003**, *187 Suppl 1*, S270.

(7) Shanmukh, S.; Jones, L.; Zhao, Y.-P.; Driskell, J. D.; Tripp, R.; Dluhy, R. A. *Anal. Bioanal Chem* **2008**, *390*, 1551.

(8) Nikoobakht, B.; El-Sayed, M. *J. Phys. Chem. A* **2003**, *107*, 3372.

(9) Tao, A.; Kim, F.; Hess, C.; Goldberger, J.; He, R.; Sun, Y.; Xia, Y.; Yang, P. *Nano Lett.* **2004**, *3*.

(10) Sauer, G.; Brehm, G.; Schneider, S.; Graener, H.; Seifert, G.; Nielsch, K.; Choi, J.; Goring, P.; Gosele, U.; Micleas, P.; Wehrspohn, R. *J. Appl. Phys* **2005**, *97*, 024308.

(11) Moskovits, M.; Jeong, D. *Chem. Phys. Lett.* **2004**, *397*, 91.

(12) Yao, J.; Pan, G.; Xue, K.; Wu, D.; Ren, B.; Sun, D.; Tang, J.; Xu, X.; Tian, Z. *Pur Appl. Chem.* **2000**, *72*, 221.

(13) Robbie, K.; Brett, M. *J. Vac. Sci. Technol. A* **1997**, *15*, 1460.

(14) Robbie, K.; Sit, J.; Brett, M. *J. Vac. Sci. Technol. A* **1998**, *16*.

(15) Driskell, J.; Shanmukh, S.; Liu, Y.; Chaney, S. B.; Tang, X.-J.; Zhao, Y.-P.; Dluhy, R. A. *J. Phys. Chem. C* **2008**, *112*, 895.

(16) Abelmann, L.; Lodder, C. *Thin Solid Films* **1997**, *305*, 1.

(17) Zhao, Y.-P.; Ye, D.-X.; Wang, G.-C.; Lu, T.-M. *Nano Lett.* **2002**, *2*, 351.

(18) Chaney, S.; Shanmukh, S.; Dluhy, R.; Zhao, Y.-P. *Nano Lett.* **2005**, *87*, 031908.

(19) Harrison, S. *Agric. Syst.* **1990**, *34*, 183.

(20) Harris, D. C. *Quantitative Chemical Analysis*; 6 ed.; W. H. Freeman and Company: New York, 2003.

(21) Pan American Health Organization; PAHO: Washington, DC, 1999, p 41 (PAHO technical paper).

(22) Naumann, D.; Helm, D.; Labischinski, H. *Nature* **1991**, *351*, 81.

(23) Bussell, R. H.; Waters, D. J.; Seals, M. K.; Robinson, W. s. *Medical Microbiology and Immunology* **1974**, *160*, 105.

(24) Waters, D. J.; Bussell, R. H. *Virology* **1973**, *55*, 554.

Table 2.1 Average y-measured and y-predicted values of the PLS processed and cross-validated prediction model for vero cell lysate samples that were diluted in water. Averages were obtained from a PLS regression model of three cell lysate media classes (samples diluted in water ten-fold from 1:10, 1:100, to 1:1000). The table illustrates that the 1:10 dilution is the optimum dilution factor since it has a low standard deviation (SD) and the smallest relative standard deviation (%RSD). (relative standard deviation is a statistical estimate of the reliability of an assay)

Y Measured Sample Ratio	**1.00E-01**	**1.00E-02**	**1.00E-03**
Y CV Predicted Sample Ratio	8.51E-02	2.16E-02	9.08E-03
SD	0.01976	0.01975	0.02238
%RSD*	23	92	246

*The relative standard deviation is defined as a statistical estimate of the reliability of an assay.

Table 2.2 Band assignments for prominent Raman shifts detected for the virus samples. [a] The presence of proteins, amino acids, and RNA contributed to the Raman shifts observed in the spectra.

Raman shift (cm^{-1})	**Assignment[a]**
1650-1680	Amide I
1606, 1004	Phenylalanine
1440-1460	C-H deformation
1295	CH_2 deformation
1230-1295	Amide III
1129	C-N and C-C stretching
1061	C-N and C-C stretching
852	“buried” tyrosine
785	Cytosine, uracil (ring, stretching)
720	Adenine
665	Guanine
520-540	S-S stretching

Table 2.3 The sensitivity and specificity of the PLS-DA processed and cross-validated prediction model for the MV genotypes A, H1 and D4 and the cell media. Data was cross-validated with venetian blinds (9 splits). [a] The sensitivity is defined as the number of predicted samples in the class divided by the number of total samples.[b] The specificity regarded as the number of predicted samples that are not in the class divided by the total number of samples.

Class	A	H1	D4	VCL
Sensitivity (Cal.)[a]	1.0	1.0	1.0	1.0
Specificity (Cal.)[b]	1.0	1.0	1.0	1.0
Sensitivity (CV)	1.0	1.0	1.0	1.0
Specificity (CV)	1.0	1.0	1.0	1.0

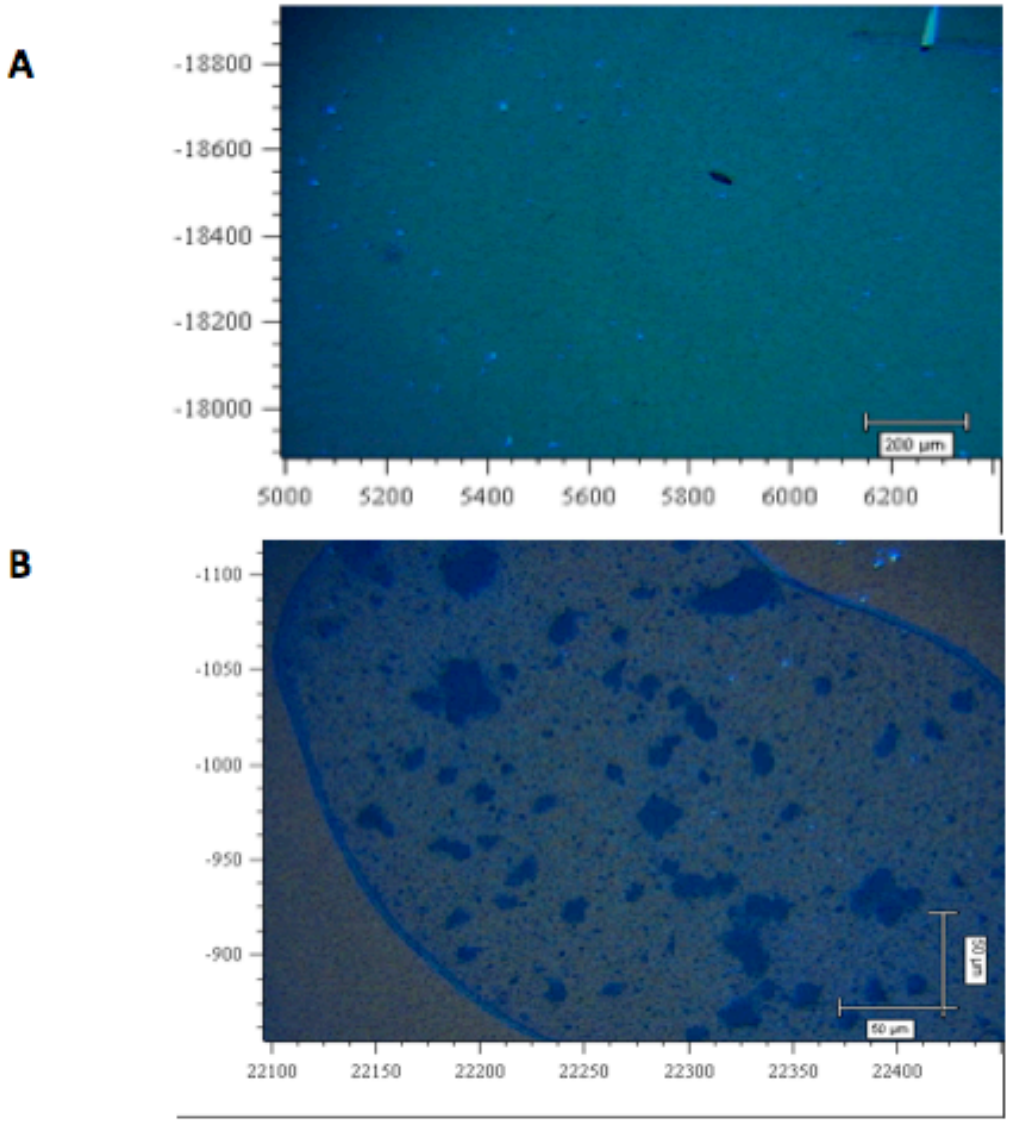

Figure 2.1 Microscopic images of Ag nanorod substrates (A) before the sample was deposited and (B) after 1µ L of the cell lysate media was applied to the SERS substrate.

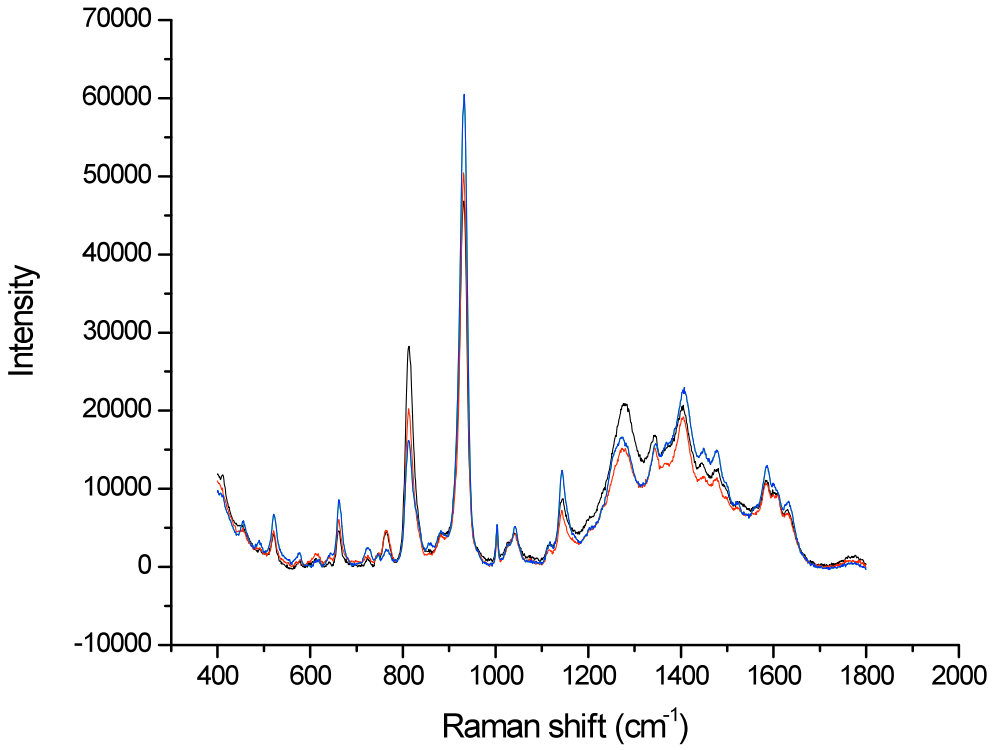

Figure 2.2 SERS spectra of the cell lysate media on a bare Ag nanorod substrate.

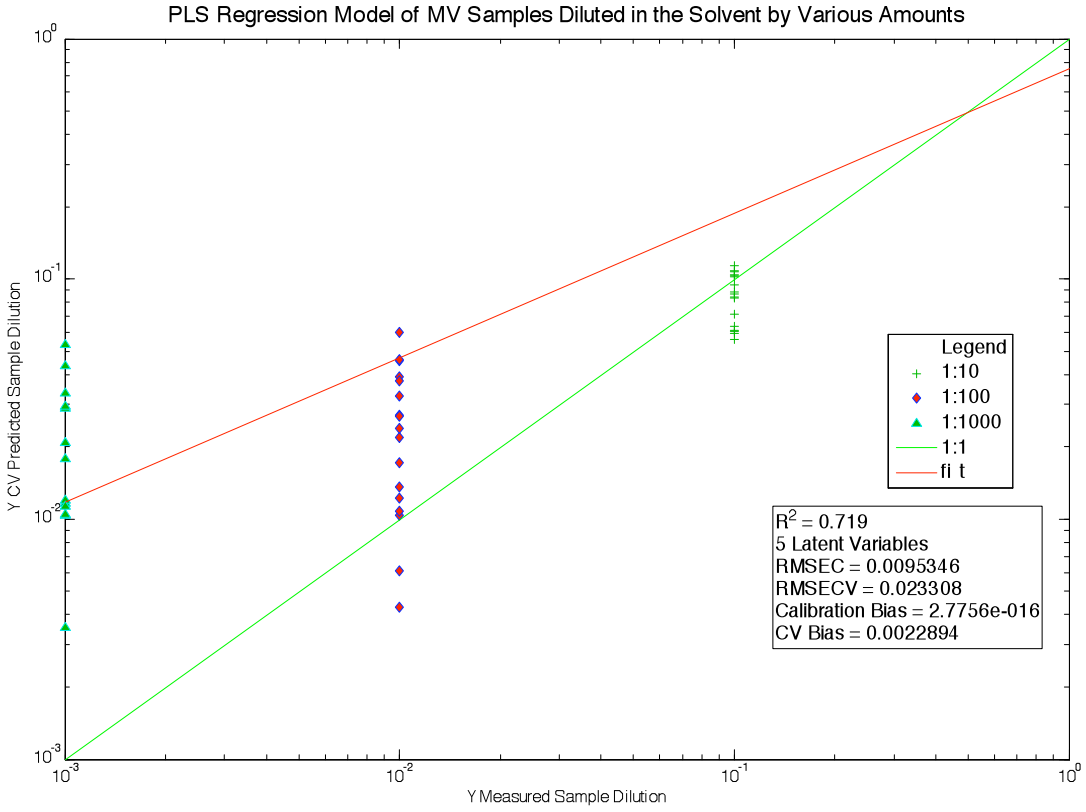

Figure 2.3 A PLS regression model illustrating the linearity between the y-measured and y-predicted values of three cell lysate media classes (samples diluted in water ten-fold from 1:10, 1:100, to 1:1000). The model was created to find the optimum dilution factor necessary for thinning out viral and media samples. Dilution of samples was necessary to prevent the formation a thick cellular layer on the nanorod surface, which would inhibit the enhancement normally exhibited by SERS.

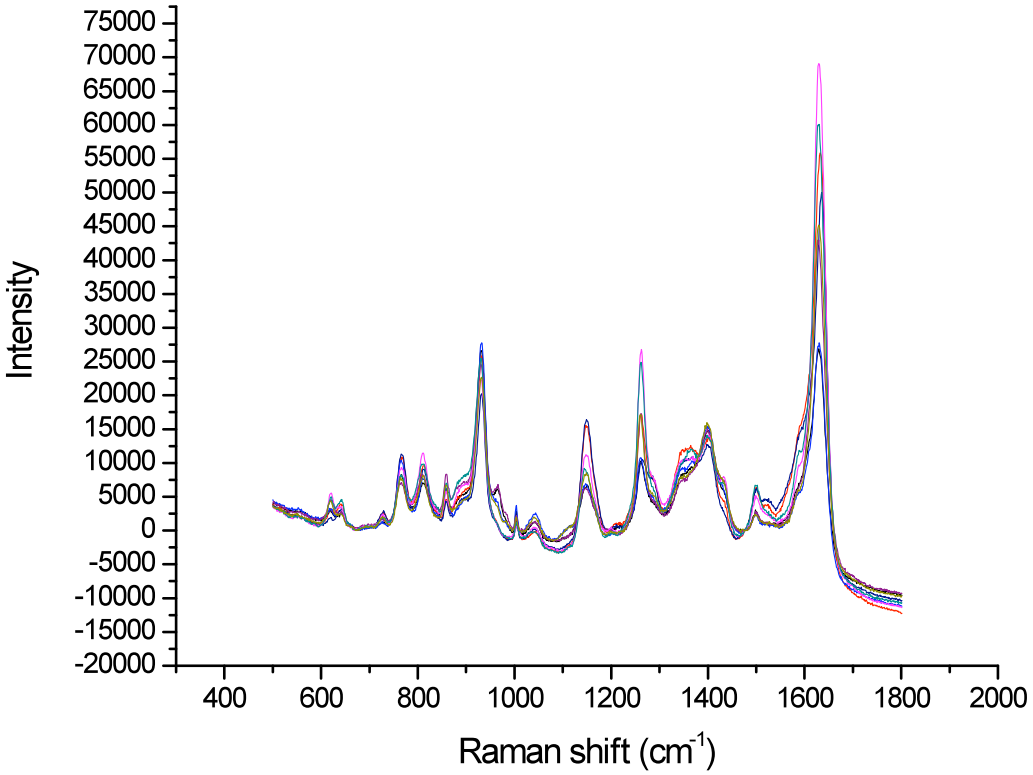

Figure 2.4 SERS spectra the A genotype of the measles virus on a bare Ag nanorod substrate.

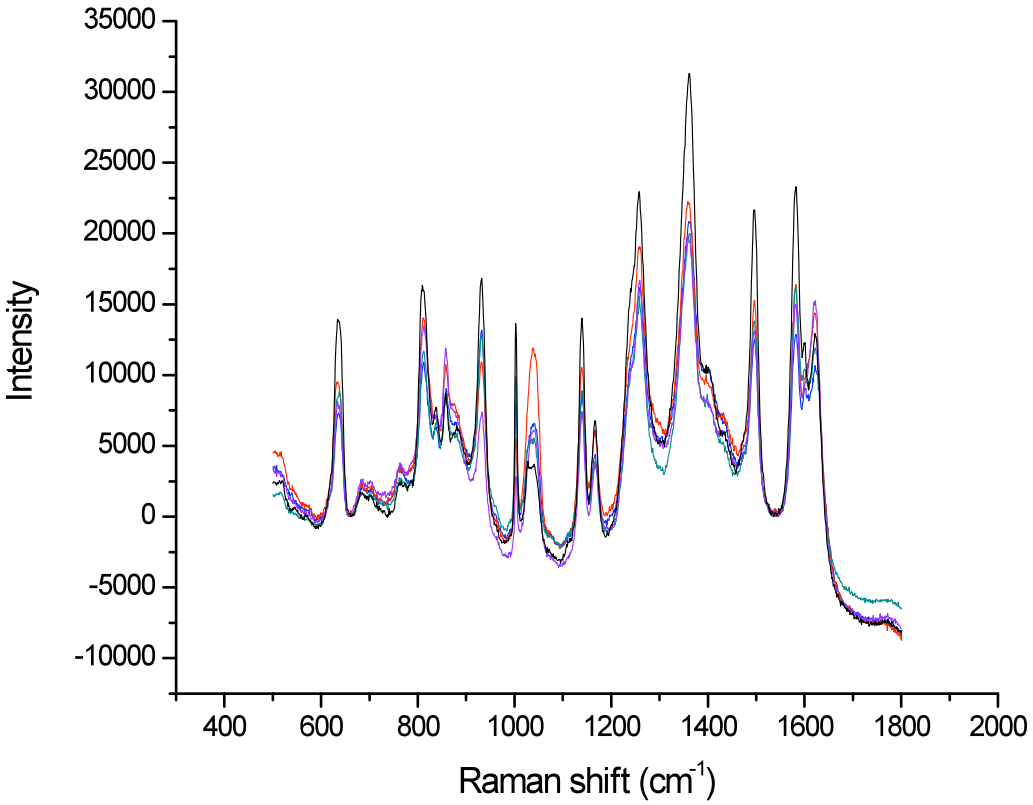

Figure 2.5 SERS spectra the H1 genotype of the measles virus on a bare Ag nanorod substrate.

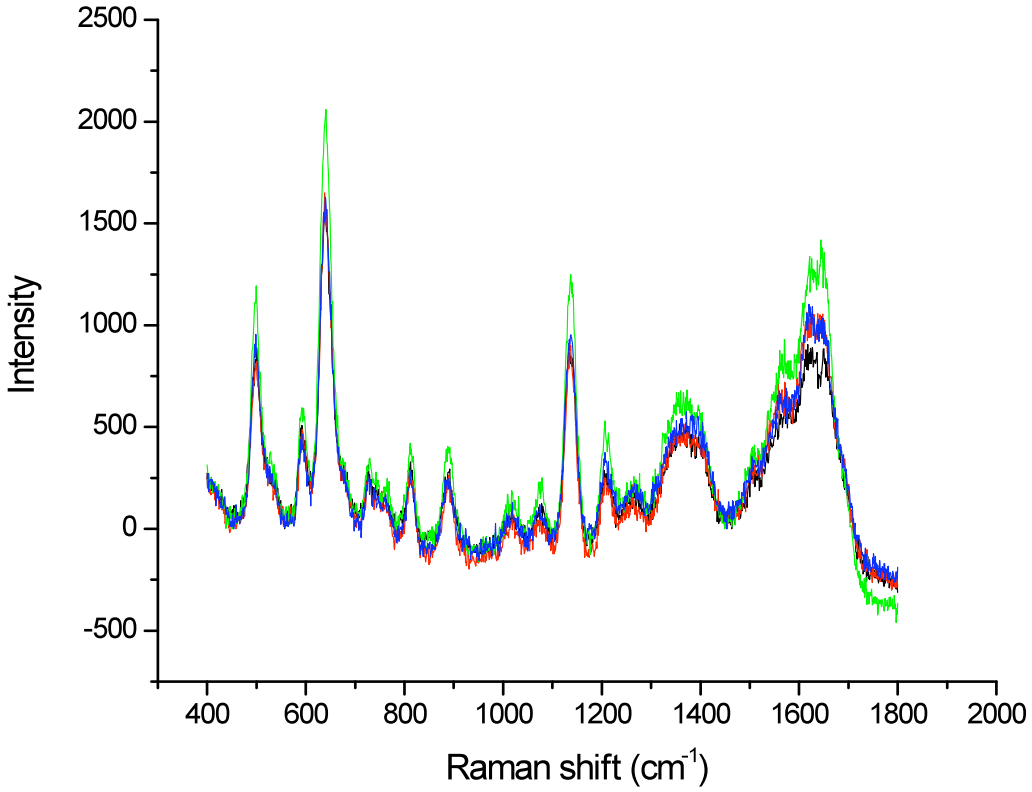

Figure 2.6 SERS spectra the D4 genotype of the measles virus on a bare Ag nanorod substrate.

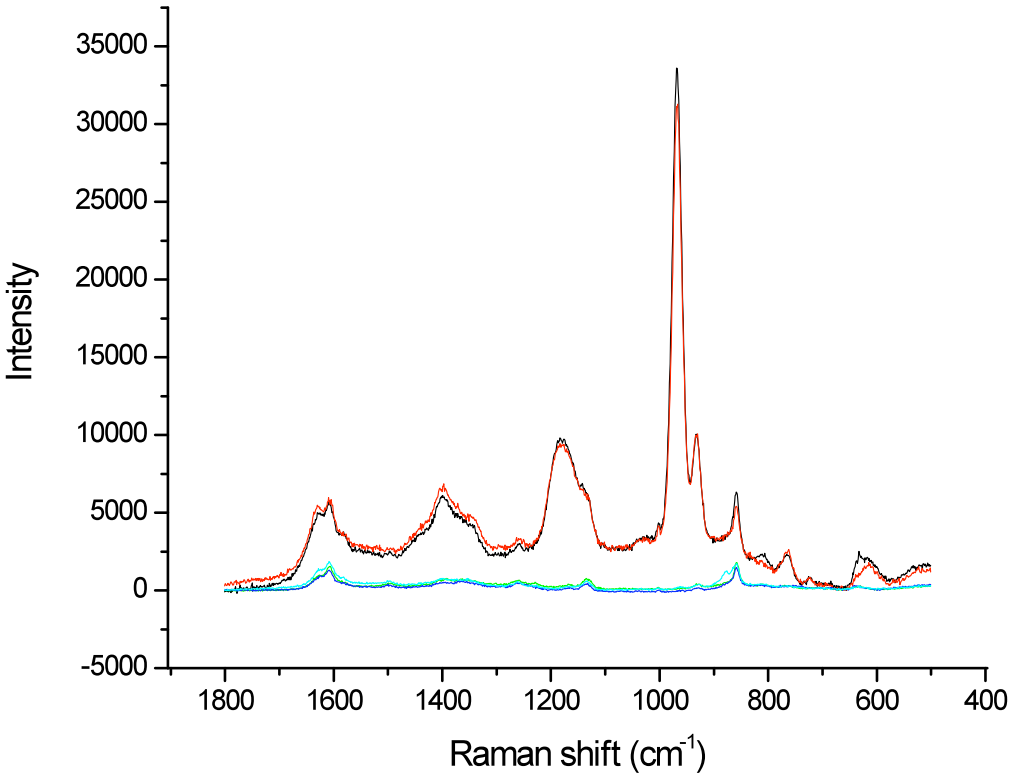

Figure 2.7 SERS spectra of molecular biological grade water (top) and the background of the bare Ag nanorod substrate.

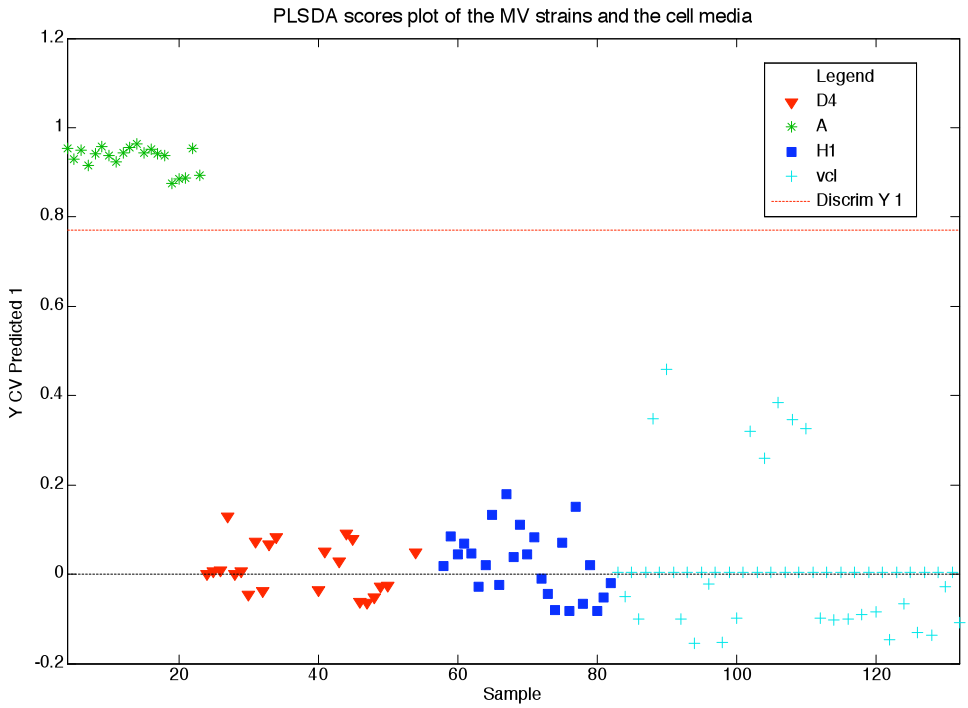

Figure 2.8 Y-predicted plot for the A genotype class prediction of SERS data. The red dash line represented the threshold for the prediction model. The threshold value defined the cut-off point for the class assignment. Samples that belonged to the A genotype class had a calculated y-predicted value that falls between the threshold (0.75) and a value that is approximately 1. Samples with y-predicted values below the threshold were identified as not belonging to the class. According to the y predicted plot, all the samples from the A genotype class were correctly identified by PLS-DA.

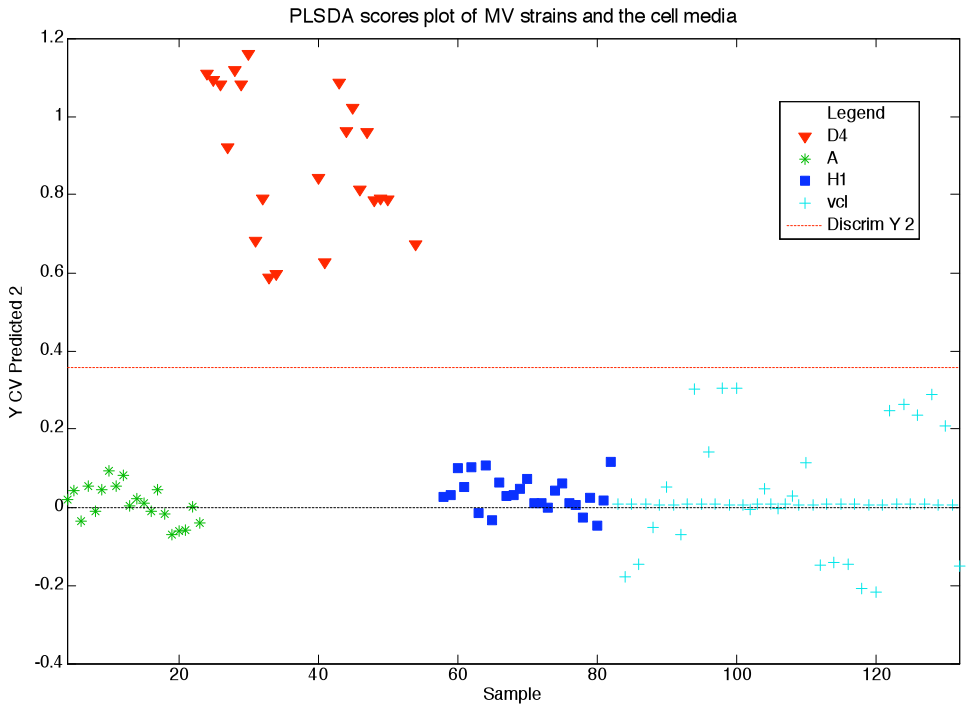

Figure 2.9 Y-predicted plot for the D4 genotype class prediction of SERS data. The red dash line represented the threshold for the prediction model. The threshold value defined the cut-off point for the class assignment. Samples that belonged to the D4 genotype class had a calculated y-predicted value that falls between the threshold (0.35) and a value that is approximately 1. Samples with y-predicted values below the threshold were identified as not belonging to the class. According to the y predicted plot, all the samples from the D4 genotype class were correctly identified by PLS-DA.

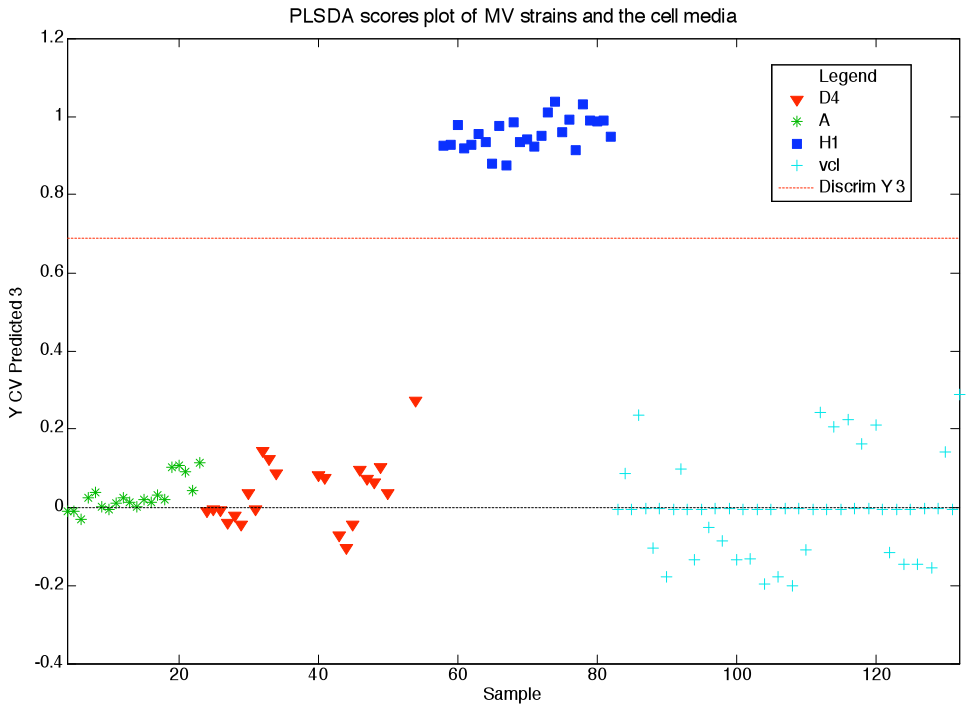

Figure 2.10 Y-predicted plot for the H1 genotype class prediction of SERS data. The red dash line represented the threshold for the prediction model. The threshold value defined the cut-off point for the class assignment. Samples that belonged to the H1 genotype class had a calculated y-predicted value that falls between the threshold (0.69) and a value that is approximately 1. Samples with y-predicted values below the threshold were identified as not belonging to the class. According to the y predicted plot, all the samples from the H1 genotype class were correctly identified by PLS-DA.

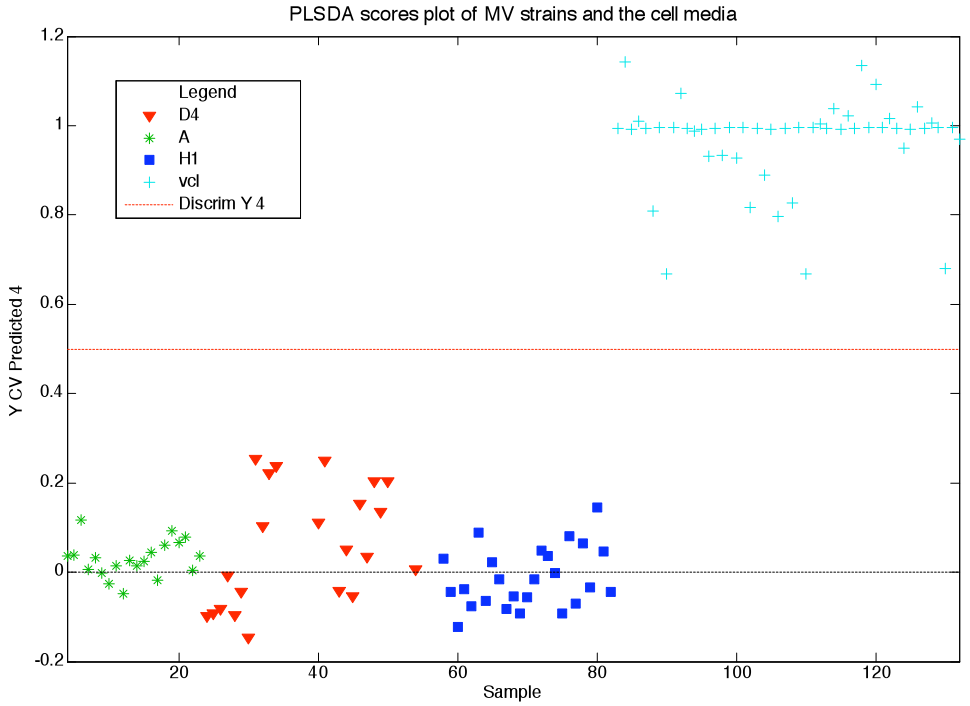

Figure 2.11 Y-predicted plot for the cell media (vcl) class prediction of SERS data. The red dash line represented the threshold for the prediction model. The threshold value defined the cut-off point for the class assignment. Samples that belonged to the vcl genotype class had a calculated y-predicted value that falls between the threshold (0.50) and a value that is approximately 1. Samples with y-predicted values below the threshold were identified as not belonging to the class. According to the y predicted plot, all the samples from the vcl genotype class were correctly identified by PLS-DA

Chapter 3

Surface-enhanced Raman Spectroscopy: A tool for the quantitative analysis of the Edmonston strain of the measles virus [2]

[2] Lynch, T., R.A. Dluhy, P. Rota, Y. Zhao, and R. Tripp. To be submitted to *Applied Spectroscopy.*

3.1 Abstract

Measles is a very contagious disease known by a prodromal illness of fever, cough, and conjunctivitis followed by the appearance of a generalized maculopapular rash. Traditionally, the measles virus (MV) can be detected using tests such as reverse transcriptase-polymerase chain reaction, enzyme-linked immunosorbent assay, and immunofluorescent antibody assay. However, these techniques might not be reliable for low limits of detection, seldom cannot provide conclusive information and, in most cases, are not time efficient. The difficulties in MV detection have driven the search for new methods that overcome the limitations associated with conventional techniques. Surface-enhanced Raman spectroscopy (SERS) demonstrates a quick, label-free spectroscopic method that is desirable for determining the detection limit of viral samples. In this study, SERS spectra of the MV were analyzed using Partial Least Squares (PLS). PLS was used to create regression plots that illustrate the relationship between spectral intensity and concentration of MV samples. PLS regression curves showed nearly linear relationships (R^2=0.995 ± 0.03) between y-predicted and y-measured data of purified MV samples at various concentrations (10^3 -10^1 pfu/ml). Information obtained using PLS suggests that SERS can potentially be used as a reliable assay finding the limit of detection of measles samples without sample amplification or labeling.

3.2 Introduction

The measles is a contagious disease that initiates in the respiratory system caused by the measles virus, spread by aerosol or respiratory droplets entering the respiratory route. An infection has an average incubation period of 14 days and infectivity from 2 to 4 days prior, until 2 to 5 days following the onset of the rash[17]. The onset of the rash coincides with the appearance of the immune response and initiation of virus clearance[18]. The disease circulates worldwide with estimates of over 30 million cases and 770,000 deaths every year[57] and remains the leading cause of vaccine-preventable child mortality. The underutilization of measles vaccine is the principal attributable cause to the current high measles morbidity and mortality[57]. In more than 95% of these deaths, they occur in low-income countries with weak health infrastructures and inaccessibility to vaccination. Its high level of infectivity and scientific evidence of the impact of measles vaccination on child survival initiates the importance of having accelerated measles detection methods.

Conventional laboratory surveillance for measles is based on detection of virus-specific antibodies and detection of viral proteins or viral RNA[1]. Detection of virus-specific antibodies such as immunoglobin M (IgM) occurs using serologic methods like immunofluorescent antibody (IFA) and enzyme-linked immunosorbent assays (ELISA or EIA) by documentation of IgG seroconversion or four-fold rise in IgG EIA titer between acute- and convalescent-phase sera, and by isolation of MV or deletion of MV RNA from a clinical specimen. Serologic methods, however, are not measles specific, meaning they cannot distinguish between wild-type infections and vaccine-associated cases because they merely measure levels of antibodies (IgG or IgM) that can be attributed to a number

of infections. Additionally, these tests are not time-efficient, have low sensitivity, poor detection limit, and frequently lead to false negatives.[2-4]

Highly viral detection sensitive methods like reverse transcription-polymerase chain reaction (RT-PCR) also do not enable the capacity to detect low levels of viral sample even though the use of the technique (*i.e.,* for the detection of MV RNA in a variety of clinical samples) has served as a valuable, alternative procedure for cases in which serologic testing results are inconclusive, inconsistent, or unavailable[1]. RT-PCR is a technique carried out through the detection of viral RNA via nucleic acid extraction and amplification. Low levels of virus typically found in a clinical samples limit the sensitivity of this viral antigen detection method. For example, previously vaccinated individuals who experience the reoccurrence of a measles outbreak have decreased amount of viral shedding, thereby low levels of RNA cannot be detected by RT-PCR. In addition to its limitations with sensitivity, RT-PCR viral RNA or viral isolation samples are often inadequate because of improper collection, storage, and processing and transportation[5]. Sample preparation alone is a lengthy and requires much precision to produce consistent and conclusive results. Likewise, it takes hours to obtain results. Finding a method that increases the reliability and speed of viral detection assays is advantageous in the future of measles surveillance and to establish a basis for further studies concerning virus discrimination.

One alternative to existing laboratory surveillance technique is surface-enhanced Raman spectroscopy (SERS), a nano-optical method that provides a fast, label free method for the determination of the viral samples. SERS is an extension of Raman spectroscopy, which is a vibrational spectroscopic technique used to provide high

structural information useful in real-world applications in biochemistry and the life sciences[6]. SERS is an extremely sensitive method that has been an emerging technique for viral pathogen detection [10,16,79,80]. In the past, Fourier transform infrared spectroscopy (FTIR) and Raman scattering have been used as vibrational spectroscopic techniques for the detection and differentiation of infectious agents [163,166-174]. These methods allow one to collect spectra that display the chemical composition of pathogens, which serve as fingerprints for detection and identification. Although both methods have been deemed successful at providing whole-organism fingerprinting, it has been found that each suffers from inherent limitations. For instance, FTIR is limited by interference from water; while Raman spectroscopy is resistant to water, it is severely limited to low scattering cross sections that translate to weak signals for pathogen detection[81]. SERS overcomes the limitation of both conventional spectroscopic methods by providing high cross sections and resistance to water.[86] SERS provides greater spectral signals to that of Raman scattering because the incoming laser beam interacts with the oscillations of plasmonic electrons in metallic nanostructures to enhance the vibrational spectra of molecules adsorbed to the surface by 14 orders of magnitude, with respect to normal Raman intensities[7-9].

Recently, SERS has been used as a biomedical-sensing device to detect viruses[10,16,80,175-177] and quantify micro and nanometric molecules [81,178]. The sensitivity and analytical utility of the SERS methodology has been proven in numerous studies [14,16,80,81,175,176]. For example, the sensitivity of the SERS technique for low level detection has been published for respiratory syncytial virus (RSV)[16] where several titers of the RSV ΔG viral strain was prepared by dilution with deionized water and small amounts of

the samples were applied to silver nanorods array (AgNR) substrates. Chemometrics was utilized in combination with SERS spectral data to produce PLS plots of the peak area at 1045 cm^{-1} verses concentration of the viral solution. PLS regression plots decreased linearly from 10^3 PFU/ml over 2 orders of magnitude therefore providing evidence of the quantitative capabilities of the SERS method when paired with chemometrics.

Scientist have previously reported the difficulties of using univariate techniques (*i.e.*, Beer-Lambert relationship) of relating changes in spectral band intensities to changes in pathogen concentration[16,81]. It is important to analyze the entire spectrum, or use specialized feature selection algorithms, since discrete patterns of multiple bands, rather than a single peak, are important for the identification[81] and quantitation. Principle least squares (PLS) is a statistical method that produces a linear regression model from large data matrices (i.e. spectral data) by projecting the predicted variable and the measured variable in new space [139]. To overcome the limitation of univariate methods, PLS is suitable for the fast and simultaneous analysis of complex mixtures with minimum sample preparation and without time-consuming separations. The use of a quantitative method based on PLS regression analysis for the identification of several viruses has been very helpful for low level detection [175].

Previously, we have demonstrated the extreme sensitivity of AgNR-SERS substrates produced using an oblique angle deposition with enhancement factors of greater than 10^8 [14,179]. Likewise, we have established the capability of using AgNR-SERS-based detection and quantitation of the RSV pathogen in combination with PLS[10]. The SERS methodology demonstrated the possibility of rapid (<60 sec) detection of various virus types on AgNR-SERS substrates in minute specimen volumes (0.50 - 1.0

μL) without biochemical manipulation of the virus sample[16]. In these previous studies SERS assays were performed with purified viruses in water and buffer. In this report, the sensitivity and specificity of the SERS method is evaluated for the measles virus in and outside a cell lysate matrix. The Edmonston strain of the measles virus was purified to isolate the viral material from the cell lysate to demonstrate the ability to achieve lower level of SERS detection. As a control, the Edmonston strain was evaluated in a cell lysate matrix. These studies indicate that the SERS methodology can be used with chemometric for measles detection, a necessary proponent for low-level measles laboratory surveillance.

3.3 Methods

Measles virus propagation. The Edmonston strain of the MV strain was used in this analysis (positive control). The strain was from a collection of samples that were clarified cell culture supernatants from Vero cells in Dulbecco's Modified Eagles Medium (DMEM; GIBCO BRL Laboratories, Grand Island, NY) without antibiotics or fetal bovine serum (FBS; Hyclone Laboratories, Salt Lake City, UT) prepared by the CDC. Measles were harvested in serum-free DMEM followed by a freeze—thaw (-70 °C/22 °C), after which the contents were vortex for 1 min. The virus titer was approximately 10^6 PFU/mL, determined by immunostaining plaque array (CDC MMR Laboratories, Atlanta, GA). The control for this study was uninfected Vero cell lysate. The control for these studies was uninfected Vero cell lysate.

Virus Purification. In trying to assess the limit of detection of MV samples using SERS- Ag nanorods substrates we postulated that large cellular debris or crystal forming buffers in the samples could interfere with the SERS signal. In the past, we have noticed

that crystal structures appear on the surface of Ag nanorods surfaces, which led to the irreproducibility of MV spectra. Two purifying materials were used to eliminate the formation of large cellular debris and crystal structures on the Ag nanorods surfaces; centrifuge tube filters (Corning Inc. Life Sciences, Lowell, MA) and micro spin desalt columns (Pierce, Rockford, IL). Aliquots of 10 μl MV samples and cell lysate control media were stored in a -70°C freezer.MV samples were thawed, vortexed and then put inside the purifying materials and centrifuged. Samples that were not used for SERS measurments were used for qRT-PCR to determine the RNA content of the purified samples.

Sample Preparation. Serial dilutions in the cellular media were performed ranging from 1:10 to 1:1000. To prevent the formation of a thick cellular layer on the surface of the Ag nanorods, MV samples were diluted in HyPure™ Molecular Biology Grade Water (Thermo Scientific, Waltham, MA) before they were placed on Ag nanorod substrates and SERS spectral collections were made.

*SERS substrate preparation.*The SERS substrates were created using a custom-designed electron beam evaporation (E-beam) system (Torr International, New Windsor, NY), as previously described.[179] Using oblique angle deposition (OAD), the angle of depositing vapor and the surface normal of the substrate is set to 86° where typically a base layer of 20 nm Ti and 500 nm Ag thin films are deposited, respectively. With increasing deposition time, randomly distributed but aligned nanorod arrays develop on the substrate. Figure 3 shows a scanning electron microscopy (SEM) image of an Ag nanorod surface of average length 860 ± 5 nm. In past studies, the overall rod length of

the nanorod substrates were 868 ± 95 nm, the diameter 99 ± 29 nm, the density 13.3 ± 0.5 rods μm^{-2}, when the average tilt angle was 71.3° ± 4.0°.[16]

SERS measurement. SERS spectra were collected using a Renishaw inVia confocal Raman microscope system (Hoffman Estates, IL) with a 785 nm near-infrared diode laser as the excitation source. Attenuated light, from a high power (300 ± 30 mW) laser, was set to ~7mW at the sample surface using a series of neutral density filters. The laser spot was focused into a ~115 μm x 11 μm spot using a 5 x objective. SERS spectra were collected from 400 to 800 cm^{-1} in the ExtendedScan mode using six coadded 10 s collection times. A 3.0-μL aliquot of the sample (i.e., intact virus or cell lysate control media) was applied to the Ag nanorod array substrate and allowed to dry overnight at room temperature prior to spectrum acquisition.

Data analysis. In the past, Ag nanorod substrates created by the oblique angle deposition (OAD) method have been used to carry out quantitative studies on microRNA mixtures.[178] However, the ability of SERS as a biosensing technique for finding the limit of detection of the measles virus (MV) has never been evaluated. For the current study, SERS spectra were collected for the Edmonson strain (positive control), cell lysate (negative control), and four dilutions (10%, 7%, 4%, and 1% concentration of the positive control). In this study, each sample was applied to several SERS substrates, and a total of fifteen spectra were collected from each sample. Each sample was then diluted in water (1:10) to thin the sample, and applied to separate substrates and allowed to dry for at least 24 hours. By visually inspecting SERS spectra, Raman band assignments of biological components were made and spectral reproducibility within and among substrates were examined. Prior to this step, the spectra were baseline corrected using

GRAMS/32 AI (v6.00, Galactic Industries Corp., Salem, NH) with 2 points and then autoscaled.

Partial Least Squares (PLS) analysis, a chemometric technique, was utilized to quantify different concentrations of the Edmonston strain of the MV. Prior to PLS, the raw SERS spectra were derivatized (1st order derivative; 9-point, 2nd order polynomial Savitzky-Golay algorithm), normalized (unit vector normalization length), and mean-centered. The processing of spectral data eliminates useless variance contributed by variation in the baseline or slight heterogeneities in the Ag nanorods substrates.[144,178] Preprocessing was carried out using PLS Toolbox v4.2 (Eigen Vector Research Inc., Wenatchee, WA) combined with the MATLAB v7.10 software (The Mathworks Inc., Natick, MA).

3.4 Results

Initial spectral analysis. Previous studies have demonstrated that silver (Ag) nanorods substrates created using oblique angle deposition (OAD) methods provided spectral reproducibility for small molecules[14] and viruses[10,16]. Hoang et al. has used Ag nanorods substrates to detect measles virus (MV) strains.[18] For the current study, SERS spectra were collected for the Edmonston strain of MV (positive control), the cell media control (negative control), and dilutions made from these samples (at 1, 4, 7, and 10% of the positive control). In this study, each sample was applied to separate SERS substrates and fifteen spectra were collected from each substrate. The instrument was set to optimum conditions (e.g., microscope objective, laser power) to allow the maximum signal-to-noise ratio without detector saturation. The spectra for each sample were baseline corrected using the GRAMS/32 program. Figure 3.1 shows the overlaid spectra

for each sample. Within this figure, the assignment of multiple bands can be made as the one at 1600 cm^{-1} for phenylalanine, the multiple bands in the 520 to 540 cm^{-1} range for S-S stretching and 1260 to 1420 cm^{-1} for amine III and C-N and C-C stretching. The spectra of the positive and negative controls are somewhat similar, however, for the spectra of the dilutions are unique and lack the reproducible desired for these samples. The spectra in this figure illustrate the difficulty of using a single band from each spectrum to show the change in intensity relative to the change in MV concentration. For example, let us examine the band at 660 cm^{-1}. The intensity increases from the first dilution to the second dilution but decreases from the second dilution to the third (Figures 3.1). However, at 1600 cm^{-1}, the intensity of the band increases from the first to the third dilution but not linearly (Figure 3.2). The plot in Figure 3.2 illustrates the misinformation that can be obtained from a concentration versus intensity plot of any spectral band. Since no single band in the SERS spectra can be used to relate the change in MV concentration, a multivariate method must be used. In the past, SERS-Ag nanorods assays have been used with chemometrics as a qualitative methodology to differentiate various genotypes of MV.[18] We assumed that using SERS and chemometrics, in a similar manner to gathering quantitative data (i.e. PCA, HCA, PLS-DA), would allow us to quantify MV samples. Partial Least Squares (PLS) analysis, a chemometric technique, was utilized to quantify different concentrations of the Edmonston strain of the MV.

PLS is a multivariate chemometric technique that decomposes spectral data into loadings and scores, building the corresponding calibration methods from these new variables.

$$X=t_1p^T_1 + t_2p^T_2 + \ldots + t_kp^T_k + \ldots + t_rp^T_r \qquad (3\text{-}1)$$

Equation 1-1illustrates how PLS decomposes the spectral data set (X) into loadings (p_i) and scores (t_i), which tell one about the sets of variables and how the samples relate to each other, respectively. PLS is advantageous for the analysis of complex mixtures because it allows for the fast and simultaneous determination of each component in the mixture without time-consuming separations. Using PLS, the regression curve in Figure 3.3 was created, which displays the spectral data using two parameters, y-measured versus y-predicted. Each spectrum is displayed as a single point (score) where the y-predicted value is determined by the loading. The y-measured values were chosen as the fraction of the positive control, which had a y-measured value of 1.0. For example, the dilution-1 class (10% of the concentration of the positive control) has a y-measured value of 1.0E-01 since it is this times the concentration of the positive control. The negative control class had a y-measured value of 0 since it contained no infectious particles. It is ideal for each class to have a y-predicted value equal to the y-measured value since the y-predicted parameter measures the ability of the PLS model to accurately estimate the concentration of the sample. In Table 3.1, notice how the y-predicted value for the positive control class (0.661) has a small relative standard deviation (RSD; 25%). The relative standard deviation (RSD) is absolute value of the standard deviation expressed as a percentage of the mean (RSD=100($s/\bar{x}$)). The RSD is a measure of a statistical estimate of the reliability of an assay. From analyzing the RSD values of each sample, it was assumed that the model was extremely erroneous. Supporting this conclusion, the root-mean-square error of cross-validation (RMSECV), the parameter that measures the total "fitting" error of predicted values in a PLS model, was high (14%). This could be due to the inability of PLS to predict the concentration of the MV samples (R^2=0.63) or that the

spectra of the MV samples contained variances from sampling. We assumed that the vast RMSECV value within the model was due to sampling since large cellular debris could be seen on the surface of Ag nanorods substrates (Figure 3.4), a feature that could decrease spectral reproducibility and the sensitive of SERS.

We suspected that the non-reproducibility seen in the MV spectra (Figure 3.1) was caused by either large cellular debris or crystal-forming substances in the MV samples. Particles (~100 μm) can be seen on the surfaces of the Ag nanorods that contain 1 μL of a MV sample (Figure 3.4b). To test this hypothesis, MV samples were purified using two methods: one that would remove cellular debris greater than 0.22 microns and another that would remove salts and other small molecules less than 1,000 molecular weight. The former method was carried out using centrifuge tube filters, which removed much of the larger cellular debris from the MV samples and left behind smaller molecules that created large crystalline structures on the surface of the Ag nanorods substrate (Figure 3.4c). The latter method, desalt spin columns, removed the smaller molecules that caused the formation of crystalline structures on the Ag nanorods surface (Figure 3.4d). To assess whether MV RNA remained in both purified samples, Real-time Polymerase Chain Reaction (qRT-PCR also known as Quantitative Reverse Transcription Polymerase Chain Reaction) was used to measure the amount of RNA in each sample.

Quantitative Polymerase Chain Reaction. As with many purification techniques, abundant proteins or salts may be partially or totally removed, although sometimes at the expenses of losing less abundant proteins which are trapped in the precipitates or adsorbed to column packings, precluding their detection.[180] To determine wheather MV RNA remained in purified MV samples, qRT-PCR experiments were performed. qRT-

PCR of purified MV samples proved that purification does not remove significant amounts of measles RNA (Table 3.2). The RNA composition of the MV samples purified with desalt spin columns was (5.40 ± 0.2) x10^3 pfu/ml, relative to the non-purified samples that has a concentration of (6.0 ± 1.0) x10^3 pfu/ml. Centrifuge tube filters, in contrast, removed nearly 62% of MV RNA (3.7 ± 0.2) x10^3 pfu/ml). It was assumed that MV RNA particles adhere to the cellulose containing filters during the purification process, whereas little MV RNA is retained in the resin of the desalt spin columns. Using SERS to analyze desalt column-purified samples, we were able to detect and identify Raman band assignments for prominent Raman shifts previously detected for MV (Figure 3.5). However, spectra obtained for the MV samples purified with centrifuge filter tubes were not reproducible and had bands low signal-to-noise ratios (not shown). Therefore for future studies, desalt spin columns were used for MV purification.

Spectral analysis. For the proceeding study, we assessed that SERS-Ag nanorods substrates and chemometrics would enable us to detect low levels of MV samples and therefore accurately predict the limit of detection of a single MV strain. SERS spectra were collected for the purified Edmonson strain (positive control) and cell lysate (negative control) media samples (Figure 3.5). Firstly, these spectra demonstrate the ability of Ag nanorods substrates as a sensing platform. Secondly, the spectra illustrate the possibility of gaining spectral reproducibility using SERS to detect the measles virus. As seen in Figure 3.5, the spectra of the positive and negative control differ greatly. One can notice the broad band at 1600 cm^{-1} for the positive control spectra, which is possibly a combination of two unresolved bands. In the spectra of the negative control, two

resolved bands are identified at the region of 1650 cm^{-1} and 1606 cm^{-1} for the amide and phenylalanine bands, respectively.

Additionally, dilutions of the positive control were made at 1, 4, 7, and 10% of the positive control sample concentration. The SERS spectra of the dilutions were compared to the spectrum for the positive control and negative control to assess the ability of SERS to capture spectra differences amongst different concentrations of measles samples (Figure 3.5). The 1650 cm^{-1} and 1606 cm^{-1} bands for amide and phenylalanine can be seen in the spectra of the dilutions much like the positive and negative controls. Amongst the dilution spectra, there are many similar characteristics including the CH_2 deformation band at 1295 cm^{-1} and the C-N and C-C stretching band at 1061 cm^{-1}. Overall, the spectral reproducibility of the purified MV samples is much higher than the raw MV samples (Figure 3.1). It is additionally essential to recognize that the negative control, which consists only of cell lysate media, produces a SERS spectrum. Since the MV samples are harvested in cell lysate, all samples should have this background signal in common, this is apparent in the first, third and fourth dilutions of the positive control (Figure 3.5). Although the spectra are similar for the dilution mixtures, the relative intensities of each band are different and do not increase or decrease in a recognizable pattern from one dilution to the next. Therefore, it would be impossible to use a univariate technique like a Beer-Lambert plot to analyze the change in spectral intensity relative to the change in MV concentration.

Chemometric analysis. Partial least squares (PLS) regression models was executed for quantitative analysis of the six measles samples. This chemometric analytical tool is a multivariate calibration tool that is more robust than univariate

methods and is able to find commonalities amongst complex datasets. Note that we realized that the relative intensities of the bands in the dilution mixtures did not have a recognizable pattern relative to the change in concentration. For example, in Figure 3.5 the intensity of the 1295 cm^{-1} for the CH_2 deformation in the spectra of the MV samples does not change linearly from the highest viral concentration to the lowest. The intensity of the band is approximately 10,000 counts for the positive control and 68,000 counts for the negative control. The band however does not decrease from dilution-1 to dilution-4, in this case it goes from 135,000, 150,000, 85,000, to 80,000 counts, respectively. Likewise, this pattern was earlier explained in Figure 3.1 for raw MV samples. Therefore, univarate techniques like the Beer-Lambert law would not be sufficient for determining a linear relationship between the change in MV concentration and change in spectral intensity of a single band. Consequently, PLS was used to create linear regression models by inputting the spectral data in the 400 to 800 cm^{-1} range.

A PLS model was created using the purified spectral data, seen in Figures 3.6. In this model, six classes were included representing the six MV samples: positive control, negative control, and dilutions 1-4. The PLS models were generated using cross validation (Venetian blinds, 9 splits). Cross validation builds a classification model with 90% of the spectra and then test the remaining 10% to measure the integrity of the model. The process is performed iteratively, for a total of 10 iterations, until each sample is withheld from the model and tested as an unknown. In Figure 3.6, each data point (score) is representative of a single SERS spectrum at various concentrations. The measured values were chosen at ratios relative to the amount of positive control (1.0) and negative control (0.0) sample within the mixture. The regression curve illustrates the linearity

between the measured and predicted values of each sample. The linearity of the purified MV sample data in Figure 3.6 is high (R^2=0.99) and the RMSECV value is low (RMSECV=0.024). This is particularly impressive given that the linearity of the raw sample data is considerable lower (R^2=0.63) than that of the purified sample data (R^2=0.99).

The validity of the PLS model can also be analyzed by looking at the average y-predicted values and its associated error (i.e. RSD). In Table 3.3, the average y-measured and y-predicted values for the purified MV samples are given, as well as the standard deviation (SD) and RSD. In Table 3.3, the SD is lower for dilution-4 than dilution-1; however, the RSD is much lower. This occurs because lower dilutions are closer to being zero and a standard of 0.01 will have a greater influence the closer the concentration. It is noticeable that the RSD becomes greater with each dilution. In contrast, the RSD for the raw data is much higher than the purified data since the reproducibility of the spectra is much lower (Table 3.1). This was expected since the crystal structures that form on the surface for the Ag nanorods substrates, due to the presence of the buffer, usually cause the reproducibility of SERS spectra to decrease along with the intensity of the spectral bands. Overall, the spectral reproducibility and PLS model linearity of the purified spectral data is much higher than the raw data. Therefore, it is advantageous to purify MV samples to allow for increased spectral reproducibility, as well as low-level detection of viral sample. Having the ability of detecting low-levels of MV samples with low error (i.e. RMSECV) suggests that one can use SERS-Ag nanorods substrates and PLS to estimate the limit of detection of MV samples.

Statistical analysis. The limit of detection (LOD) is defined as the smallest amount of an analyte that can clearly be distinguished from the blank.[155,162] The LOD of molecular substances can be estimated using statistical methods like the Student's T-test as described in previous methods.[162] In this portion of the study, only purified MV sample data was considered. Likewise, a null hypothesis was made: that the predicted concentration of the lowest dilution in Figure 3.5 (concentration= $5.4x10^1 \pm 0.2\ x10^1$ pfu/ml) was near the LOD. From Table 3.1, the y-predicted values for the 15 scores of the lowest dilution were compared to the values for the negative control. The Data Analysis toolbar in Microsoft Excel (For Windows XP, Microsoft Corporation, Santa Rosa, CA) was used to analyze the data using the Student's T-Test: Two-Sample Assuming Equal Variances. According to the t-test, if *t stat* < *t critical two-tail* the null is rejected. In Table 3.4, since *t stat* (3.64) > *t critical two-tail* (2.76) it was valid to assume that the mean y-predicted concentration of the lowest MV dilution (dilution-4) was near the mean y-predicted negative control, and thereby also near the LOD. Using the relationship that the LOD is equal to the estimated mean of the blank sample plus 2 or 3 standard deviations (LOD= $\overline{X} + \sigma t$) and inputting this LOD value into the y-value of equation of the fit line (Figure 3.6), the actual LOD was determined to be $(7.07 \pm 0.4)\ x\ 10^1$ pfu/ml.

3.5 Discussion

The study reported here illustrates the utility of SERS for the fast and accurate detection and quantification of measles virus samples at various concentrations. This experiment demonstrates that SERS can be used as a label-free technique to detect the measles virus, and that the method could possibly provide useful quantitative information

about varying concentrations of measles virus samples. In the past, SERS has been coupled with chemometrics as a qualitative methodology. It has been used for the differentiation of virus genotypes using multivariate chemometric methods like PLS-DA, PCA, and HCA.[10,18,81] Univariate methods, however, cannot be used to relate the changes in spectral intensity with concentration amongst molecular samples. Such a concept can be seen in Figure 3.1 where the change in intensity of the 1295 cm^{-1} band is not related to the variation in viral concentration. SERS, nonetheless, can be utilized as a quantitative method when combined with chemometric methods like PLS.[178]

PLS is a multivariate technique that decomposes complex spectral data into corresponding models using newly acquired variables. Using PLS for our study, the noticeable contributions of each sample to the variance were visually observed by looking at the standard deviation (SD) in each class (Figure 3.2). The relative standard deviation (RSD) for rose with the decrease of viral concentration. For example, the RSD of dilution-1 class ($6._0 \times 10^2 \pm 9._6 \times 10^2$ pfu/ml) was 52% whereas the RSD of the dilution-3 class ($2.4 \times 10^2 \pm 0.4 \times 10^2$ pfu/ml) was 191% (Figure 3.2). It was expected that the RSD would increase with a decrease in viral concentration but not to a value larger than the RSD of the negative control (65%). Judging by the large RSD values of the sample dilutions, and RMSECV of the model (0.14), it was concluded that the PLS could not accurately estimate the concentration of the raw samples. It was hypothesized that sampling issues caused the error of the model. This theory was formulated by visual inspection of Ag nanorods substrate surfaces that contained MV samples. Apparent on these samples were large particles caused either by large cellular debris and crystal-

forming small molecules within the MV samples. Purifying MV samples using various methods tested the hypothesis.

Initially, two purification methods were used to remove substances that were thought to lower the sensitivity of the SERS assay: centrifuge filter tubes and desalt spin columns. qRT-PCR was used to verify the presence of MV RNA in purified samples. PCR results confirmed that RNA was present in purified samples but highest for samples purified using desalt spin columns (Table 3.3). In a comparison between the spectra of purified measles samples with literature references of Raman band assignments, the major bands were assigned to components of the virus and cell culture media (Figure 3.).[163] For example, bands at 1650, 1606, and 1290 cm^{-1} could be visualized for the presence of amide I, phenylalanine, and amide III, respectively, in the purified samples. Likewise, bands in the range of 600 and 800 cm^{-1} were representative of nucleotides (i.e. cytosine, guanine) present in measles samples. A PLS model was created using the spectral data of the purified MV samples. This model gave high linearity (R^2=0.99) and a low RMSECV value (0.024). Additionally, the RSD values of the dilutions were less than 33%, excluding dilution-4. The RSD value of the dilution-4 was expected to be high because it exceeding the limit of detection. When comparing the y-predicted data of dilution-4 with the negative control, it was concluded that the limit of detection (LOD) of this assay was $(7.07 \pm 0.4) \times 10^1$ pfu/ml. This estimation of the LOD is epidemiologically relevant because viral shedding of measles by an infected host can be within the range of 1 to about 10^4 pfu/ml and scientists can seroconvert with as little as 10 pfu of the virus although the vaccine dosage is approximately 10^3 pfu/ml. Nonetheless, more testing should be done to measure lower levels of the virus using the SERS-AgNR assay.

3.6 Acknowledgements

The research was funded by the Faculty in Infectious Disease at the UGA and Centers for Disease Control and Prevention (UGA/CDC FID) Seed Grant. The author thanks Paul Rota, Marcus Collins, and the Centers for Disease Control (CDC) for supplying the measles samples and Yiping Zhao for the use of the e-beam evaporator.

3.7 References

1. Clements, C.; Strassburg, M.; Cutts, F., The epidemiology of measles. *World Health Stat Q* **1992,** *45*, 285-91.
2. Bottomley, L.; Zhao, Y.; Tripp, R.; Dluhy, R., Georgia Research Alliance FY2009 Collaboration Planning Grant. University of Georgia, Georgia Institute of Technology, CDC MMR and Herpesvirus Branch: Athens, Atlanta, 2009; p 21.
3. (a) Riddell, M. A.; Mossa, M. J.; Hauer, D.; Monzec, M.; Griffin, D. E., Slow clearance of measles virus RNA after acute infection. *J of Clin Virol* **2007,** *39*, 312-317; (b) Mancuso, J.; Krauss, M.; Audet, S.; Beeler, J., ELISA underestimates measles antibody seroprevalence in US military recruits. *Vaccine* **2008,** *26* (38), 4877-4878; (c) Jenkerson, S.; Beller, M.; Middaugh, J.; Erdman, D., False positive rubeola IgM tests [letter]. *N Engl J Med* **1995,** *332*, 1103-4.
4. Rota, P.; Bellini, W., Update on the global distribution of genotypes of wild type measles viruses. *J Infect Dis* **2003,** *187 Suppl 1* (10 (2)), S270-6.
5. Carey, P. R., *Biochemical applications of Raman and resonance Raman spectroscopies*. Academic Press: New York, 1982; p 262.
6. (a) Driskell, J.; Shanmukhy, S.; Liu, Y.; Hennigan, S.; Jones, L., Infectious agent detection with SERS-active silver nanorod arrays prepared by oblique angle deposition. *IEEE Sensors Journal* **2008,** *8*, 863-870; (b) Patel, I.; Premarsiri, W.;

Moir, D.; Ziegler, L., Barcoding bacterial cells: a SERS-based methodology for pathogen identification *J. Raman Spectrosc* **2008,** *39*, 1660-1672; (c) Shanmukh, S.; Jones, L.; Driskell, J.; Zhao, Y. P.; Dluhy, R.; Tripp, R., Rapid and sensitive detection of respiratory virus molecular signatres using a silver nanorod array SERS substrate. *Nano Lett.* **2006,** *6* (11), 2630-2636; (d) Shanmukh, S.; Jones, L.; Zhao, Y.-P.; Driskell, J. D.; Tripp, R.; Dluhy, R. A., Identification and classification of repiratory syncytial virus (RSV) strains by surface-enhanced Raman Spectroscopy and mulitvariate statistical techniques. *Anal. Bioanal Chem* **2008,** *390*, 1551-1555.

7. (a) Amiali, N.; Mulvey, M.; Sedman, J.; Louie, M.; Simor, A., et al., Rapid identification of coagulase-negative staphylococci by Fourier transform infrared spectroscopy. *Journal of Microbiological Methods* **2007,** *68*, 236–242; (b) Harz, M.; Rösch, P.; Popp, J., Vibrational spectroscopy - A powerful tool for the rapid identification of microbial cells at the single-cell level. *Cytometry Part A* **2009,** *75*, 104–113; (c) Huang, W.; Griffiths, R.; Thompson, I.; Bailey, M.; Whiteley, A., Raman microscopic analysis of single microbial cells. *Analytical Chemistry* **2004,** *76*, 4452–4458; (d) Hutsebaut, D.; Maquelin, K.; De Vos, P.; Vandenabeele, P.; Moens, L., et al.; , Effect of culture conditions on the achievable taxonomic resolution of Raman spectroscopy disclosed by three Bacillus species. *Analytical Chemistry* **2004,** *76*, 6274–6281; (e) Kalasinsky, K.; Hadfield, T.; Shea, A.; Kalasinsky, V.; Nelson, M., et al., Raman chemical imaging spectroscopy reagentless detection and identification of pathogens: Signature development and evaluation. . *Analytical Chemistry* **2007,** *79*, 2658–2673; (f) Kirschner, C.; Maquelin, K.; Pina, P.; Thi, N.; Choo-Smith, L., et al., Classification and identification of enterococci: a comparative

phenotypic, genotypic, and vibrational spectroscopic study. . *Journal of Clinical Microbiology* **2001,** *39*, 1763–1770; (g) Maquelin, K.; Choo-Smith, L.; van Vreeswijk, T.; Endtz, H.; Smith, B., et al. , Raman spectroscopic method for identification of clinically relevant microorganisms growing on solid culture medium. . *Analytical Chemistry* **2000,** *72*, 12–19; (h) Maquelin, K.; Kirschner, C.; Choo-Smith, L.; Ngo-Thi, N.; van Vreeswijk, T., et al. , Prospective study of the performance of vibrational spectroscopies for rapid identification of bacterial and fungal pathogens recovered from blood cultures. . *Journal of Clinical Microbiology* **2003,** *41*, 324–329; (i) Naumann, D.; Helm, D.; Labischinski, H., Microbiological characterizations by FT-IR spectroscopy. . *Nature* **1991,** *351*, 81–82; (j) Rebuffo, C.; Schmitt, J.; Wenning, M.; von Stetten, F.; Scherer, S., Reliable and rapid identification of Listeria monocytogenes and Listeria Species by artificial neural network-based Fourier transform infrared spectroscopy. *Applied Environmental Microbiology* **2006,** *72*, 994

8. Driskell, J. e. a., Rapid and Sensitive Detection of Rotavirus Molecular Signatures Using Surface Enhanced Raman Spectrscopy. *PLoS ONE* **2010,** *5* (4), 1-9.
9. Hossain, M. K.; Ozaki, Y., Surface-enhanced Raman scattering: facts and inline trends. *Current Science* **2009,** *97* (2), 192-201.
10. (a) Willets, K.; Duyne, R. P. V., *Ann. Rev. Phys. Chem.* **2007,** *58*, 267-297; (b) Aroca, R., in Surface-Enhanced Vibrational Spectroscopy. In *An associated database of almost 5800 references is available at* www.spectroscopynow.com [Online] Wiley: Chichester, 2006; (c) Kneipp, K.; Kneipp, H., *Surface-enhanced Raman Scattering*. Springer-Verlag: Berlin, 2006; p 464.

11. (a) Alexander, T., Development of methodology based on commercialized SERS-active substrates for rapid discrimination of Poxviridae virions. . *Analytical Chemistry* **2008,** *80*, 2817–2825; (b) Alexander, T., Surface-enhanced Raman spectroscopy: A new approach to rapid identification of intact viruses. *Spectroscopy* **2008** *23*, 36–42; (c) Bao, P.; Huang, T.; Liu, X.; Wu, T., Surface-enhanced Raman spectroscopy of insect nuclear polyhedrosis virus. Journal of Raman *Spectroscopy* **2001,** *32*, 227–230.

12. Driskell, J. D.; Primera-Pedrozo, O. M.; Dluhy, R. A.; Zhao, Y.; Tripp, R. A., "Quantitative Surface-Enhanced Raman Spectroscopy Based Analysis of MicroRNA Mixtures,". *Appl. Spectrosc.* **2009,** *63*, 1107-1114.

13. Driskell, J.; Shanmukh, S.; Liu, Y.; Chaney, S. B.; Tang, X.-J.; Zhao, Y.-P.; Dluhy, R. A., The Use of Aligned Silver Nanorod Arrays Prepared by Oblique Angle Deposition as Surface Enhanced Raman Scattering Substrates. *J. Phys. Chem. C* **2008,** *112*, 895-901.

14. Kramer, R., *Chemometric Techniques for Quantitative Analysis* 1ed.; CRC Press: New York, 1998.

15. Chaney, S.; Shanmukh, S.; Jones, L.; Zhao, Y.; Driskell, J., *Appl. Phys. Lett.* **2005,** *87*, 31908-31910.

16. Chin, W. W.; Marcolin, B. L.; Newsted, P. R., A partial least squares latent variable modelling approach for measuring interaction effects: Results from a Monte Carlo simulation study and voice mail emotion/adoption study. In *The 17th International Conference on Information Systems,*, Cleveland, OH, 1996.

17. Hoang, V. Detection and Classification of Measles Virus By Surface-Enhanced Raman Scattering (SERS) Spectroscopy and Fourier Transform Infrared (FTIR) Spectroscopy. Univ of GA, Athens, 2008.

18. Canas, B.; Pineiro, C.; Calvo, E.; Lopez-Ferrer, D.; Gallardo, J. M., Trends in sample preparation for classical and second generatoin proteomics. *J. Chromatogr. A* **2007,** *1153* (1-2), 235-258.

19. (a) Harris, D. C., *Quantitative Chemical Analysis*. 6 ed.; W. H. Freeman and Company: New York, 2003; (b) Burns, M.; Valdivia, H., Modelling the limit of dectection in real-time quantitative PCR. *Eur Food Res Technol* **2008,** *226*, 1513-1524.

Table 3.1 PLS regression model parameters and results for raw MV samples at various concentrations. A Venetian blinds algorithm with 9 splits was used for cross validation.

	Positive Control	Dilution 1	Dilution 2	Dilution 3	Dilution 4	Negative Control
Y Measured Sample Ratio	1.000	0.100	0.079	0.040	0.010	0.000
Y CV Predicted Sample Ratio	0.661	0.097	0.090	0.091	-0.008	0.265
Range	0.614	0.175	0.414	0.681	0.241	0.646
SD	0.165	0.051	0.120	0.175	0.076	0.171
%RSD	25	52	134	191	915	65

Table 3.2 Real time Polymerase Chain Reaction results for MV samples that were purified using centrifuge tube filters (filter) and desalt spin columns (column), compared to samples that were not purified (raw). The cyclic threshold and quantity of each samples is given and were obtained from a calibration plot of the MV standards 1-4.

Purification Method	**Ct**	**Quantity (pfu/ml)**
Filter	25.0 ± 0.1	$3.70 \times 10^3 \pm 2.0 \times 10^2$
Column	24.44 ± 0.06	$5.40 \times 10^3 \pm 2.0 \times 10^2$
Raw	24.3 ± 0.1	$6.0 \times 10^3 \pm 1.0 \times 10^3$
Standard 1	26.9	10^3
Standard 2	30.8	10^4
Standard 3	33.8	10^5
Standard 4	37.5	10^6

Table 3.3 PLS regression model parameters and results for purified MV samples at various concentrations. A Venetian blinds algorithm with 9 splits was used for cross validation.

	Positive Control	Dilution 1	Dilution 2	Dilution 3	Dilution 4	Negative Control
Y Measured Sample Ratio	1.000	0.100	0.079	0.040	0.010	0.000
Y CV Predicted Sample Ratio	0.987	0.103	0.080	0.062	0.004	-0.013
Range	0.112	0.066	0.049	0.085	0.047	0.041
SD	0.04	0.02	0.02	0.02	0.01	0.01
%RSD	4	19	25	33	244	75

Table 3.4 The limit of detection, the smallest amount that is clearly distinguishable from the blank, can be estimated using statistical measures like the student's t-test. The lowest dilution (dilution-4) was estimated to be near the limit of detection. The Student's T-Test: Two-Sample Assuming Equal Variances was used used to test the null hypothesis, that the predicted concentration of dilution-4 was near that of the negative control. Since t stat > t critical two-tail the null was not rejected.

T-Test: Two-Sample Assuming Equal Variances		
	Variable 1	**Variable 2**
Mean	0.00409	-0.0133
Variance	0.000215	0.000128
Observations	15	15
Pooled Variance	0.000172	
Hypothesized Mean Difference	0	
df	28	
t Stat	**3.64**	
P(T<=t) one-tail	0.000554	
t Critical one-tail	2.47	
P(T<=t) two-tail	0.00111	
t Critical two-tail	**2.76**	

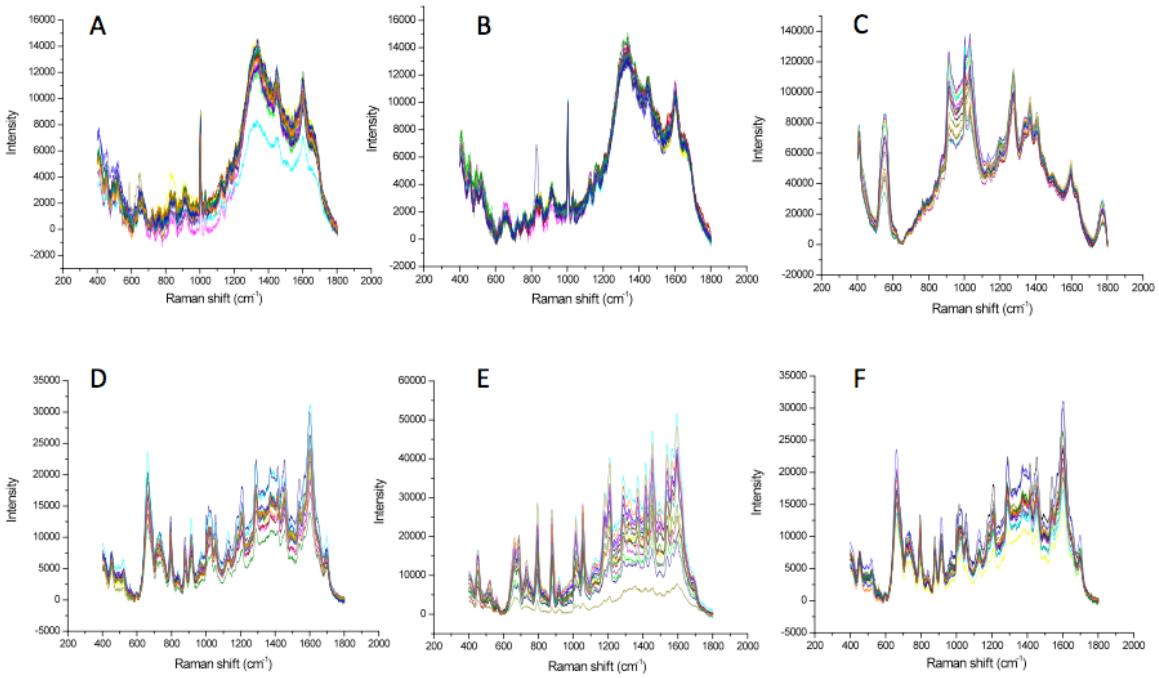

Figure 3.1 Fifteen SERS spectra of raw (A) positive control ($6.0 \times 10^3 \pm 1.0 \times 10^3$ pfu/ml), (B) negative control, (C) Dilution-1 ($6.0 \times 10^2 \pm 9.6 \times 10^2$ pfu/ml), (D) Dilution-2 ($4.2 \times 10^2 \pm 0.7 \times 10^2$ pfu/ml), (E) Dilution-3 ($2.4 \times 10^2 \pm 0.4 \times 10^2$ pfu/ml), and (F) Dilution-4 ($6.0 \times 10^1 \pm 1.0 \times 10^1$ pfu/ml) samples. Individual spectra collected from separate substrates are presented to illustrate the spectral reproducibility. All spectra have been baseline corrected.

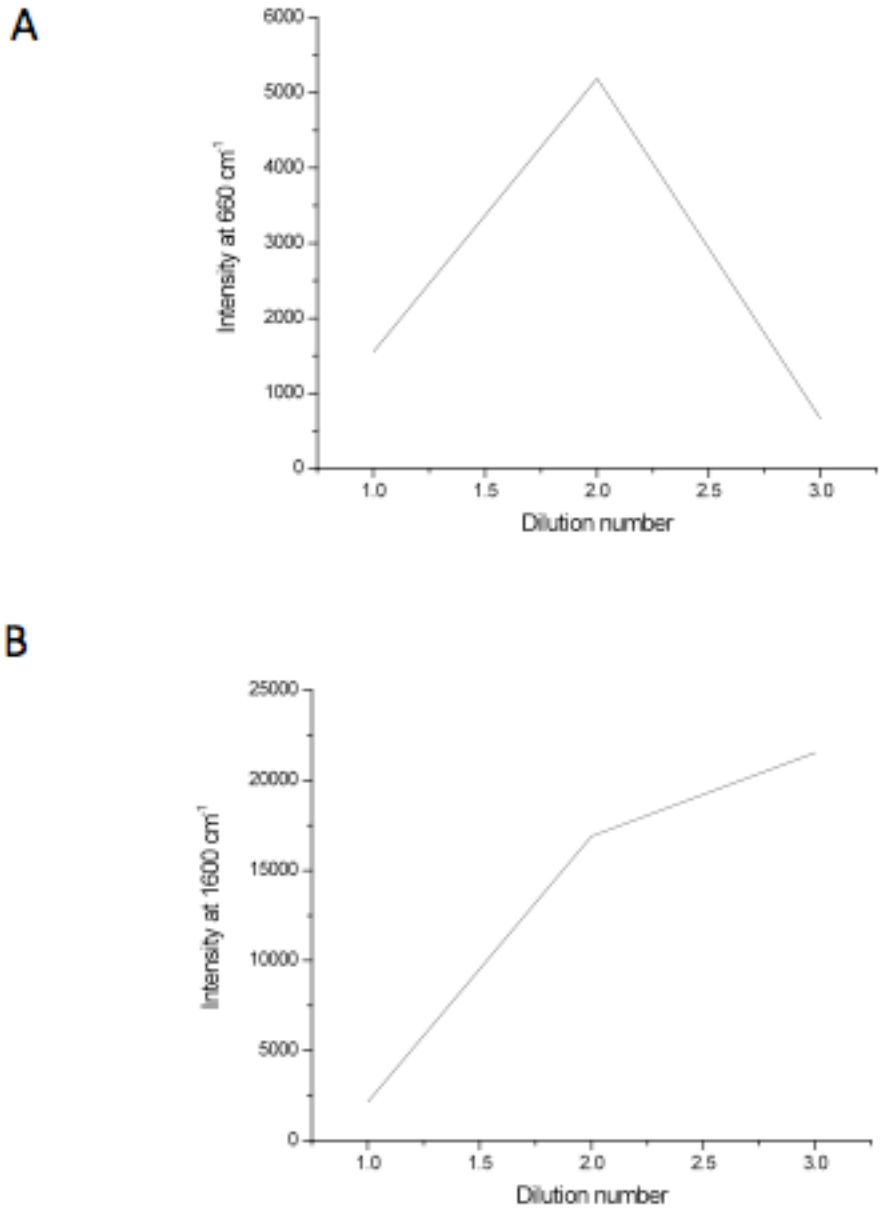

Figure 3.2 The intensity at two different Raman shifts (A) 660 and (B)1600 cm^{-1} relative to the dilutions of the Edmonston strain. The plots demonstrate the difficulty of using a single band from the spectra of the diluted MV samples to show the change in intensity relative to the concentration. At 600 cm^{-1}, the band increases in intensity from dilution-1 to diluiton-2 but decreases from dilution-2 to dilution-3. However, at 1600 cm^{-1}, the intensity of the band increases from dilution-1 to dilution-3 but not linearly.

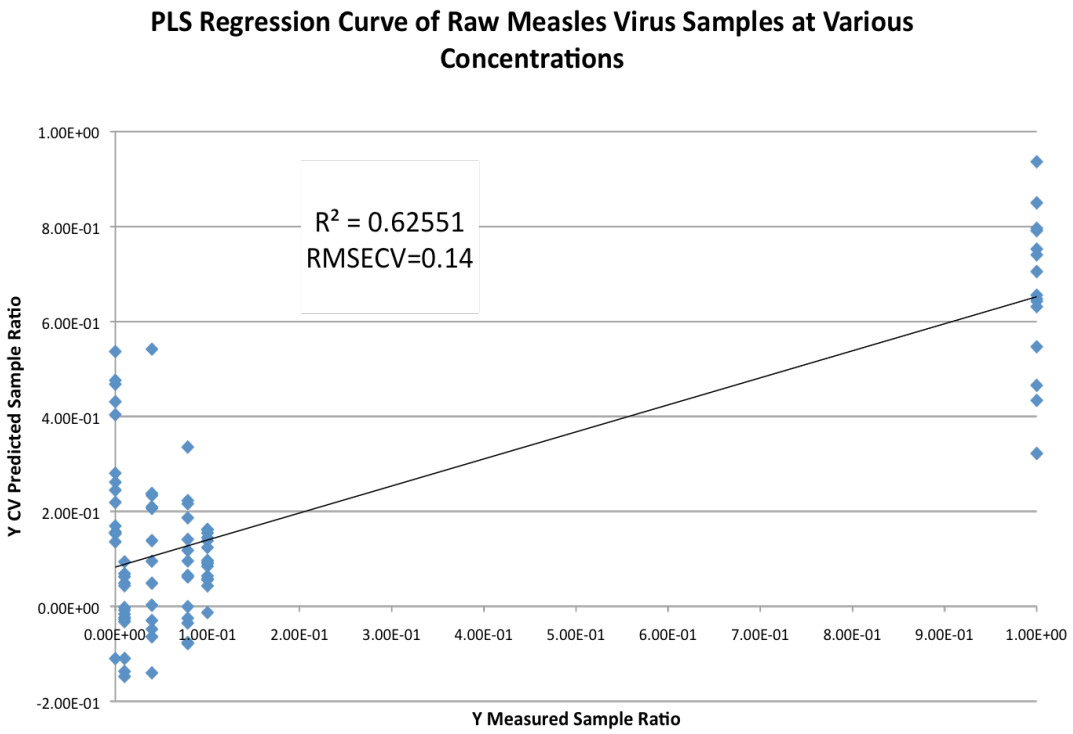

Figure 3.3 PLS results for raw Edmonston strain (MV) samples at various concentrations. The first to last classes go from left to right and represent the positive control, dilution-1, dilution-2, dilution-3, dilution-4, and negative control. Solid line is the equation of the line formed by the various classes.

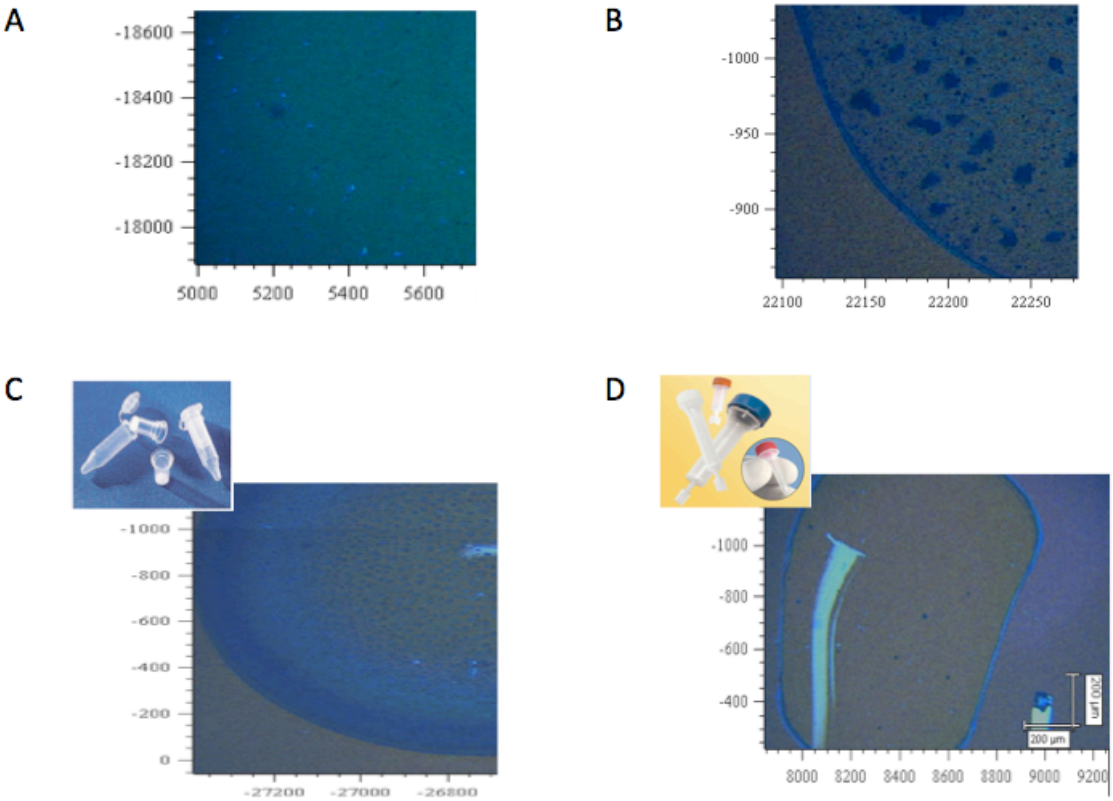

Figure 3.4 Microscopic images of (A) a bare Ag nanorod substrate and substrates containing 1 µL of a MV sample (B) that was not purified, (C) purified with a centrifuge tube filter, and (B) purified with a desalt spin column. The sample purified with the centrifuge tube filter is darker in color and contains a crystal-forming substance. Whereas, the sample purified with the desalt spin column is fairly clear and contains no crystal-forming substances.

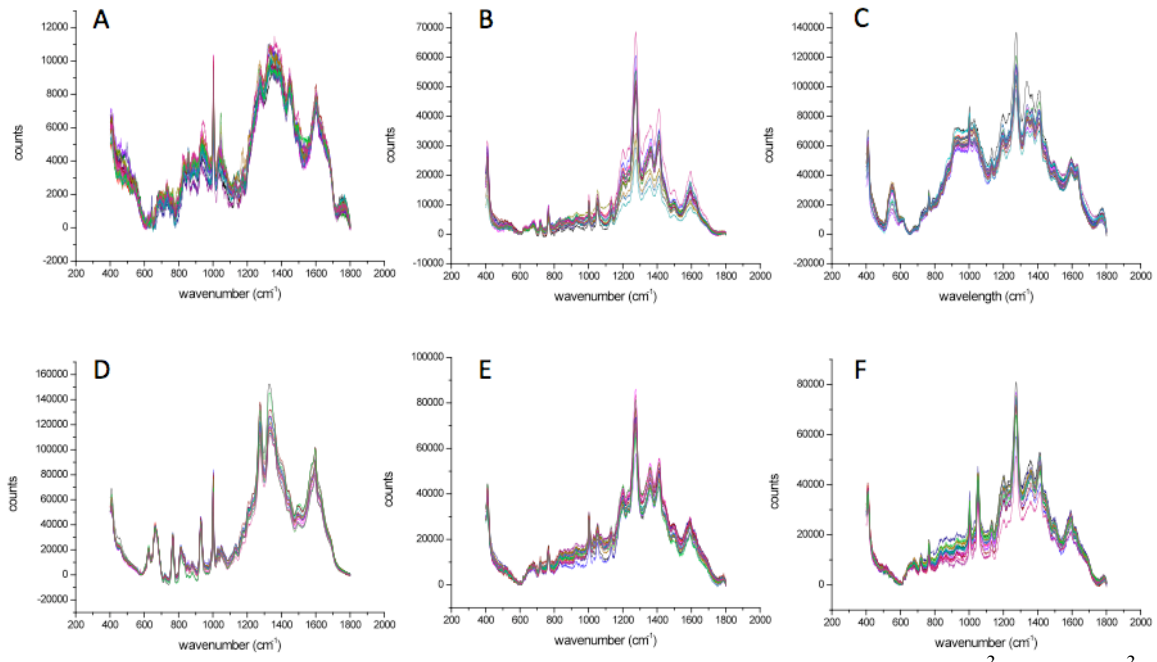

Figure 3.5 Fifteen SERS spectra of purified (A) positive control ($5.4 \times 10^3 \pm 0.2 \times 10^3$ pfu/ml), (B) negative control, (C) Dilution-1 ($5.4 \times 10^2 \pm 0.2 \times 10^2$ pfu/ml), (D) Dilution-2 ($3.8 \times 10^2 \pm 0.6 \times 10^2$ pfu/ml), (E) Dilution-3 ($2.2 \times 10^2 \pm 0.3 \times 10^2$ pfu/ml), and (F) Dilution-4 ($5.4 \times 10^1 \pm 0.2 \times 10^1$ pfu/ml) Edmonston strain samples . Individual spectra collected from separate substrates are presented to illustrate the spectral reproducibility. All spectra have been baseline corrected.

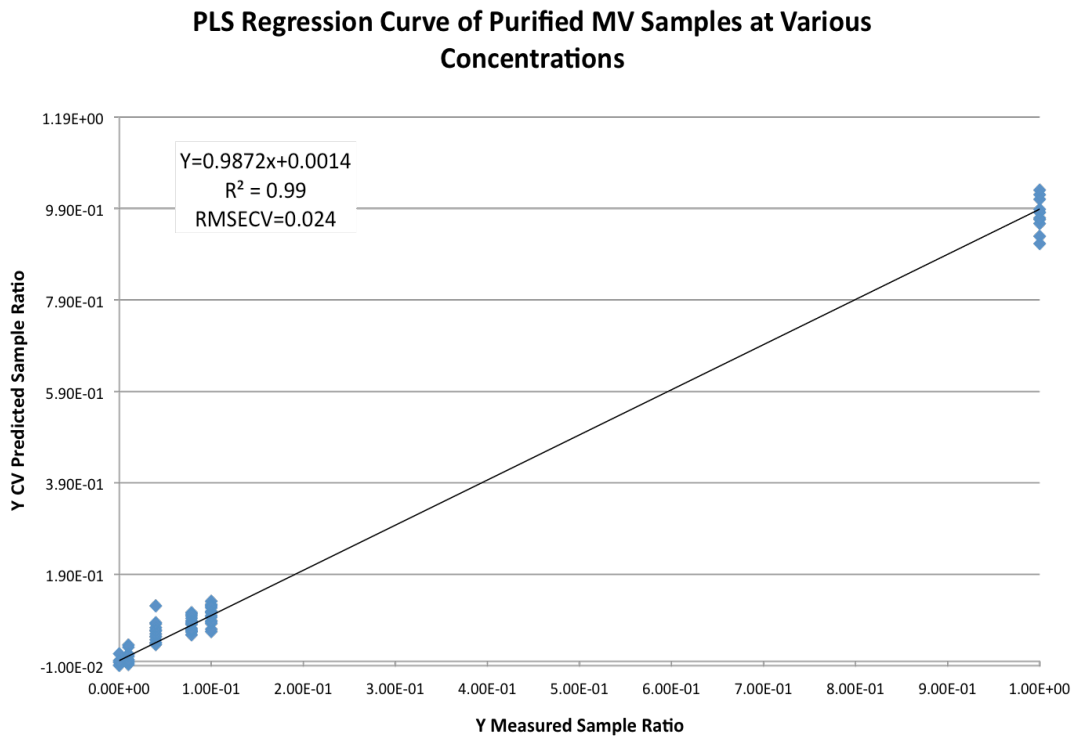

Figure 3.6 PLS results for purified Edmonston strain (MV) samples at various concentrations. The first to last classes go from left to right and represent the positive control, dilution-1, dilution-2, dilution-3, dilution-4, and negative control. Solid line is the equation of the line formed by the various classes.

Chapter 4

Conclusion and Future Work

Measles is a very contagious disease known by a prodromal illness of fever, cough, and conjunctivitis followed by the appearance of a generalized maculopapular rash. The disease initiates in the respiratory system caused by the measles virus, which is spread by aerosol or respiratory droplets entering the respiratory tract. Traditionally, the MV can be detected using polymerase chain reaction (PCR), enzyme-linked immunosorbent assay (ELISA), and indirect immunofluorescent antibody assay (IFA).[2,62] However, each technique is not time efficient and can lead to false negative results. The difficulties in MV detection have driven the search for new methods for detection that overcome the limitations associated with conventional methods. In 2004, Hoang et al. demonstrated that SERS may be used as a label-free spectroscopic method for detecting individual MV strains. Since SERS is a spectroscopic technique in which the analyte is adsorbed onto a nanometrically roughened metal surface that serves as a platform to enhance the Raman scattered signal by up to 14 orders of magnitude.[7,181] Hoang et al. established that Ag nanorod arrays fabricated by an oblique angle deposition method produce highly sensitive and reproducible SERS substrates with enhancements $>10^8$.[14,179] The fast and low-level detection of the virus is so pertinent because the measles infection has an average incubation period of 14 days and infectivity from 2 to 4 days prior, until 2 to 5 days following the onset of the rash. The onset of the rash coincides with the appearance of the immune response and initiation of virus clearance. Therefore, a

sensitive, quick, and low-level detection technique is important for the surveillance of the measles.

In the past, studies have demonstrated the capability of using Ag nanorod-based SERS to detect the measles virus.[18] In these studies, Hoang et al. proved that the SERS technique is sufficiently sensitive to identify the molecular spectra of individual MV strains.[182] The selectivity of the technique was illustrated by chemometric analysis of the spectral data. Chemometrics is a multivariate statistics pattern recognition technique used to group variables together rather than focus on only one variable at a time. For the case of studying the measles, dimension reduction methods like principle components analysis (PCA), Hierarchical Cluster Analysis (HCA) and Principle Component Analysis (PCA) were used to differentiate amongst various genotypes of the measles, specifically the H1, D4, and A strains. Since the measured Raman shifts were also characteristic of the chemical composition of the samples, SERS presented a helpful method for vibrational analysis of the virus samples.

Although, Ag nanorods-based SERS has been employed with chemometrics to provide qualitative data, it has been recently utilized to perform quantitative analysis.[178] Using Partial Least Squares (PLS) to analyze SERS spectral data, PLS models (i.e. regression curves) can be produced and used to determine the limit of detection of measles viral samples. PLS is a supervised multivariate analytical technique that decomposes spectral data into loadings and scores, building corresponding predicted plots of the sample concentrations. This multivariate technique is suitable for the analysis of viral samples because complex mixtures—especially ones containing proteins, RNA,

and amino acids—allow for fast and simultaneous determination of each component in a mixture without time-consuming separations and with minimum sample preparation.

The use of Ag nanorods-based SERS with chemometrics is particularly important in regards to achieving low-level detection. It was initially assumed that low-level detection and consequently the limit of detection for common strains of the measles could be determined because of the sensitivity and selectivity available with the Ag nanorods-SERS assay and chemometric PLS method, respectively. In past studies SERS substrates have demonstrated extreme sensitivity (~10^9 enhancement factor) and with minute specimen volumes (0.8 ± 0.3 μL) without biochemical manipulation.[14] In this study we have used Ag nanorods-based SERS assays with PLS to quantify MV samples. PLS regression curves accurately (RMSECV=0.024) estimated low molecular concentrations (10^3 -10 pfu/ml) of MV samples with high linearity (R^2=0.99). We estimated the limit of detection (LOD) using this model to be (7.07 ± 0.4) x 10^1 pfu/ml, which using lower concentrations to train the PLS model may lead to even lower detection limits.[178] This is epidemiologically relevant because viral shedding of measles by an infected host can be within the range of 1 to about 10^4 pfu/ml and scientists can seroconvert with as little as 10 pfu of the virus although the vaccine dosage is approximately 10^3 pfu/ml.

In conclusion, the data from the Ag nanorod-SERS based assays and chemometric studies proved that the two methods, when used together, could serve as potential spectroscopic techniques for measles quantification. Specifically, the high sensitivity of the SERS technique allows for the quick and accurate detection of the MV at low viral concentration. In the past, chemometrics (i.e. PLS-DA) has proven to be a selective technique for the classification of various MV genotypes. PLS, the chemometric

technique that PLS-DA was based on, will therefore offer the same selectivity. Therefore, the detection of the measles virus at various concentrations demonstrates the ability of Ag nanorod substrates and PLS to provide the sensitivity and selectivity essential for low-level viral detection of the MV.

4.1 References

(1) Bottomley, L.; Zhao, Y.; Tripp, R.; Dluhy, R.; University of Georgia, Georgia Institute of Technology, CDC MMR and Herpesvirus Branch: Athens, Atlanta, 2009, p 21.

(2) Riddell, M. A.; Mossa, M. J.; Hauer, D.; Monzec, M.; Griffin, D. E. *J of Clin Virol* **2007**, *39*, 312.

(3) Mancuso, J.; Krauss, M.; Audet, S.; Beeler, J. *Vaccine* **2008**, *26*, 4877.

(4) Jenkerson, S.; Beller, M.; Middaugh, J.; Erdman, D. *N Engl J Med* **1995**, *332*, 1103.

(5) Rota, P.; Bellini, W. *J Infect Dis* **2003**, *187 Suppl 1*, S270.

(6) Carey, P. R. *Biochemical applications of Raman and resonance Raman spectroscopies*; Academic Press: New York, 1982.

(7) Willets, K.; Duyne, R. P. V. *Ann. Rev. Phys. Chem.* **2007**, *58*, 267.

(8) Aroca, R. In *An associated database of almost 5800 references is available at www.spectroscopynow.com;* Wiley: Chichester, 2006.

(9) Kneipp, K.; Kneipp, H. *Surface-enhanced Raman Scattering*; Springer-Verlag: Berlin, 2006.

(10) Shanmukh, S.; Jones, L.; Zhao, Y.-P.; Driskell, J. D.; Tripp, R.; Dluhy, R. A. *Anal. Bioanal Chem* **2008**, *390*, 1551.

(11) Bao, P.-D.; Huang, T.-Q.; Liu, X.-M.; Wu, T.-Q. *J. Raman Spectrosc* **2001**, *32*, 227.

(12) Driskell, J.; Kwarta, K. M.; Lipert, R. J.; Porter, M. D. *Anal. Chem* **2005**, *77*, 6147.

(13) Abelmann, L.; Lodder, C. *Thin Solid Films* **1997**, *305*, 1.

(14) Driskell, J.; Shanmukh, S.; Liu, Y.; Chaney, S. B.; Tang, X.-J.; Zhao, Y.-P.; Dluhy, R. A. *J. Phys. Chem. C* **2008**, *112*, 895.

(15) Chaney, S. B.; Shanmukh, S.; Dluhy, R. A.; Zhao, Y.-P. *Appl. Phys. Lett.* **2005**, *87*, 31908.

(16) Shanmukh, S.; Jones, L.; Driskell, J.; Zhao, Y. P.; Dluhy, R.; Tripp, R. *Nano Lett.* **2006**, *6*, 2630.

(17) Brereton, R. G. *Chemometrics: Data Analysis for the Laboratory and Chemical Plant.* ; John Wiley & Sons Ltd.: Chichester, 2003.

(18) Hoang, V., Univ of GA, 2008.

(19) Fraser, K. *Measles virus and its biology*; Academic Press: London, New York, 1978.

(20) Panum, P. *Medical Classics* **1938**, *3*, 829.

(21) Cherry, J.; Feigin, R. D.; P.G. Shackelford; Hinthorn, D. R.; Schmidt, R. R. *J. Pediatri* **1973**, *82*, 802.

(22) Edmonson, M. B.; Addiss, D. G.; McPherson, J. T.; Berg, J. L.; Circo, S. R.; Davis, J. P. *JAMA* **1990**, *263*, 2467.

(23) Mathias, R. G.; Meekison, W. G.; Arcand, T. A.; Schechter, M. T. *Am. J. Public Health* **1989**, *79*, 475.

(24) Ozanne, G.; d'Halewyn, M. A. *J. Clin. Microbiol.* **1992**, *30*, 564.

(25) McNeill, W. *Plagues and Peoples*; Anchor Press/Doubleday: Garden City, New York, 1976.

(26) Rhazes, A.-B. *Treatise on the Smallpox and Measles*; J Brindley: London, 1748.

(27) Rolleston, J. *The History of the Acute Exanthemata*; William Heinemann: London, 1937.

(28) Black, F. *Science* **1975**, *258*, 1739.

(29) Lucas, J. *London Med J* **1790**, *11*, 325.

(30) Von Pirquest, C. *Deutsch Med Wochesnschr* **1908**, *35*, 1297.

(31) Tellez-Nagel, I. *Science* **1966**, *154*, 899.

(32) Connolly, J.; Allen, I.; Hurwitz, L., et al. *Lancet* **1967**, *1*, 542.

(33) Ender, J.; Peebles, T. *Proc. Soc. Exp. Biol. Med.* **1954**, *86*, 277.

(34) Smaron, M.; Saxon, E.; Wood, L., et al. *J Virol Methods* **1991**, *33*, 223.

(35) Kobune, F.; Sakata, H.; Sugiura, A. *J Virol* **1990**, *1990*.

(36) Ono, N.; Tatsuo, H.; Hidaka, Y., et al. *J Virol* **2001**, *75*, 4399.

(37) Norrby, E.; Enders-Ruckle, G.; ter Meulen, V. *J. Infect Dis* **1975**, *232*, 262.

(38) Albrecht, P.; Herrmann, K.; Burns, G. *J. Virol Methods* **1981**, *3*, 251.

(39) Knipe, D. M. In *Fields' Virology*; 5 ed.; Howley, P. M., Griffin, D. E., Lamb, R., Martin, M., Eds.; Lippincott Williams & Wilkins: Philadelphia, 2007; Vol. 1.

(40) Longhi, S. In *Current Topics in Microbiology and Immunology* Springer Berlin Heidelberg: 2009; Vol. 329, p 103.

(41) Klingele, M.; MHartter, H.; Adu, F., et al. *J Med Virol* **2000**, *62*, 91.

(42) Rima, B.; Earle, J.; Baczko, K., et al. *J. Gen. Virol* **1997**, *78*, 97.

(43) Rota, J.; Hummel, K.; Rota, P., et al. *Virology* **1992**, *188*, 135.

(44) Giraudon, P.; Jacquier, M.; Wild, T. *Virus Res* **1988**, *18*, 137.

(45) Sheshberadaran, H.; Norrby, E. *Virology* **1986**, *152*, 58.

(46) Tamin, A.; Rota, P.; Wang, Z.-D., et al *J Infect Dis* **1994**, *170*, 795.

(47) Buckland, R.; Giraudon, P.; Wild, F. *J Gen Virol* **1989**, *70*, 435.

(48) Robbie, K.; Brett, M. *J. Vac. Sci. Technol. A* **1997**, *15*, 1460.

(49) Riddell, M.; Rota, J.; Rota, P. *J. Virol* **2005**, *2*, 87.

(50) WHO *Part I. World Health Organization Weekely Epidemiological Record* **2001**, *76*, 242.

(51) Mulders, M.; Truong, A.; Muller, C. *Vaccine* **2001**, *19*, 2245.

(52) Rota, J.; Bellini, W.; Rota, P. *In: Thompson RCA*; Molecular epidemiology of infectious diseases ed.; Kluwer Academic/ Lippincott Raven Publishers: London, 2000; Vol. 168.

(53) Bellini, W.; Rota, P. *Emerg Infect Dis* **1998**, *4*, 1.

(54) Rota, J.; Heath, J.; Rota, P. *J Infect Dis* **1996**, *173*, 32.

(55) Rima, B.; JAP, E.; Baczko, K. *Curr top Microbiol Immnol* **1995**, *191*, 65.

(56) Rota, P.; Rota, J.; Bellini, W. *Semin Virol* **1995**, *6*, 379.

(57) Clements, C.; Strassburg, M.; Cutts, F. *World Health Stat Q* **1992**, *45*, 285.

(58) Venczel, L.; Rota, J.; Dietz, V.; Morris-Glasgow, V.; Siqueira, M.; Quirogz, E.; Rey, G.; Quadros, C. d. *J Infect Dis* **2003**, *187 (Suppl 1)*, S140.

(59) Pan American Health Organization; PAHO: Washington, DC, 1999, p 41 (PAHO technical paper).

(60) Anderson, J.; Barrett, T.; Scott, G. R. *Manual on the diagnosis of rinderpest*.

(61) Bernd Kochanowski, U. R. *Quantitative PCR Protocols*; Humana Press: New Jersey, 1999.

(62) Morfina, F.; Beguin, M.; Lina, B.; Thouvenot, D. *Vaccine* **2002**, *20*, 1541.

(63) Helfand, R.; Kebede, S.; Alexander, J. *J. Infect Dis* **1996**, *173*, 1470.

(64) Lieven, A.; Burunell, P. *J. Clin. Microbiol.* **1986**, *24*, 391.

(65) Onzanne, G.; Halewyn, M. *J. Clin. Microbiol.* **1992**, *30*, 564.

(66) Helfand, R.; Heath, J.; Anderson, L. *J. Infect Dis* **1997**, *175*, 195.

(67) Scheld, W. M. *Infections of the Central Nervous Systems* 3ed.; Lippincott Williams & Wilkins: Philadelphia, 2004.

(68) Dietz, V.; Rota, J.; Izurieta, H.; Carrasco, P.; Bellini, W. *Bull World Health Organ* **2004**, *82*, 852.

(69) Pelletier, M. J. In *Handbook of Vibrational Spectroscopy*; John Wiley & Sons: Chichester, 2002, p 467.

(70) McCreery, R. L. In *Raman Spectroscopy for Chemical Analysis*; John Wiley & Sons: New York, 2000, p 155.

(71) Ingle, J. D.; Crouch, S. R. *Spectrochemical Analysis*; Prentice Hall: Englewood Cliffs, NJ, 1988.

(72) Pommier, C. J.; Walton, L. K.; Ridder, T. D.; Denton, M. B. In *Handbook of Vibrational Spectroscopy*; Ingle, J. D., Crouch, S. R., Eds. Chichester, 2002; Vol. 1, p 507.

(73) Baldwin, K. J.; Batchelder, D. N.; Webster, S. In *Handbook of Raman Spectroscopy: From the Research Laboratory to the Process Line*; Dekker, M., Ed.; I.R. Lewis
H.G.M. Edwards: New York, 2001.

(74) Treado, P. J.; Nelson, M. P. In *Handbook of Vibrational Spectroscopy*; John Wiley & Sons: 2002.

(75) Tian, Z.; Ren, B.; Wu, D. *J. Phys. Chem. B* **2002**, *106*, 9463.

(76) Vo-Dihn, T. *Trac-Trends* **1998**, *17*, 557.

(77) Ferraro, J. R.; Nakamoto, K.; Brown, C. W. *Introductory Raman Spectroscopy*; 2 ed.; Academic Press, 2003.

(78) Kneipp, K.; Kneipp, H.; Itzkan, I.; Dasari, R. R.; Feld, M. S. *J. Phys. : Condens. Matter* **2002**, *14*, R597.

(79) Patel, I.; Premarsiri, W.; Moir, D.; Ziegler, L. *J. Raman Spectrosc* **2008**, *39*, 1660.

(80) Driskell, J.; Shanmukhy, S.; Liu, Y.; Hennigan, S.; Jones, L. *IEEE Sensors Journal* **2008**, *8*, 863.

(81) Driskell, J. e. a. *PLoS ONE* **2010**, *5*, 1.

(82) Michaels, A. M.; Nirmal, M.; Brus, L. E. *J. Am. Chem. Soc.* **1999**, *121*, 9932.

(83) Ethchegoin, P. e. a. *Chem Phys Lett* **366**, *366*, 115.

(84) Otto, A.; Mrozek, I.; Grabhorn, H.; Akemann, W. *J. Phys. : Condens. Matter* **1992**, *4*, 1143.

(85) Otto, A. *Indian J. Phys.* **2003**, *77B*, 63.

(86) Hossain, M. K.; Ozaki, Y. *Current Science* **2009**, *97*, 192.

(87) Zeman, E. J.; Schatz, G. C. *J. Phys. Chem.* **1987**, *91*, 634.

(88) Moskovitis, M. *J. Chem. Phys.* **1978**, *69*, 4159.

(89) Haynes, C.; Van Duyne, R. *J. Phys. Chem. B.* **105**, *105*, 5599.

(90) Sherry, L.; Chang, S.; Shatz, G.; van Duyne, R. P.; Wiley, B.; Xia, Y. *Nano Lett.* **2005**, *5*, 2034.

(91) McFarland, A.; van Duyne, R. P. *Nano Lett.* **2003**, *3*, 1057.

(92) Haes, A.; Haynes, C.; McFarland, A.; Zou, S.; Schatz, G. C.; van Duyne, R. P. *MRS Bull.* **2005**, *30*, 368.

(93) Haes, A.; van Duyne, R. P. *Anal Bioanal Chem* **2004**, *379*, 920.

(94) Miller, M.; Lazarides, A. *J. Phys. Chem. B* **2005**, *109*, 21556.

(95) Mock, J.; Barbic, M.; Smith, M.; Schultz, D.; Schultz, S. *J. Chem. Phys.* **2002**, *116*, 6755.

(96) Haynes, C.; McFarland, A.; Smith, M.; Hulteen, J.; van Duyne, R. P. *J. Phys. Chem. B* **2002**, *106*, 1898.

(97) Schatz, G. C.; Young, M. A.; van Duyne, R. P. In *Surface-Enhanced Raman Scattering: Physics and Applications*; Kneipp, K., Kneipp, H., Moskovitis, M., Eds.; Springer-Verlag: Berlin, 2006.

(98) Kelly, K.; Coronado, E.; Zhao, L.; Schatz, G. *J. Chem. Phys. B.* **2003**, *107*, 668.

(99) Link, S.; El-Sayed, M. A. *J. Phys. Chem. B* **1999**, *103*, 8410.

(100) Draine, B.; Flatau, P. *J. Opt. Soc. Amer* **1994**, *11*, 1491.

(101) Jensen, T.; Kelly, K.; Lazarides, A.; Schatz, G. C. *J. Cluster Sci* **1999**, *10*, 295.

(102) Yang, W.; Schatz, G. C.; van Duyne, R. P. *J. Chem. Phys.* **1995**, *103*, 869.

(103) Novotny, L.; Bian, R.; Xie, X. *Phys. Rev. Lett.* **1997**, *79*, 645.

(104) Bian, R.; Dunn, R.; Xie, X.; Leung, P. *Phys. Rev. Lett.* **1995**, *75*, 4772.

(105) Taflove, A. *Computational Electrodynamics: The Finite-Difference Time Domain Method*; Artech House: Boston 1995.

(106) Jung, L.; Campbell, C.; Chinowsky, T.; Mar, M.; Yee, S. *Langmuir* **1998**, *14*, 36.

(107) Haes, A.; van Duyne, R. P. *J. Am. Chem. Soc.* **2002**, *124*, 10596.

(108) Zhang, X.; Hicks, E.; Zhao, J.; Schatz, G. C.; van Duyne, R. P. *Nano Lett.* **2005**, *5*, 1503.

(109) Green, M.; Liu, F.; Cohen, L.; Kollensperger, P.; Cass, T. *Faraday* **2006**, *132*, 269.

(110) Kattumuri, V.; Chandrasekhar, M.; Guha, S. *Appl. Phys. Lett.* **2006**, *88*.

(111) Kneipp, K.; Flemming, J. *J. Mol. Struct.* **1986**, *145*, 173.

(112) Koglin, E.; Sequaris, J. M.; Valenta, P. *J. Mol. Struct.* **1982**, *79*, 185.

(113) Nabiev, I.; Sokolov, K.; Voloshin, O. *J. Raman Spectroscopy* **1982**, *21*, 333.

(114) Otto, C.; van de Tweel, T.; de Mul, F.; Greve, J. *J. Raman Spectroscopy* **1986**, *17*, 289.

(115) Thornton, J.; Force, R. *Appl. Spec.* **1991**, *45*, 1522.

(116) Suh, J.; Moskovits, M. *J. Am. Chem. Soc.* **1986**, *108*, 4711.

(117) Vo-Dinh, T.; Hiromoto, M.; Begun, G.; Moody, R. *Anal Chem* **1984**, *56*.

(118) Nikoobakht, B.; El-Sayed, M. *J. Phys. Chem. A* **2003**, *107*, 3372.

(119) Tao, A.; Kim, F.; Hess, C.; Goldberger, J.; He, R.; Sun, Y.; Xia, Y.; Yang, P. *Nano Lett.* **2004**, *3*.

(120) Sauer, G.; Brehm, G.; Schneider, S.; Graener, H.; Seifert, G.; Nielsch, K.; Choi, J.; Goring, P.; Gosele, U.; Micleas, P.; Wehrspohn, R. *J. Appl. Phys* **2005**, *97*, 024308.

(121) Moskovits, M.; Jeong, D. *Chem. Phys. Lett.* **2004**, *397*, 91.

(122) Yao, J.; Pan, G.; Xue, K.; Wu, D.; Ren, B.; Sun, D.; Tang, J.; Xu, X.; Tian, Z. *Pur Appl. Chem.* **2000**, *72*, 221.

(123) Haynes, C.; Van Duyne, R. *J. Phys. Chem. B* **2001**, *105*, 5599.

(124) Felidj, N.; Aubard, J.; Levi, G.; Krenn, J.; Hohenau, A.; Schider, G.; Leitner, A.; Aussenegg, F. *Appl. Phys. Lett.* **2003**, *82*, 3095.

(125) Robbie, K.; Sit, J.; Brett, M. *J. Vac. Sci. Technol. A* **1998**, *16*.

(126) Abelmann, L.; Lodder, C. *Thin Solid Films* **1997**, *305*, 1.

(127) Zhao, Y.-P.; Ye, D.-X.; Wang, G.-C.; Lu, T.-M. *Nano Lett.* **2002**, *2*, 351.

(128) Kemsley, E.; Ruault, S.; Wilson, R. *Food Chem.* **1995**, *54*, 321.

(129) Frank, I. E.; Friedman, J. H. *Technometrics* **1993**, *35*, 109.

(130) Chevallier, S.; Bertrand, D.; Kohler, A.; Courcoux, P. *J. Chemom.* **2006**, *20*, 221.

(131) Tran, T.; Wehrens, R.; Buydens, L. *Chemometrics Intell. Lab. Syst.* **2005**, *77*, 3.

(132) Maggio, R.; Cerretani, L.; Chiavaro, E.; Kaufman, T.; Bendini, A. *Food Control* **2010**, *21*, 890.

(133) Martens, H.; Naes, T. *Multivariate calibration* Wiley: Chichester, 1989.

(134) Geladi, P.; Kowalski, B. R. *Anal Chimica Acta* **1986**, *185*, 1.

(135) Nocairi, H.; Qannari, E.; Vigneau, E.; Bertrand, D. *Comput. Stat. Data Anal.* **2005**, *48*, 139.

(136) Baker, M.; Rayens, W. *J. Chemom.* **2003**, *17*, 166.

(137) Wise, B. M.; Shaver, J. M.; Gallagher, N. B.; Windig, W.; Bro, R.; Koch, R. S.; Eigenvector Research, Inc.: 2006.

(138) Adams, M. *Chemometrics in analytical spectroscopy*; 2 ed.; The Royal Society of Chemistry: Cambridege, 2004.

(139) Kramer, R. *Chemometric Techniques for Quantitative Analysis* 1ed.; CRC Press: New York, 1998.

(140) Chin, W. W.; Newsted, P. R. In *Statistical strategies for small sample research*; Hoyle, R. H., Ed.; Sage: Thousand Oaks, CA, 1999, p 307.

(141) Fornell, C.; Bookstein, F. L. *Journal of Marketing Research* **1982**, *19*, 440.

(142) Dijkstra, T. *Journal of Econometrics* **1983**, *22,*, 67.

(143) Garthwaite, P. H. *Journal of the American Statistical Association* **1994**, *89*, 122.

(144) Chin, W. W.; Marcolin, B. L.; Newsted, P. R. In *The 17th International Conference on Information Systems,* Cleveland, OH, 1996.

(145) McDonald, R. P. *Multivariate Behavioral Research* **1996**, *31*, 239.

(146) Chin, W. W.; Marcolin, B. L.; Newsted, P. R. *Information Systems Research* **2003**, *14*, 189.

(147) Cassel, C. M.; Hackl, P.; Westlund, A. H. *Journal of Applied Statistics* **1999**, *26*, 435.

(148) Lohmöller, J.-B. *Latent variable path modelling with partial least squares*; Physica Verlag: Heidelberg, Germany, 1989.

(149) Lyng et al. *BMC Cancer* **2007**, *7*.

(150) Haenlein, M.; Kaplan, A. M. *Understanding Statistics* **2004**, *3*, 283.

(151) Blackie, M. J.; Dent, J. B. *Systems Simulation in Agriculture*; Elsevier Science & Technology: London, 1979.

(152) Harrison, S. *Agric. Syst.* **1990**, *34*, 183.

(153) Mayer, D.; Stuart, M.; Swain, A. *Agric. Syst.* **1994**, *45*, 93.

(154) Analla, M. *Agric. Syst.* **1998**, *57*, 115.

(155) Burns, M.; Valdivia, H. *Eur Food Res Technol* **2008**, *226*, 1513.

(156) Saunders, G.; Parkes, H., (eds) *Analytical molecular biology: quality and validation*; RSC: Cambridge, 1999.

(157) Foy, C.; Parkes, H. *Clin Chem* **2001**, *47*, 990.

(158) McNaught, A.; Wilkinson, A. *Compendium of chemical terminology--IUPAC Recommendations*; Blackwell: Amsterdam, 1997.

(159) Kochanowski, B.; Reischl, U. *Quantitative PCR Protocols*; Humana Press: New Jersey, 1999.

(160) Takeda, M. *The Journal of Clinical Investigation* **2008**, *118*, 2386.

(161) Chaney, S.; Shanmukh, S.; Dluhy, R.; Zhao, Y.-P. *Nano Lett.* **2005**, *87*, 031908.

(162) Harris, D. C. *Quantitative Chemical Analysis*; 6 ed.; W. H. Freeman and Company: New York, 2003.

(163) Naumann, D.; Helm, D.; Labischinski, H. *Nature* **1991**, *351*, 81.

(164) Bussell, R. H.; Waters, D. J.; Seals, M. K.; Robinson, W. s. *Medical Microbiology and Immunology* **1974**, *160*, 105.

(165) Waters, D. J.; Bussell, R. H. *Virology* **1973**, *55*, 554.

(166) Amiali, N.; Mulvey, M.; Sedman, J.; Louie, M.; Simor, A., et al. *Journal of Microbiological Methods* **2007**, *68*, 236.

(167) Harz, M.; Rösch, P.; Popp, J. *Cytometry Part A* **2009**, *75*, 104.

(168) Huang, W.; Griffiths, R.; Thompson, I.; Bailey, M.; Whiteley, A. *Analytical Chemistry* **2004**, *76*, 4452.

(169) Hutsebaut, D.; Maquelin, K.; De Vos, P.; Vandenabeele, P.; Moens, L., et al.; *Analytical Chemistry* **2004**, *76*, 6274.

(170) Kalasinsky, K.; Hadfield, T.; Shea, A.; Kalasinsky, V.; Nelson, M., et al. *Analytical Chemistry* **2007**, *79*, 2658.

(171) Kirschner, C.; Maquelin, K.; Pina, P.; Thi, N.; Choo-Smith, L., et al. *Journal of Clinical Microbiology* **2001**, *39*, 1763.

(172) Maquelin, K.; Choo-Smith, L.; van Vreeswijk, T.; Endtz, H.; Smith, B., et al. *Analytical Chemistry* **2000**, *72*, 12.

(173) Maquelin, K.; Kirschner, C.; Choo-Smith, L.; Ngo-Thi, N.; van Vreeswijk, T., et al. *Journal of Clinical Microbiology* **2003**, *41*, 324.

(174) Rebuffo, C.; Schmitt, J.; Wenning, M.; von Stetten, F.; Scherer, S. *Applied Environmental Microbiology* **2006**, *72*, 994.

(175) Alexander, T. *Analytical Chemistry* **2008**, *80*, 2817.

(176) Alexander, T. *Spectroscopy* **2008** *23*, 36.

(177) Bao, P.; Huang, T.; Liu, X.; Wu, T. *Spectroscopy* **2001**, *32*, 227.

(178) Driskell, J. D.; Primera-Pedrozo, O. M.; Dluhy, R. A.; Zhao, Y.; Tripp, R. A. *Appl. Spectrosc.* **2009**, *63*, 1107.

(179) Chaney, S.; Shanmukh, S.; Jones, L.; Zhao, Y.; Driskell, J. *Appl. Phys. Lett.* **2005**, *87*, 31908.

(180) Canas, B.; Pineiro, C.; Calvo, E.; Lopez-Ferrer, D.; Gallardo, J. M. *J. Chromatogr. A* **2007**, *1153*, 235.

(181) Stiles, P.; Dieringer, J.; Shah, N.; van Duyne, R. P. *Ann. Rev. Anal. Chem* **2008**, *1*, 601.

(182) Driskell, J.; Seto, A.; Jones, L.; Jokela, S.; Dluhy, R.; Zhao, Y.; Tripp, R. *Biosens. Bioelectron.* **2008**, *24*, 923.